Linking molecular, electrical, and behavioral rhythms in the brain's biological clock

By

Jeffrey R. Jones

Dissertation

Submitted to the Faculty of the

Graduate School of Vanderbilt University

in partial fulfillment of the requirements

for the degree of

DOCTOR OF PHILOSOPHY

in

Neuroscience

May, 2015

Nashville, TN

Approved:

Terry L. Page, Ph.D.
Douglas G. McMahon, Ph.D.
Danny G. Winder, Ph.D.
Christopher S. Colwell, Ph.D.

Copyright © 2015 by Jeffrey R. Jones
All Rights Reserved

To my families, old and new:

Mom, Dad, and Andrew
&
Lisa, Mendel, Watson, and
Cricket

ACKNOWLEDGMENTS

First and foremost, I need to acknowledge my funding sources that allowed me to carry out my dissertation research:

This work was financially supported from 2010 to 2012 by the NIH Training in Fundamental Neuroscience Grant T32MH064913 awarded to Mark Wallace and Doug McMahon. From 2012 to present, this work was supported by the NIH Ruth L. Kirschstein National Research Service Award (NRSA) Individual Predoctoral Fellowship F31NS092213 awarded to Jeff Jones.

Secondly, I would like to thank the wide variety of people who have been both supportive and influential throughout my time in graduate school, in no particular order:

The McMahon Lab

Post-docs:	Chris Ciarleglio, Holly Resuehr, Michael Risner, and Chad Jackson
Graduate students:	Noah Green, Heng Dai, Michael Tackenberg, and David Sprinzen
Research staff:	Lili Xu and Laurel Young

Thesis Committee

Terry Page, Doug McMahon, Danny Winder and Chris Colwell

Others

Mark Wallace, John "Doc V" Veillette, Carl Johnson, Terry Jo Bichell, and Juliane Krueger

Third, I would like to again thank Doug McMahon, my dissertation advisor. He was the reason I came to Vanderbilt, and he was immensely supportive during my time in graduate school. He was everything I could have asked for from a mentor and boss.

Finally, I want to thank my wife, Lisa Funkhouser-Jones – she is an amazing scientist and a constant source of inspiration. I couldn't have done this without her.

Jeff Jones

March 13th, 2015

TABLE OF CONTENTS

Page

LIST OF TABLES

Page

LIST OF FIGURES

Page

PREFACE

When I was applying to graduate school in the Fall of 2008, I knew I wanted to study neuroscience. Specifically, because of my undergraduate research project, I wanted to use electrophysiology to study learning and memory in the hippocampus. At the time, Vanderbilt's direct-entry Neuroscience Ph.D. program was for Systems and Cognitive Neuroscience – fMRI, human psychophysics, monkeys, and so on. Vanderbilt also had an alternative entry track into Cellular/Molecular Neuroscience through its Interdisciplinary Graduate Program, or IGP. IGP required students to take an rigorous course load the first year of graduate school covering all aspects of general biology. I did not want to study humans or monkeys, and I must admit that I did not want to intensively study areas of biology outside of neuroscience, so I did not apply to Vanderbilt. Instead, I applied to a variety of other schools all over the country, and ultimately, in the Fall of 2009, I started in the Neurobiology and Behavior program at Columbia University in New York City.

My time at Columbia introduced me to cutting-edge neuroscience techniques about which I had no idea, such as optogenetics, two-photon microscopy, and calcium imaging. It was an extremely intellectually stimulating environment. However, as I progressed through my first-year rotations, I struggled to find a laboratory that I wanted to join. This was compounded by the fact that, despite what I had thought when I applied to Columbia, I absolutely did not like the big-city lifestyle. So in the mid-summer of 2010, around the time I would have to choose a "home" laboratory out of my rotation choices, I was strongly considering dropping out of graduate school. Luckily, Lisa Funkhouser, my now wife, was a graduate student at Vanderbilt, and she suggested that I contact the head of Vanderbilt's neuroscience program, Doug McMahon, who was understanding enough to invite me to Nashville for an interview. I soon transferred to Vanderbilt and began work in Doug's lab as a second-year graduate student. Essentially, I did my laboratory rotations at Columbia and chose none of the labs to join; instead, I happened to choose Doug's lab at Vanderbilt as my home laboratory (**Fig. P-1**).

Figure P-1 Doug's laboratory in Medical Research Building III, Vanderbilt University.

Nashville was very different from New York City, and Vanderbilt was very different from Columbia, but perhaps the biggest change of all was being thrown into the world of circadian neurobiology in Doug's lab. Most people vaguely know of circadian rhythms, but of all the topics covered in my undergraduate neuroscience program, I think we spent maybe five minutes of one lecture explaining that there is a part of the hypothalamus called the "suprachiasmatic nucleus" or SCN that serves as the brain's circadian pacemaker. Doug assured me this system was ideal for electrophysiology (which was a technique I strongly wanted to learn as a graduate student), as these clock neurons had the rather remarkable property of not only spontaneously firing action potentials, but modulating their firing rates with the circadian cycle. I was given my own electrophysiology rig (**Fig. P-2**), and spent the first year or two in Doug's lab learning how to patch SCN neurons from our lab's line of mice that express green fluorescent protein as a real-time output of the molecular clockworks within each neuron (see **Chapter III**).

Figure P-2 My electrophysiology rig in Doug's lab.

Recording from these neurons led me to the realization that in order to truly understand circadian neurophysiology, I would also need to be able to *manipulate* the firing rates of these neurons. To do this, I needed to introduce the new technology of optogenetics to the SCN, which would allow me to shine light on genetically-engineered SCN neurons to directly increase or decrease their firing rates (see **Chapter II**). Doug was fully on-board with this, and sent me off to a variety of places to learn the techniques necessary to pioneer the use of optogenetics in the circadian system: to the "Optogenetics Innovation Laboratory" course at Stanford led by the inventor of optogenetics itself, Karl Deisseroth; to a summer school on neurophysiology at the Université Paris Descartes; and to a spring course on imaging in neuroscience in Québec. Even though there was competition from others in the field, in February 2015 our work paid off and we published a manuscript detailing for the first time the use of both *in vitro* and *in vivo* optogenetics in the SCN. In this dissertation, I thus present the culmination of nearly five years of work detailing the links between the molecular and electrical rhythms in the brain's biological clock and their circadian behavioral output.

CHAPTER I

The multi-component circadian system

1.1: Circadian rhythms and the suprachiasmatic nucleus

Understanding the interaction between gene networks, neuron electrical activity, and neural circuits that ultimately give rise to behavior is a key unsolved question in neurobiology that has broad impacts on such areas as synaptic plasticity, neurodevelopment, and neuropsychiatric disease (Spitzer, 2006; Takahashi et al., 2008; Gerstner and Yin, 2010). For instance, the discovery of a gene that is implicated in, say, depression or anxiety does not directly cause such a disorder per se; instead, the altered gene or gene network disrupts the function of neurons and circuits that ultimately mediate these complex behaviors. A useful model system to study this interaction is the mammalian brain's biological clock, the suprachiasmatic nucleus (SCN). The SCN neural circuit contains around 20,000 neurons, each approximately 10 μm in diameter, located above the optic chiasm and adjacent to the third ventricle at the base of the hypothalamus (Abrahamson and Moore, 2001). It receives light input from the retina via the retinohypothalamic tract and outputs information to the rest of the body through efferent connections with other hypothalamic nuclei (see **Sections 1.4** and **1.5**). Importantly, the SCN is a multi-component circadian oscillator consisting of molecular and electrical rhythms in individual neurons that, together as a network, regulate circadian rhythms in behavior and physiology (Colwell, 2011; **Fig. I-1**). In this chapter, I will discuss the individual components that make up the mammalian circadian system. This section in particular will discuss the basics of circadian rhythms and the evidence supporting the role of the SCN as the master circadian pacemaker in mammals.

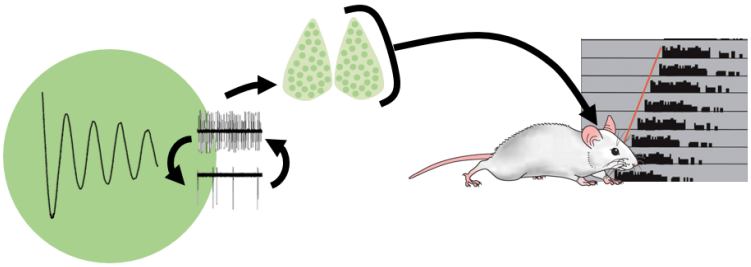

Figure I-1 The multi-component SCN circadian system.

Networked SCN circuit activity consisting of individual SCN neurons, each exhibiting autonomous molecular and electrical rhythms, ultimately gives rise to circadian rhythms in behavior and physiology.

The term "circadian" (from the Latin words *circa* and *dium*, meaning about a day) was first coined in 1957 by Franz Halberg, one of the founders of modern chronobiology (Kuhlman et al., 2007). However, circadian rhythms themselves were first described in

the 4th century B.C.E. by Androsthenes, a Greek historian and ship captain under Alexander the Great, who identified and recorded a diurnal pattern of leaf movement in the tamarind tree *Tamarindus indicus* (Harmer et al., 2001). Over two millennia later, the French scientist Jean-Jacques d'Ortous de Mairan performed what is considered the first experiment investigating circadian rhythms. de Mairan observed that the leaves of the "touch-me-not" plant *Mimosa pudica* (so-called because its leaves rapidly close when touched) exhibited an diurnal rhythm of leaf opening and closing. He then performed the simple experiment of putting the plant into his cupboard – in constant darkness – and discovered that its leaf opening rhythms continued in the absence of sunlight. However, despite this astounding result, de Mairan did not believe that the *Mimosa* had an "internal clock;" instead, he thought that other uncontrolled factors such as temperature or light leak signaled the plant to open and close its leaves (Kuhlman et al., 2007). A little over a century later, the Swiss botanist Augustin de Candolle expanded upon de Mairan's findings by observing that the leaf opening rhythms of the Mimosa plant in constant darkness occurred an hour earlier each day, demonstrating that the plant's leaf rhythms had an endogenous free-running period of less than 24 hours (Roenneberg and Merrow, 2005).

Although there were a small number of observations of circadian or diurnal rhythms in mammals throughout antiquity (such as Herophilus of Alexandria's measurements of daily changes in human pulse rate; Tamarkin et al., 1985), the first rigorous circadian experiment in mammals was performed in 1866 by William Ogle. Ogle noted that his own body temperature increased in the early morning and decreased in the evening, and these changes in body temperature were independent of variations in light (Kirsch, 2011). This was expanded upon a few decades later by Sutherland Simpson and J. J. Galbraith, who showed that the body temperature rhythms of monkeys persisted in both constant darkness and constant light (Buijs and Kalsbeek, 2001). Indeed, human circadian rhythms were shown to be endogenous by two independent experiments in 1962. In the first, the French geologist Michel Siffre lived for two months in total isolation in an underground cave (Silver and Rainbow, 2013); in the second, Jurgan Aschoff and Rutger Wever isolated test subjects in a bunker below Munich (Aschoff et al., 1967). Each of these experiments demonstrated that human circadian rhythms were endogenous, with a free-running period of slightly longer than 24 hours. Through the next century, the characteristics of circadian rhythms were established by Aschoff, Colin Pittendrigh, and Erwin Bunning (Weaver, 1998). Namely, for a rhythm to be considered circadian, (*1*) it had to have an endogenous free-running period lasting approximately 24 hours, (*2*) it had to exhibit temperature compensation (that is, the period of the rhythm persists over a range of physiological temperatures), and (*3*) it had to be entrainable by exposure to an external stimulus, such as light, termed a *Zeitgeber* (Kuhlman et al., 2007). However, the neural locus of circadian rhythmicity in mammals was not identified until 1972, when Robert Moore and Victor Eichler and Freidrich Stephan and Irving Zucker independently

determined that lesions to a small pair of bilateral nuclei in the hypothalamus of rats – the SCN – abolished circadian rhythmicity in drinking behavior, locomotor activity, and adrenal corticosterone rhythms (Moore and Eichler, 1972; Stephan and Zucker, 1972). Thus, these experiments demonstrated that the SCN was necessary to produce circadian rhythms in behavior and physiology.

Another important discovery implicating the SCN as the source of circadian rhythmicity in mammals came from a study that used the (at the time) groundbreaking [14C]-deoxyglucose technique to measure *in vivo* glucose utilization in rats. William Schwartz and Harold Gainer found that the rate of glucose consumption in the SCN, measured as the optical density of [14C]-deoxyglucose-labeled brain sections on an autoradiograph, varied drastically with the time of day. Whereas glucose consumption in other areas of the brain remained relatively constant during the day and night, glucose consumption in the SCN was much higher during the day phase of the circadian cycle (Schwartz and Gainer, 1977). This is consistent with Shin-Ichi Inouye and Hiroshi Kawamura's subsequent discovery of increased electrical activity in the *in vivo* SCN during the day (Inouye and Kawamura, 1979; see **Section 1.3**) and is likely due to the increased activity of the ATP-dependent sodium-potassium pump at this time of day (Colwell, 2011). Again, however, these experiments solely demonstrate the necessity of the SCN for generating circadian rhythmicity, not its sufficiency.

Later experiments tested the sufficiency of the SCN as a circadian pacemaker by transplanting fetal brain tissue into the third ventricle of rats (Sawaki et al., 1984) or hamsters (Lehman et al., 1987) with lesioned SCNs, which causes behavioral arrhythmicity. Amazingly, transplanting fetal SCN tissue restored circadian rhythms in locomotor behavior, while transplanting control fetal tissue had no effect. The fetal SCN tissue appeared to integrate into the host brain, developing retinal afferents and, possibly, efferents into extra-SCN brain areas. In 1990, a landmark experiment by Martin Ralph and colleagues used *tau* mutant golden hamsters, which have a shortened period of locomotor activity (see **Section 1.2**), to demonstrate that the period of locomotor rhythms is determined by the SCN itself (Ralph et al., 1990). A graft containing the SCN from *tau* hamsters or wild-type hamsters was transplanted into the third ventricle of an SCN-lesioned host animal of either genotype. Ralph and colleagues demonstrated that not only did an SCN graft restore locomotor rhythms in an arrhythmic host animal, but also that the period of the restored locomotor rhythm depended solely on the period of the donor SCN, regardless of the genotype of the lesioned host animal. That is, a SCN-lesioned wild-type hamster transplanted with a SCN graft from a *tau* mutant hamster would have a short period of locomotor activity, while a SCN-lesioned *tau* mutant hamster transplanted with a SCN graft from a wild-type hamster would have a normal period of locomotor activity. The dependency of the period of restored locomotor activity in an arrhythmic host on the period of the donor SCN even holds when the host and donor animals are different species,

which typically have differing inherent periods of locomotor activity (Sollars et al., 1995). Intriguingly, Rae Silver and colleagues determined that the ability of a donor SCN to restore locomotor activity rhythms in a SCN-lesioned host animal does not depend on the reestablishment of synapses with the host brain (Silver et al., 1996). Hamster SCN grafts that were encapsulated within a semi-permeable membrane that prevented neural connections but allowed for the diffusion of humoral signals still restored locomotor activity rhythms when transplanted into an SCN-lesioned host. Together, these studies definitively establish the sufficiency of the SCN in generating circadian rhythms in behavior and physiology.

1.2: The mammalian molecular clockworks

Our current understanding of the molecular clockworks within the SCN is that of a transcriptional / translational feedback loop (TTFL) consisting of a number of so-called clock genes that undergo a cycle of transcription, translation, and degradation once every ~24 hours, after which the cycle repeats, signifying a new circadian "day" (Takahashi et al., 2008).

As is often the case in biology, the discovery of the molecular clockworks in the mammalian SCN was preceded by the discovery of these clock genes in simpler model organisms. In the 1970s, Ron Konopka and Seymour Benzer's landmark study using ethyl methanesulfonate (EMS) mutagenesis in the fruit fly *Drosophila melanogaster* demonstrated that there was a genetic determinant of circadian period in eclosion and locomotor activity (Konopka and Benzer, 1971). This gene – the first identified clock gene – was termed *period*, and the identified *Drosophila* mutants, per^{S}, $per^{L,}$ and per^{0}, exhibited a shortened, lengthened, or abolished period of circadian activity, respectively. Around the same time, another clock gene, *Frequency*, was discovered by Jerry Feldman and Marian Hoyle to be necessary for the persistence of rhythms in conidiation (that is, the production of asexual spores) in the fungus *Neurospora crassa* (Feldman and Hoyle, 1973). Thus, these studies showed that individual genes could definitively impact circadian rhythms in behavior. However, genes that influence circadian behavior in mammals were not discovered for nearly two decades, first in hamsters, then in mice.

In 1988, Martin Ralph and Michael Menaker made the serendipitous discovery that a golden hamster (*Mesocricetus auratus)* shipped to them by their animal supplier had a dramatically shortened period of circadian locomotor activity. After performing breeding experiments with the hamster, they discovered that the mutation responsible for the change in circadian period occurred at a single autosomal locus they termed *tau* (from the mathematical symbol for the period of an oscillation; Ralph and Menaker, 1988). Whereas wild-type golden hamsters have a period of locomotor activity of approximately 24 hours, heterozygous *tau* mutants had a period of 22 hours, and homozygous *tau*

mutants had a period of 20 hours. A few years later, the laboratory of Joseph Takahashi undertook a similar experiment to that of Konopka and Benzer in which they performed forward *N*-ethyl-*N*-nitrosourea (ENU) mutagenesis in mice and screened the animals for changes in their period of locomotor activity (Vitaterna et al., 1994). They generated 304 offspring from the mutagenized parent mice, and 303 of them had wild-type periods of activity. One of the mice, however, exhibited an abnormally long period of locomotor activity. Subsequent breeding experiments identified an exon 19 mutation (Δ19) in a gene aptly termed *Clock* (circadian locomotor output cycles kaput) as the cause of this altered circadian behavior, and implicated the basic helix-loop-helix (bHLH)-PAS (*Period-Arnt-Single-minded*) transcription factor *Clock* itself as an essential gene for normal circadian rhythms in behavior.

These seminal findings by the Menaker and Takahashi laboratories paved the way for the rapid discovery of additional components of the mammalian molecular clockworks over the next decade. Both forward genetic screening in mice and homologous cloning approaches proved key to these discoveries. A mammalian ortholog of *Drosophila per* was discovered independently by two groups in 1997 (Sun et al., 1997; Tei et al., 1997); however, it soon became clear that unlike the single copy of *per* in *Drosophila*, mice have three paralogs of *per*, termed *mPer1*, *mPer2*, and *mPer3* (Bae et al., 2001). Likewise, the mouse clock gene *Cryptochrome* was found to have two paralogs, *Cry1* and *Cry2*, each orthologous to the photoreceptive protein *cryptochrome* that was identified in *Drosophila* (van der Horst et al., 1999). Yet another bHLH-PAS gene, *Bmal1* (brain and muscle ARNT-like protein 1), was found by two independent groups in 1997 to be an essential determinant of circadian rhythms in mammals (Hogenesch et al., 1997; Ikeda and Nomura, 1997). The discovery of these clock genes and proteins in the 1990s led to the development of a model of the mammalian molecular clockworks in which clock genes and proteins cycle in a TTFL consisting of positive and negative elements, similar to models proposed for such diverse organisms as *Drosophila*, *Arabidopsis*, and *Neurospora* (Mackey, 2007).

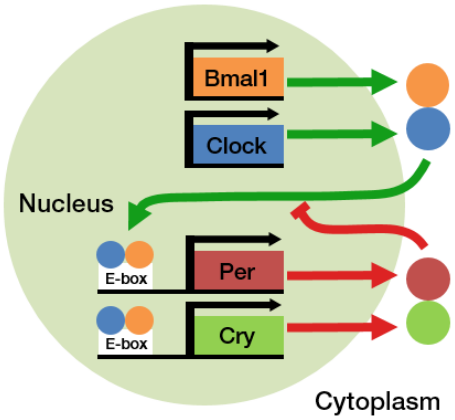

Figure I-2 The core mammalian transcriptional/translational feedback loop.

The SCN molecular clock consists of the positive effectors *Bmal1* and *Clock*, which are transcribed, translated, dimerize, and return to the nucleus to activate the transcription of the negative effectors *Per* and *Cry*. *Per* and *Cry* are transcribed, translated, dimerize, and return to the nucleus to inhibit their own transcription. Progressive phosphorylation of the PER/CRY complex results in its degradation, allowing the cycle to start over. Green lines, positive loop; red lines, negative loop; bent arrows, promoters; arrow line endings, positive regulation; flat line endings negative regulation; colored circles, clock proteins.

The molecular clockworks found in each SCN neuron consists of positive, negative, and accessory loops that, together, form a TTFL that cycles once every ~24 hours (Welsh et al., 2010; **Fig. I-2**). In the positive loop, the clock genes *Bmal1* and *Clock* (or *Npas2*, see (Debruyne, 2008) are translated into bHLH-PAS proteins that heterodimerize outside the nucleus and subsequently enter the nucleus and bind to specific *cis*-regulatory elements, termed enhancer boxes or E-boxes (with a canonical sequence of 5'-CACGTG-3'), on the promoters of target genes (Takahashi et al., 2008). A subset of these so-called "clock-controlled genes" collectively form the negative loop of the TTFL, wherein the BMAL1/CLOCK heterodimer binds to the E-boxes of the *Per* and *Cry* genes and initiates their transcription. Translated PERs and CRYs then heterodimerize outside the nucleus, and the resulting proteins are then phosphorylated by the enzymes casein kinase 1ε/δ (for PER) or AMPK or DYRK1A/GSK-3β (for CRY1 and CRY2, respectively; Kurabayashi et al., 2010). This phosphorylated PER/CRY complex then translocates to the nucleus and is able to directly inhibit the BMAL1/CLOCK heterodimer, effectively inhibiting its own transcription (Lowrey and Takahashi, 2011). Of course, for this mechanism to be useful as (or even considered) a circadian pacemaker, the PER and CRY proteins in the negative loop must be degraded for a new cycle of transcription and translation to begin. Indeed, the stability, or degradation rate, of the PER/CRY complex determines the period of the molecular clockworks, and this stability is determined by the phosphorylation state of the complex (Merrow et al., 2006). For example, the abnormally short period of circadian

locomotor activity in *tau* mutant golden hamsters was later found to be due to a gain-of-function mutation in casein kinase 1ε that increases the rate of phosphorylation of PER (Lowrey et al., 2000). The phosphorylation of PER by casein kinase 1ε/δ targets it for ubiquitination by βTrCP, and the ubiquitinated PER is then degraded by the 26S proteasome. Similarly, the phosphorylation of CRY by AMPK targets it for FBXL3-mediated ubiquitination and 26S proteasome degradation (Takahashi et al., 2008). After this cycle of transcription, translation, and degradation, the molecular clockworks then starts a new cycle, thus signaling the start of another ~24-hour circadian day.

Much of what we know about the function of the molecular clockworks in mammals comes from studying the behavioral phenotypes of mice with mutations in or knockouts of various clock and clock-related genes. Below is an abbreviated table describing the effects of these mutations on locomotor activity rhythms in mice; the effects of some of these mutations on molecular and electrophysiological circadian rhythms will be examined in **Chapter III**.

Table I-1 Locomotor activity phenotypes of various clock gene mutants.

Mutation	Phenotype	References
Per1$^{-/-}$	0.5 to 1 hour shorter period	Bae et al., 2001; Cermakian et al., 2001
Per2$^{-/-}$	1.5 hour shorter period or arrhythmic	Zheng et al., 1999; Bae et al., 2001
Per1$^{-/-}$*; Per2*$^{-/-}$	Arrhythmic	Bae et al., 2001
Cry1$^{-/-}$	1 hour shorter period	van der Horst et al., 1999
Cry2$^{-/-}$	1 hour longer period	van der Horst et al., 1999
Cry1$^{-/-}$; *Cry2*$^{-/-}$	Arrhythmic	van der Horst et al., 1999
Bmal1$^{-/-}$	Arrhythmic	Bunger et al., 2000
Clock$^{\Delta 19/\Delta 19}$	4 hour longer period or arrhythmic	Vitaterna et al., 1994
Clock$^{-/-}$	0.4 hour shorter period	Debruyne et al., 2006

In addition to the "core" positive and negative loops consisting of *Per*, *Cry*, *Bmal1*, and *Clock*, additional "accessory" gene/protein loops have been discovered that contribute to the overall precision and robustness of the mammalian molecular clockworks (Lowrey and Takahashi, 2011). The expression of *Bmal1* itself has been shown to be regulated by the clock-controlled genes *RORα*, *RORβ*, and *RORγ* and *REV-ERBα* and *REV-ERBβ* (Guillaumond et al., 2005). *RORα/β/γ* and *REV-ERBα/β* are transcribed when E-boxes on their promoters are bound by BMAL1/CLOCK. The genes are subsequently translated and returned to the nucleus, wherein RORs and REV-ERBs bind to RREs (RevErbA/ROR response elements, with the canonical sequence 5'-(A/T)A(A/T)NT(A/G)GGTCA-3') on the promoter of *Bmal1* and activate or repress, respectively, its expression (Minami et al., 2013). Yet another accessory loop consisting of the PAR-bZIP (proline- and acidic amino acid-rich basic leucine zipper) activators *Dbp*, *Tef*, and *Hlf* and the repressor *E4bp4* act on D-box elements (with a canonical sequence of 5'-TTATG(C/T)AA-3') of various clock genes including *Per*, *Cry*, *RevErb*, and *Ror* to modulate their transcription (Minami et al.,

2013). Importantly, the core molecular clockworks is also influenced by post-transcriptional regulation (such as by RNA binding proteins) and post-translational regulation (such as by sumoylation, acetylation, and chromatin remodeling (Lowrey and Takahashi, 2011). Thus, it is increasingly clear that the simplified model of the core TTFL in SCN neurons is not sufficient to establish the near-24 hour rhythm of the mammalian molecular clockworks.

While much of what we know about the mammalian molecular clockworks was discovered by using classical molecular biology techniques including polymerase chain reaction (PCR), Western and Northern blotting, and *in situ* hybridization, these strategies all lack the single-sample, longitudinal temporal resolution available for, for example, studying circadian rhythms in locomotor activity. In 2000, real-time reporters of the mammalian molecular clockworks were independently developed by three groups. Shin Yamazaki and colleagues, using rats, and Shun Yamaguchi and colleagues, using mice, created transgenic lines that expressed bioluminescent firefly luciferase under control of the *mPer1* promoter (Yamaguchi et al., 2000; Yamazaki et al., 2000). The laboratory of my thesis advisor, Douglas McMahon, instead used the *mPer1* promoter to drive a degradable form of enhanced green fluorescent protein (GFP) in "*Per1*::d2EGFP" mice (Kuhlman et al., 2000). Importantly, the SCN has the remarkable property of being able to be organotypically cultured and have its molecular (and physiological, see below) rhythms persist indefinitely (Mirmiran et al., 1995). Organotypic SCN sections could therefore be monitored for bioluminescence or fluorescence rhythms in these transgenic mice over multiple circadian cycles (Yamazaki et al., 2000; Quintero et al., 2003). A few years later, another line of knock-in mice was developed by the Takahashi lab in which luciferase is fused to the PER2 protein (Yoo et al., 2004). In the work presented in this dissertation, I take advantage of the real-time reporting capability of these "PER2::LUC" mice (**Chapter II**; Jones et al., 2015) and the McMahon lab's *Per1*::d2EGFP mice (**Chapter III**) to investigate the workings of the mammalian molecular clockworks.

1.3: Circadian electrical activity

The identification of the SCN as being necessary for behavioral rhythmicity in mammals (see **Section 1.1**) strongly suggested that the SCN was the master pacemaker in the brain. However, at that time, there were no experiments proving that the SCN in and of itself exhibited autonomous rhythms. In 1979, Shin-Ichi Inouye and Hiroshi Kawamura had the ingenious idea to test this hypothesis using *in vivo* electrophysiology to record from the SCN and extra-SCN brain areas in awake, behaving animals (Inouye and Kawamura, 1979). They observed that both of these regions exhibited circadian rhythms in multi-unit activity, that is, the action potential frequency or firing rate of the population of cells near the recording electrodes. Surprisingly, when they used a Halasz microknife (essentially a rotatable loop of wire) to isolate an "island" of the hypothalamus that contained the SCN,

they found that while the circadian rhythm in multi-unit activity in the isolated SCN persisted in the absence of connections to the rest of the brain, the rhythm of activity outside the SCN was abolished. Later experiments in which the isolated SCN of awake, behaving rats was recorded continuously for up to 35 days exhibited free-running multi-unit activity rhythms, similar to previously observed free-running rhythms in behavior (Inouye and Kawamura, 1982). Thus, these groundbreaking electrophysiological experiments suggested that the SCN was indeed the central circadian pacemaker.

A true confirmation of the endogenous pacemaker activity of the SCN would require its complete isolation from the rest of the brain. While Inouye and Kawamura's SCN island technique eliminated a majority of connections from the rest of the brain, this technique could not guarantee the complete absence of synaptic coupling or extra-SCN humoral influences on its electrical activity. A few years later, the advent of the acute *in vitro* SCN slice preparation allowed Daniel Green and Rhanor Gillette and Gerard Groos and Jan Hendriks to independently investigate whether the SCN of rats exhibited a circadian rhythm in electrical activity when entirely removed from the brain (Green and Gillette, 1982; Groos and Hendriks, 1982). These groups recorded extracellular single-unit activity (that is, the putative electrical activity from a single cell) from individual SCN neurons throughout the day in an *in vitro* SCN slice and found that, as a population, the neurons exhibited a diurnal variation in firing rate. Importantly, the observed high spike frequency during the day and low spike frequency at night corresponded to the light cycle and behavioral activity of the animal from which the SCN was obtained. Thus, these experiments demonstrated that the SCN maintained its *in vivo* electrical activity rhythmicity *in vitro* for at least one circadian cycle. The subsequent development of the organotypic SCN culture detailed above allowed for the continuous recording of single SCN neurons for up to 66 hours and showed conclusively that firing rate rhythms continued indefinitely *in vitro* (Bos and Mirmiran, 1990). Indeed, *in vitro* firing rate rhythms in the organotypic SCN have been recorded for over eight days (Ikeda et al., 2003).

While *in vitro* recording in the SCN revealed that the SCN *circuit* produces endogenous rhythms in electrical activity, at the time, it remained unclear whether SCN neurons *per se* could generate these rhythms. The first evidence of sustained single-cell electrical rhythms came from recordings in the ocular pacemaker of the sea snail *Bulla gouldiana*. *Bulla* eyes express circadian rhythms in compound action potential frequency when recorded *in vitro* from the optic nerve and these rhythms were shown to be localized to a group of so-called basal retinal neurons located, fittingly, at the base of the retina (McMahon and Block, 1987a, 1987b). Surprisingly, when these neurons were completely dissociated from one another, they continued to exhibit daily spontaneous changes in membrane conductance (Michel et al., 1993). This suggested that, at least in some organisms, single neurons could sustain circadian rhythms in electrical activity. In 1995, David Welsh and colleagues

expanded on this discovery in a landmark study using dissociated SCN neurons from rats (Welsh et al., 1995). They cultured isolated SCN neurons onto a multielectrode array –an arrangement of microelectrodes used to record extracellular electrical activity – and recorded spontaneous action potentials over multiple days. These spontaneous action potentials in individual SCN neurons were similar to those observed in the intact SCN circuit, and, importantly, the rhythms were independently generated: even though functional synapses had formed between these dissociated neurons, the recorded action potential frequency rhythms were not synchronized. Indeed, when action potentials were reversibly blocked with the voltage-gated sodium channel blocker tetrodotoxin, the rhythms in individual neurons reemerged with an unaltered phase. Thus, these results and later experiments by other laboratories strongly suggested that individual SCN neurons could generate circadian rhythms in electrical activity (Liu et al., 1997; Herzog et al., 1998).

These and other experiments *in vivo* and *in vitro* have elucidated the nature of these electrical activity rhythms in SCN neurons. While a number of neurons in the brain, including cerebellar Purkinje, vestibular nucleus, and hippocampal neurons, spontaneously (and repetitively) fire action potentials in the absence of synaptic drive due to a set of intrinsic ionic currents (Häusser and Clark, 1997; Cohen and Miles, 2000; Darlington et al., 2002), neurons in the SCN are unique among those in the brain in that they can modulate their firing *rate* in a circadian manner (Kuhlman and McMahon, 2006). On average, SCN neurons exhibit a peak firing rate of around 8 to 12 Hz (that is, action potentials per second) during the circadian day, and a trough in firing rate of around 1 Hz or less during the circadian night; however, most SCN neurons are thought to be active for only 4 to 6 hours of the day (VanderLeest et al., 2007). This unique rhythmic action potential generation in SCN neurons is currently understood to be due to two differing ionic mechanisms: basal potassium conductance and spike-associated conductances, the first contributing to the day-night variation in firing rate, and the second contributing to spontaneous generation of action potentials themselves (**Fig. I-3**; Kuhlman, 2007).

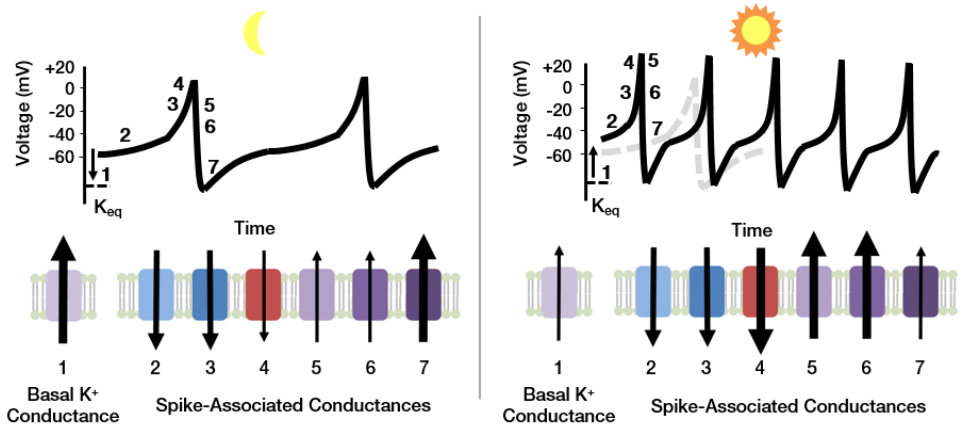

Figure I-3 Ionic mechanism of spontaneous firing rhythms in SCN neurons.

Daily rhythms in spontaneous firing rate in SCN neurons are generated by a collection of rhythmic, intrinsic ionic currents. (**1**) Leak K^+ channel; (**2**) Persistent Na^+ channel; (**3**) Voltage-gated Na^+ channel; (**4**) L-type Ca^{2+} channel; (**5**) FDR K^+ channel; (**6**) A-type K^+ channel; (**7**) BK channel. Size of arrows represents relative size of current passing through channels. Left, nighttime regulation of firing rate; right, daytime regulation of firing rate.

Individual SCN neurons exhibit diurnal rhythms in resting membrane potential alongside their diurnal variation in firing rate such that they are nearly 10 mV more depolarized during the day than in the night (that is, around -45 mV during the day and -55 mV at night). Importantly, this depolarization during the day coincides with a *decrease* in membrane potassium conductance in these neurons (and, conversely, the nightly hyperpolarization coincides with an *increase* in potassium conductance). As in other neurons, the equilibrium potential for potassium in SCN neurons is negative or hyperpolarized compared to the resting membrane potential of the cell. Thus, increasing potassium conductance during the night phase of the circadian electrical activity rhythm brings the resting membrane potential further away from the membrane voltage necessary to generate an action potential, termed the spike threshold (in the SCN, this value is around -35 to -40 mV). Conversely, decreasing potassium conductance allows the resting membrane potential to drift away from the equilibrium potential for potassium towards the spike threshold, making the neuron more likely to fire an action potential (Colwell, 2011). The reduced potassium conductance, and, consequently, the reduced *overall* membrane conductance during the day also contributes to an increased sensitivity to the intrinsic ionic currents that generate action potentials in SCN neurons. Ohm's law states that a change in voltage is proportional to a change in current times resistance (V = IR). As conductance is by definition the inverse of resistance, a decreased conductance during the day in these neurons results in a higher magnitude voltage change for a given change in current (Kuhlman, 2007). The channels responsible for these rhythms in basal potassium

conductance are currently unknown. The rhythms in basal potassium conductance are sensitive to tetraethyl ammonium, a non-specific potassium channel blocker, and are thought to be generated by twin-pore "leak" potassium channels. Many of these leak potassium channel genes are transcribed in the SCN, including those for TWIK-1, TRAAK, TASK-1, TASK-2, and TREK-1; however, specific pharmacological blockers for these channels are unavailable (Colwell, 2011).

In addition to the daily fluctuation in basal potassium conductance, various "spike-associated conductances" (some of which are also modulated in a circadian manner) are also involved in repetitive, spontaneous firing in SCN neurons (Kuhlman and McMahon, 2006). A requirement for this autonomous generation of action potentials that is shared by both extra-SCN neurons that spontaneously fire action potentials and SCN neurons themselves is an intrinsic, depolarizing drive towards spike threshold. In SCN neurons this is accomplished by a persistent, slowly-inactivating depolarizing current that works through sodium channels that are blocked by the voltage-gated sodium channel blocker TTX and the neuroprotective drug riluzole (Kononenko et al., 2004). There is no current evidence for circadian modulation of this channel's conductance; as such, it is thought to largely contribute to the generation of action potentials independently of the SCN's circadian modulation of firing rate. Indeed, a circadian modulation of membrane potential persists in the presence of TTX or prolonged intracellular dialysis. Other studies have identified the sodium channels responsible for this *persistent* depolarization as Nav1.8 and Nav1.9, encoded by the genes *SCN8A* and *SCN9A*, respectively (Colwell, 2011). Additional voltage-gated sodium channels and nimodipine-sensitive L-type calcium channels also work together with the persistent sodium channel and, ultimately, produce the large depolarization or "spike" comprising an action potential (Pennartz et al., 2002). Intriguingly, currents mediated by the L-type calcium channel Cav1.3, encoded by the genes *CACNA1C* and *CACNA1S*, are rhythmically expressed within the SCN, exhibiting a large conductance during the day and minimal conductance at night (Jackson et al., 2004). Thus, the increased current through these L-type calcium channels allows an SCN neuron to rapidly reach spike threshold and peak depolarization levels during the day phase of the circadian cycle, which contributes to a faster firing rate.

Rapid depolarization during the day phase does not in and of itself lead to faster action potential generation in SCN neurons. This depolarization must in turn be met with a rapid repolarization and a short enough after-hyperpolarization such that the neuron can quickly begin to fire another action potential (Kuhlman and McMahon, 2006). SCN neurons accomplish this with an assortment of potassium channels, including fast delayed rectifier (FDR) potassium channels (Kv3.1 and Kv3.2, encoded by *Kcnc1* and *Kcnc2*, respectively) and A-type potassium channels (Kv4.1 and Kv4.2, encoded by *Kcnd1* and *Kcnd2*, respectively). When FDR potassium channels in the SCN are blocked by the broad-spectrum voltage-gated potassium channel blocker 4-aminopyridine, SCN neurons

exhibit a significantly slower repolarization (thus decreasing spike frequency) and a disruption of circadian rhythms in firing frequency (Itri et al., 2005). Similarly, when these channels are genetically knocked out in a *Kcnc1*$^{-/-}$; *Kcnc2*$^{-/-}$ double knockout mouse line, spontaneous firing rate is reduced in the day phase of the circadian cycle and the width of individual action potentials is greatly increased (Kudo et al., 2011). Importantly, the conductances of FDR potassium channels are higher in the day phase and lower in the night phase of the circadian cycle. Thus, these studies show that FDR potassium channels are essential parts of the repolarization phase of the action potential that is necessary for a rapid daytime firing rate in SCN neurons; however, as 4-aminopyridine is not selective for FDR potassium channels, other potassium channels may be involved in this regulation of firing rate. Indeed, the I_A current mediated by A-type voltage-gated potassium channels in the SCN also exhibits diurnal rhythms; however, there is no evidence for rhythmic expression of the Kv4.1 and Kv4.2 channels responsible for this current (Itri et al., 2010). Finally, calcium-activated BK "big potassium" potassium channels (encoded by *Kcnma1*) play an important role in both the repolarization and the after-hyperpolarization phases of action potential generation in the SCN. Current through BK channels is elevated in the night phase of the circadian cycle. Pharmacologically blocking this current with the scorpion toxin iberiotoxin or knocking out the channel in *Kcnma1*$^{-/-}$ mice dampens, but does not abolish, the day-night difference in firing rate in SCN neurons (Meredith et al., 2006; Pitts et al., 2006). However, suppressing BK currents in this manner does increase spike frequency in the night phase of the circadian cycle. Thus, it is likely that elevated nighttime BK current lengthens after-hyperpolarization duration, and, indeed, studies have shown that this current alone may contribute up to 40% of the after-hyperpolarization in SCN neurons (Cloues and Sather, 2003).

Traditional electrophysiological methods that have been used to study circadian electrical activity in the SCN include the *in vitro* techniques of cell-attached and whole-cell patch clamp recording and multielectrode array recording, or the *in vivo* technique of multiunit recording. A major problem with these techniques is that they are largely only able to monitor and not manipulate electrical activity in SCN neurons. While neuronal firing rate can be manipulated pharmacologically, such as with TTX, or ionically, such as with high or low potassium extracellular medium, these methods are not directed to SCN neurons and have nonspecific effects. The recent invention of optogenetics has given neuroscientists the tools necessary to directly decrease or increase firing rate with high temporal and spatial resolution (Boyden et al., 2005). With this technology, light-sensitive proteins can be transgenically or virally expressed in specific neurons and light of particular wavelengths can be shined onto these neurons to manipulate their firing rates. In this dissertation, I show for the first time that the SCN can be optogenetically manipulated both *in vitro* and *in vivo* (Jones et al., 2015; **Chapter II**). Another problem with traditional electrophysiology is that it is difficult to measure the activity of many neurons simultaneously, such as those that comprise the SCN neural circuit. While many

neurons can be recorded using multielectrode arrays, the spatial resolution of this technique is limited. Genetically-encoded calcium sensors (Brancaccio et al., 2013) or voltage-sensors (Cao et al., 2013) allow for the simultaneous imaging of an entire neural circuit with high spatial and temporal resolution. I briefly discuss this technique as a future direction in **Chapter IV**. The combination of optogenetic manipulation of firing rate and genetically-encoded calcium or voltage sensor imaging allows for all-optical electrophysiology (Hochbaum et al., 2014) which could be applied to the SCN in the future.

1.4: The SCN neural network

The fact that dispersed, dissociated SCN neurons generate independent circadian rhythms in spontaneous firing rate (see **Section 1.3**) or PER2::LUC bioluminescence (see **Section 1.2**) demonstrates that individual SCN neurons are cell-autonomous molecular and electrical oscillators. However, cell autonomy within the SCN is limited: the inputs onto and outputs of the SCN depend on the networked connectivity among individual neurons (Welsh et al., 2010). The SCN network is commonly divided into two main areas based on neuropeptide content: a ventrolateral "core" region immunopositive for the neuropeptides vasoactive intestinal peptide (VIP, ~24% of SCN neurons), gastrin releasing peptide (GRP, ~14%), calretinin (~14%), substance P (~2%) and neurotensin (~4%), and a dorsomedial "shell" region immunopositive for the neuropeptides arginine vasopressin (AVP, ~37% of SCN neurons), somatostatin (~3%) and met-enkephalin (~3%; Moore, 2013; **Fig. I-4**; note that these numbers are from rat SCN, although other mammals such as mice have similar percentages). Additionally, most, if not all, neurons in the SCN produce the neurotransmitter γ-aminobutyric acid (GABA; Wagner et al., 1997). Neurons in the SCN are morphologically homogenous with the exception of GRP-positive neurons, which have significantly smaller somata than VIP-positive or AVP-positive neurons. Overall, the shell is slightly larger than the core, containing 57% of the total number of SCN neurons and having a volume of ~2,200,000 μm^3 (compared to a core volume of ~1,400,000 μm^3; Moore, 2013).

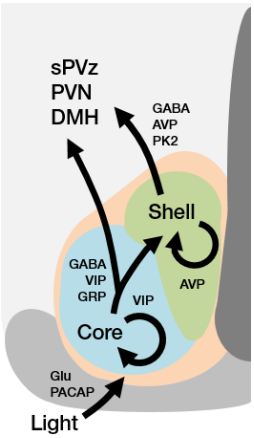

Figure I-4 Coupling factors within the SCN neural network.

Retinal input onto the SCN through the retinohypothalamic tract releases glutamate (Glu) and pituitary adenylate cyclase activating polypeptide (PACAP) onto neurons in the core region of the SCN, which are immunopositive for vasoactive intestinal peptide (VIP), gastrin releasing peptide (GRP), and GABA. GABA acts as a coupling factor within both the SCN core itself and within the SCN shell, which is immunopositive for arginine vasopressin (AVP). These neuropeptides (including prokineticin 2, PK2) and neurotransmitters are released from the SCN to downstream regions including the subparaventricular zone (sPVz), paraventricular nucleus (PVN), and dorsomedial hypothalamus (DMH). Light gray, optic chiasm; dark gray, third ventricle.

There is clearly a neurochemical and neuroanatomical difference between the core and shell regions of the SCN, and, fittingly, there is also a functional difference between these divisions of the SCN network. The VIPergic SCN core, located adjacent to the optic chiasm, receives retinal input from melanopsin-containing intrinsically photoreceptive retinal ganglion cells (ipRGCs) through the retinohypothalamic tract. As such, neurons in this region of the SCN (core, ventrolateral, or VIP-positive SCN neurons) are also called "retinorecipient" neurons (Ruan et al., 2008). ipRGCs release the neurotransmitters glutamate and PACAP (pituitary adenylate cyclase-activating polypeptide) onto AMPA/NMDA and PAC1 receptors, respectively, on neurons in the SCN core. This leads to an increase in intracellular calcium, which in turn activates a variety of downstream signaling cascades that ultimately converge to promote the transcription and translation of the core clock genes *Per1* and *Per2* (Irwin and Allen, 2010). Thus, light information is able to directly influence the molecular clock by acting through retinorecipient core SCN neurons. A number of experiments have shown that the SCN core is essential for the maintenance of normal circadian rhythmicity. In 1999, Joseph LeSauter and Rae Silver elegantly demonstrated that circadian rhythms in the locomotor activity of hamsters persisted when a targeted SCN lesion spared the core region of the SCN. They also found that fetal SCN grafts containing the SCN core could restore locomotor rhythmicity in

SCN-lesioned host animals, but grafts lacking the core failed to restore these rhythms (LeSauter and Silver, 1999). Thus, they showed that the SCN core is both necessary and sufficient for circadian rhythms in locomotor activity; a few years later, they also demonstrated that the core is essential for circadian rhythms in other behaviors (drinking and gnawing), physiology (body temperature and heart rate), and hormone secretion (melatonin and cortisol; Kriegsfeld et al., 2004). *In vitro* experiments using cultured SCN slices from *Per1-luc* mice that express a bioluminescent readout of the molecular clockworks (see **Section 1.2**) have also supported the idea that the core is crucial for coherent circadian rhythms. When an SCN slice is bisected into two sections, one containing and one lacking the core, both sections contained cells that exhibited bioluminescence rhythms. In the section containing the core, these individual rhythms were synchronized; however, in the section *lacking* the core, the rhythms were out of synchrony, suggesting that some coupling factor is present in the core region of the SCN (Yamaguchi et al., 2003).

The most likely candidate for this core coupling factor is a secreted neuropeptide, as the genetic deletion of the secretory vesicle proteins IA-2 and IA-2β significantly disrupts circadian rhythms in electrical activity and physiology (Kim et al., 2009). Indeed, Kazuyuki Shinohara and colleagues were able to identify a rhythmic release of the neuropeptide VIP from cultured SCN slices by collecting the culture medium every two hours for up to six days, which suggests that the release of VIP is essential for normal SCN activity (Shinohara et al., 1995). In the SCN, VIP acts on the Gs/Gq-coupled G-protein coupled receptor VPAC2 (vasoactive intestinal peptide receptor 2, encoded by *Vipr2*), which is expressed throughout the core and the shell, and regulates both circadian electrical activity by closing potassium channels (Pakhotin et al., 2006) and the molecular clockworks by influencing intracellular calcium dynamics through a Gq-mediated pathway (Brancaccio et al., 2013). VIP application during the night phase of the circadian cycle has also been shown to induce the expression of the core clock genes *Per1* and *Per2*, and this induction is at least partially due to the activation of protein kinase A and CREB (calcium/cyclic AMP response element binding protein; Nielsen et al., 2002). Consistent with VIP's depolarizing effects on circadian electrical activity, SCN neurons from VPAC2 receptor-deficient *Vipr2*$^{-/-}$ mice are chronically hyperpolarized and those from VIP-deficient VIP$^{-/-}$ mice do not exhibit circadian rhythms when recorded on a multielectrode array (Cutler et al., 2003; Brown et al., 2007). Intriguingly, although the exogenous application of VIP onto an SCN slice normally causes an acute induction of SCN neuron firing rate in a time-dependent manner (similar to phase shifts induced by light; Reed et al., 2001), this VIP-induced firing rate increase is dependent on the transcription of *Per1* (Kudo et al., 2013); I investigate this curious finding further in **Chapter III**. SCN slices from *Vipr2*$^{-/-}$ mice do not show a circadian variation in levels of *Per1* and *Per2* mRNA as measured by *in situ* hybridization or *Per1*-promoter mediated transcription as measured by *Per1-luc* bioluminescence. Similarly, SCN slices from VIP$^{-/-}$ mice exhibit blunted population-level

Per1-promoter mediated transcription as read out by *Per1*::d2EGFP fluorescence; however, the *single cell* fluorescence rhythms remained robust even in the absence of VIP (Ciarleglio et al., 2009). In 2005, Sara Aton and colleagues found that although single-cell firing rate rhythms only persist in a subset of SCN neurons from *Vipr2*$^{-/-}$ or VIP$^{-/-}$ mice that are dissociated and cultured at high density on a multielectrode array, the rhythms that persist are not synchronized. Importantly, daily application of a VPAC2 agonist to the cultured neurons restores firing rate synchrony in VIP$^{-/-}$ but not *Vipr2*$^{-/-}$ neurons (Aton et al., 2005). Thus, together, these results suggest that VIP plays an important role in coupling individual neuronal oscillators within the SCN.

VIP produced by the core region of the SCN is both necessary and sufficient for synchronized neuronal rhythms (in that genetic ablation of VIP or its receptor results in asynchronous molecular and electrical rhythms and that exogenous application of a VPAC2 agonist is able to resynchronize rhythms in VIP$^{-/-}$ SCN neurons, respectively); however, it is not the only putative coupling agent within the SCN. Synaptic transmission involving the neurotransmitter GABA occurs alongside humoral release of VIP and other neuropeptides in SCN neurons (Moore and Speh, 1993). The synaptic release of GABA appears to be circadian, as there is a higher frequency of spontaneous inhibitory post-synaptic currents in SCN neurons in the dorsomedial shell region in the late day and early subjective night than in the late subjective night (Itri et al., 2004). In the SCN, GABA acts on ionotropic $GABA_A$ receptors and metabotropic $GABA_B$ receptors expressed throughout the SCN. Interestingly, unlike in most areas of the brain, GABA may be both excitatory and inhibitory in SCN neurons. The level of intracellular chloride within SCN neurons is set by a balance between the rhythmically-expressed sodium-potassium-chloride cotransporter NKCC1 (encoded by *SLC12A2*) and the chloride-potassium symporter KCC2 (encoded by *SLC12A5*), which raise and lower intracellular chloride levels, respectively. As $GABA_A$ receptors selectively conduct chloride ions, the excitatory or inhibitory nature of GABA acting on these receptors in SCN neurons therefore depends on the level of intracellular chloride (Choi et al., 2008). Exogenous GABA acts through $GABA_A$ receptors to produce phase shifts (through acute application) or synchronization (through daily application) in dissociated SCN neurons (Liu and Reppert, 2000). However, Aton and colleagues found that pharmacologically blocking both $GABA_A$ and $GABA_B$ receptors did not affect the synchrony of *Per1-luc* rhythms in SCN slices, and, surprisingly, improved the stability and precision of PER2::LUC rhythms in dissociated SCN neurons (Aton et al., 2006). Therefore these results demonstrate that GABA is sufficient, but not necessary, for synchrony and neural coupling within the SCN. Other presumed coupling factors within the core of the SCN include GRP, which can produce phase shifts in firing rate rhythms in wild-type SCN neurons and synchronize asynchronous *Per1-luc* rhythms in *Vipr2*$^{-/-}$ SCN slices (Maywood et al., 2006), and neurotensin, which can also produce phase shifts in firing rate rhythms in the SCN (Meyer-Spasche et al., 2002).

Although VIP is produced solely within the ventrolateral core of the SCN, the VPAC2 receptor to which it binds is expressed throughout the SCN, and the SCN shell receives dense projections from the core (Mohawk and Takahashi, 2011). Thus, rhythmic VIP release and synaptic connections from the SCN core serve to synchronize asynchronous rhythms within both the core and the shell regions of the SCN. Indeed, as light information, and thus a mechanism by which the internal circadian oscillator is entrained to the outside world, is transmitted exclusively into the retinorecipient core, it is perhaps unsurprising that core coupling factors mediate synchrony both within and outside the core itself. VIPergic core neurons synchronize the core SCN through ipsilateral projections within the core of one SCN hemisphere and through contralateral projections to the core of the other hemisphere; similarly, AVPergic shell neurons project both ipsilaterally and contralaterally. However, there are few, if any, reciprocal connections from the shell region of the SCN back onto the core (Moore, 2013). The influence that AVPergic neurons in the shell have on SCN network function is not fully understood. AVP within the SCN acts upon vasopressin receptors 1a and 1b (V1a and V1b; encoded by *Avpr1a* and *Avpr1b*, respectively). Although *Avpr1a* mRNA is rhythmically expressed within the SCN, neither exogenous application of AVP nor the pharmacological blockade of V1a and V1b receptors has apparently any effect on circadian gene expression (Watanabe et al., 2000). Instead, AVP and its receptors seem to play a modulatory role within the SCN. Maywood and colleagues demonstrated that pharmacologically blocking V1a and V1b receptors in cultured SCN slices from both *Vipr2*$^{-/-}$ and VIP$^{-/-}$ mice prevented a long-term restoration of dampened PER2::LUC bioluminescence rhythms (Maywood et al., 2011). Likewise, Yoshiaki Yamaguchi and colleagues showed that *Per1-luc* rhythms from V1a$^{-/-}$; V1b$^{-/-}$ double knockout mice rapidly entrain in response to a phase shift induced by cycloheximide; as such, AVP-mediated communication through these receptors within the SCN appears to be critical to resisting external perturbations to the system (Yamaguchi et al., 2013). SCN slices from V1a$^{-/-}$ mice also show attenuated rhythms of *prokineticin 2* (*PK2*) mRNA, which codes for a key output component of the SCN (Li et al., 2009); thus, AVP may modulate SCN output onto other brain areas as well as contributing to circadian robustness within the SCN itself.

1.5: Outputs of the SCN

Through its interconnected network of single-cell molecular and neuronal oscillators, the SCN is able to produce a coherent, synchronized rhythm of electrical activity and neuropeptide release. The state of the network (that is, the phase or period of the oscillator) is able to be altered by light input onto the system through the retinohypothalamic tract (see **Section 1.4**). Similarly, the network can be modulated by non-photic inputs from the geniculohypothalamic tract, which projects from the intergeniculate leaflet of the thalamus to release neuropeptide Y and GABA onto the SCN, and by serotinergic (5-hydroxytryptamine, 5-HT) projections from the medial and dorsal

raphe nucleus (Abrahamson and Moore, 2001). However, for the SCN to influence behavior and physiology as the body's pacemaker, its phase and period must be communicated to the rest of the body. To do this, the SCN releases the neurotransmitter GABA and a variety of neuropeptides from both the core and shell regions onto downstream targets. Whereas GABA is released from both the core and shell, particular output neuropeptides are released from each SCN region: those released from the core include VIP, GRP, and TGF-α (transforming growth factor α), and those released from the shell include AVP, PK2, and CLC (cardiotrophin-like cytokine; **Fig. I-4;** Li et al., 2012).

Neurons in the SCN exhibit a circadian rhythm in AVP levels that is mirrored by the observed rhythm of AVP concentration within the cerebrospinal fluid, suggesting that AVP released by the SCN has widespread effects throughout the brain. In 2004, Ehab Tousson and Hilmar Meissl demonstrated that AVP is a key output factor of the SCN by using multielectrode arrays to record from acute and organotypic hypothalamic slices (Tousson and Meissl, 2004). They found spontaneous firing rate rhythms within not only the SCN, but also the surrounding hypothalamus. Spontaneous firing rate in structures outside the SCN became arrhythmic when the SCN was ablated, but reemerged in the presence of an SCN graft, which suggested that a humoral factor released by the SCN (but not synaptic connectivity) was necessary for the persistence of extra-SCN firing rate rhythms. Importantly, the ability of an SCN graft to restore firing rate rhythms outside the SCN in an SCN-lesioned slice was prevented by an AVP receptor antagonist and periodic application of exogenous AVP could restore firing rate rhythms outside the SCN independently of a graft. Thus, release of AVP from the SCN is able to modulate extra-SCN firing rate and, presumably, downstream behavior and physiology. *In vivo* infusion of AVP or an AVP receptor antagonist into the SCN of hamsters or rats, respectively, did not have any apparent effect on circadian locomotor activity (Albers et al., 1984). AVP does, however, seem to play a role in hormonal release in general and in the release of corticosterone in particular, as the infusion of AVP is able to suppress the increase in corticosterone levels found in SCN-lesioned rats, and infusion of an V1 receptor antagonist causes elevated corticosterone levels in animals with an intact SCN (Kalsbeek et al., 1996).

mRNA levels of another putative output factor of the SCN, PK2, have been shown to be rhythmic by a number of methods, which suggests that *PK2* is a clock-controlled gene (Zhang et al., 2009). In fact, the same BMAL1/CLOCK heterodimer that activates *Per* and *Cry* transcription (see **Section 1.2**) also binds to E-box elements in the promoter region of *PK2*, and *PK2* mRNA rhythms are absent in $Clock^{-/-}$ and $Cry^{-/-}$ mice (which have a disrupted molecular clock; Cheng et al., 2002). PK2 itself appears to have a direct effect on the circadian rhythmicity of many behaviors and physiological functions. Infusing PK2 into the lateral ventricle of rats during the night phase of the circadian cycle when PK2 levels are normally low inhibits locomotor activity rhythms. Even more strikingly, in 2006,

Jia-Da Li and colleagues demonstrated that knocking out PK2 in *PK2*$^{-/-}$ mice resulted in a significant disruption of circadian rhythms in a variety of ostensibly SCN-driven behavioral and physiological outputs, including rhythms in locomotor activity, sleep/wake, body temperature, and plasma glucocorticoid levels (Li et al., 2006). Other studies have shown that knocking out the prokineticin 2 receptor (PKR2) in *PKR2*$^{-/-}$ mice also disrupts circadian rhythms in locomotor activity and thermoregulation, suggesting that PK2 (and its receptor) are necessary for a coherent circadian output from the SCN (Prosser et al., 2007).

In 2001, the laboratory of Charles Weitz reported that TGF-α was a putative SCN output molecule that could influence circadian behavior (Kramer et al., 2001). When TGF-α was infused into the third ventricle of mice, it reversibly inhibited locomotor activity and disrupted normal sleep/wake rhythms. mRNA levels of TGF-α in the SCN are rhythmic, exhibiting maximal levels in the early day phase of the circadian cycle (around circadian time [CT] 3) and minimal levels around subjective dusk. However, later studies did not find a circadian rhythm in protein levels of TGF-α in the SCN of hamsters (Lindley et al., 2008). Similarly to TGF-α, CLC is rhythmically expressed in the SCN, with a peak occurring during the late day phase of the circadian cycle (around CT 9), and has been implicated as a key circadian regulator of locomotor activity (Kraves and Weitz, 2006). In 2006, Weitz and colleagues demonstrated that an acute infusion of CLC into the third ventricle of mice reversibly disrupts circadian rhythms in locomotor activity, while infusion of neutralizing antibodies against GP130, the receptor for CLC, reversibly increases locomotor activity during the day (when CLC is maximally expressed). Thus, both TGF-α and CLC act as inhibitory output signals of the SCN for locomotor activity; however, their role in other clock-controlled behaviors is unknown.

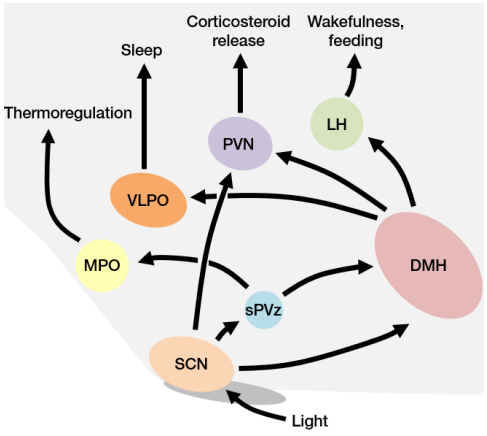

Figure I-5 Outputs of the suprachiasmatic nucleus.

The SCN directly synapses onto the subparaventricular zone (sPVz), the paraventricular nucleus (PVN), and the dorsomedial hypothalamus (DMH). These areas in turn are connected to other hypothalamic and thalamic nuclei including the medial preoptic area (MPO), the ventrolateral preoptic nucleus (VLPO), and the lateral hypothalamus (LH) to regulate circadian rhythms in behavior and physiology.

Surprisingly, the SCN does not form widespread synaptic connections throughout the brain (Saper et al., 2005). The SCN instead projects monosynaptically to a relatively small number of hypothalamic and thalamic nuclei, with the majority of its projections synapsing in the dorsal and ventral subparaventricular zone (sPVz), the dorsomedial hypothalamus (DMH), and the paraventricular nucleus of the thalamus (PVN; **Fig. I-5**). A number of additional sparse connections from the SCN to the bed nucleus of the stria terminalis, lateral septum, arcuate nucleus, amygdala, and habenula have also been identified neuroanatomically (Abrahamson and Moore, 2001). Importantly, the limited connectivity of the SCN may partially explain the differences between nocturnal and diurnal animals. Rhythms of both firing rate and clock gene expression within the SCN are similar in nocturnal and diurnal animals (with each exhibiting a peak in firing rate and in *Per* expression during the day phase of the circadian cycle), which suggests that the difference between the activity periods of these animals must be due to differences in downstream brain regions. However, surprisingly, the overall distribution of efferent projections from the SCN does not seem to significantly differ between nocturnal and diurnal animals (Saper et al., 2005b). Lesion studies have identified that relay neurons in the dorsal and ventral sPVz appear to be necessary for sustained circadian rhythms in sleep and wakefulness and locomotor activity or body temperature rhythms, respectively. Thus, the SCN must project to relay neurons within the sPVz to control these aspects of behavior and physiology. Major targets of the sPVz include the DMH and the medial preoptic area (MPO). Although the SCN projects directly to the DMH, there are many more connections from the sPVz to the DMH, which suggests that the sPVz modulates the

connection between the SCN and DMH. Consequently, DMH lesions greatly diminish or abolish circadian rhythms in sleep and wakefulness, feeding, locomotor activity, and corticosteroid release (Chou et al., 2003). The MPO, on the other hand, receives circadian information through the sPVz to modulate rhythms in body temperature. Corticosteroid and melatonin release from the PVN are under circadian control through projections from the SCN itself and from those through the DMH (through the sPVz). Finally, sleep and wakefulness, which is perhaps the aspect of mammalian behavior and physiology that is most obviously under circadian regulation, is controlled by neurons in the ventrolateral preoptic nucleus (VLPO) and the lateral hypothalamus (LH), respectively (Saper et al., 2005b). However, the interplay between the so-called sleep homeostat – the VLPO and LH – and circadian drive from the SCN in the regulation of sleep and wakefulness is not completely understood.

In this chapter, I have elaborated on the individual components of the multi-component circadian system, from the molecular clock and electrical activity rhythms in individual SCN neurons to the SCN network and its control of circadian behavior and physiology. However, for these individual components to come together as a coherent circadian oscillator, there must be connections or links between them. In **Chapter II**, I briefly introduce our current knowledge of the interrelationship between both circadian electrical activity and the molecular clockworks and circadian electrical activity and behavior and physiology. I follow this with my own research investigating this relationship entitled "Manipulating circadian clock neuron firing rate resets molecular circadian rhythms and behavior." In **Chapter III**, I subsequently introduce our current knowledge of the link between the molecular clock and circadian electrical activity and present my own research on the link between them entitled "The core clock gene *Per1* links molecular and electrical circadian rhythms." Finally, in **Chapter IV**, I conclude by describing how my dissertation research advances the field of circadian neurobiology and how my research has the potential to, in the future, positively impact human health, and I introduce a number of pilot experiments I have performed and future experiments expanding upon my dissertation work that directly follow from them.

CHAPTER II

Linking electrical activity rhythms to the molecular clockworks and behavior

2.1: Evidence for a relationship between electrical activity rhythms and the molecular clockworks and circadian behavior and physiology

Although the step-by-step depiction of the multi-component circadian oscillator presented in **Chapter I** suggests that rhythmic electrical activity is driven by, or solely an output of, the molecular clockworks (and indeed, I explore this directional relationship in depth in **Chapter III**), there have been a number of studies suggesting that electrical activity in the SCN may actually feedback onto or even drive circadian gene expression rhythms.

This somewhat unintuitive relationship between these two components of the circadian system was first discovered in 2002 by Michael Nitabach and colleagues using the circadian system of *Drosophila* (Nitabach et al., 2002). As mentioned in **Section 1.2**, a subset of pacemaker neurons in the *Drosophila* brain exhibit circadian rhythms in clock gene expression; these neurons, like those of the mammalian SCN, also exhibit electrical activity rhythms. Nitabach and colleagues used a targeted reverse genetic approach to introduce a modified *Drosophila* open rectifier potassium channel (dORK channel, encoded by *Ork1*) or the mammalian inward rectifying potassium channel $K_{ir}2.1$ (encoded by *Kcnj2*) specifically to the lateral pacemaker neurons (LN_vs) of *Drosophila*. dORK channels, which act as a constitutively open, potassium selective "leak" channel, and $K_{ir}2.1$ channels, which have a high open probability at the resting membrane potential, act to hyperpolarize neurons by decreasing their input resistance and driving their resting membrane potential towards the hyperpolarized equilibrium potential for potassium (**See Section 1.3**). Thus, the genetic targeting of these channels to LN_v neurons can be used to specifically "silence" circadian electrical activity both *in vitro* and *in vivo*. As expected, electrically silencing these *Drosophila* pacemaking neurons causes the animal's normal circadian rhythms in locomotor activity to become arrhythmic. Surprisingly, abolishing circadian electrical activity also stops the free-running rhythms of PERIOD (PER) and TIMELESS, two of the core clock proteins in the *Drosophila* circadian system. These results and other similar experiments performed by Nitabach and colleagues demonstrate that, at least in *Drosophila*, electrical activity rhythms are necessary inputs onto the molecular clockworks (Nitabach et al., 2006). However, when $K_{ir}2.1$ channels are conditionally expressed in the pacemaker neurons of adult *Drosophila*, the rhythmicity of PER is not severely affected even though behavioral rhythms are impaired (Depetris-Chauvin et al., 2011). Thus, the exact relationship between circadian electrical activity and the molecular clockworks in *Drosophila* remains unclear.

Whether circadian electrical activity could "feed back" onto the molecular clockworks in the mammalian SCN was first investigated in 2005 by Shun Yamaguchi and colleagues, who used cultured *Per1-luc* SCN slices to observe the molecular clock state (as read out by bioluminescence) in individual neurons over multiple days (Yamaguchi et al., 2003). Bioluminescence was recorded from neurons in these slices for at least two circadian cycles, after which the voltage-gated sodium channel blocker TTX was applied to the slice to block action potentials. Chronic application of TTX caused a dramatic reduction in the amplitude of the single-cell bioluminescence rhythms that progressively dampened over time, and this reduction in bioluminescence amplitude occurred in parallel with a reduction in *Per1* and *Per2* mRNA and PER1 and PER2 protein during both the day and night phase of the circadian cycle. After seven days of continuous treatment, the TTX was washed out of the slice and, surprisingly, the amplitudes of the single-cell bioluminescence rhythms immediately returned to their pre-treatment levels. Importantly, on the third day after TTX washout, the peak times of bioluminescence in individual SCN neurons were highly correlated with the peak times prior to TTX application, which suggests that the neurons remained in phase even in the absence of electrical activity feedback from the membrane. A closer look at the data however suggests that the phase relationships between individual neurons is not completely preserved in the first one to two days after TTX washout. One caveat to these results is that while the concentration of TTX used in these experiments was, according to Yamaguchi and colleagues, sufficient to inhibit action potential generation without affecting membrane potential, potassium current, or the sodium-potassium ATPase, other studies have shown that TTX causes acute membrane depolarization in a subset of SCN neurons (Colwell, 2011).

Although the results by Yamaguchi and colleagues suggested that the molecular clockworks continues "ticking" even in the absence of circadian electrical activity, in 2009, Alexis Webb and colleagues more closely investigated the effects of TTX on the molecular clockworks as read out by single-cell bioluminescence in cultured PER2::LUC SCN slices (Webb et al., 2009). Each SCN neuron showed a significant decrease in bioluminescence amplitude, as expected. However, unexpectedly, only about 13% of recorded neurons maintained rhythmicity throughout two six-day TTX treatments interspaced by a six-day washout period. Conversely, 50% of recorded neurons became arrhythmic during TTX treatment and nearly 38% of recorded neurons either gained or lost bioluminescence rhythmicity during the second TTX treatment period. Thus, in these experiments, TTX actually stops the molecular clockworks in a subset of SCN neurons, but again, TTX may have nonspecific effects on membrane electrical activity beyond its role in blocking voltage-gated sodium channels. Gabriella Lundkvist and colleagues addressed this issue by using *Per1-luc* SCN slices cultured in extracellular medium containing 0 mM potassium, which hyperpolarizes neurons and therefore prevents them from firing action potentials without directly blocking voltage-gated ion channels (Lundkvist et al., 2005). Experimental slices that were initially cultured in this 0 mM potassium medium did not

exhibit any *Per1* rhythmicity as read out by bioluminescence. The slices were kept in the hyperpolarizing medium for either 18, 24, or 30 hours, after which the medium was switched to control extracellular medium. Bioluminescence rhythms were restored in control medium; however, the rhythms were six hours out of phase from one another (that is, rhythmicity in the slices kept in hyperpolarizing medium for 18, 24, or 30 hours reemerged with peak times occurring at 24, 30, or 36 hours in culture), which suggests that the molecular clockworks itself was stopped when the SCN was hyperpolarized.

While the link between circadian electrical activity and the molecular clockworks is perhaps more unintuitive, our current knowledge of precisely how electrical activity rhythms in general and firing rate rhythms in particular within the SCN influence circadian outputs in behavior and physiology (see **Section 1.5**) also remains unclear. In 1987, William Schwartz and colleagues investigated whether circadian electrical activity was necessary for the SCN to keep accurate time *in vivo* by continuously infusing either artificial cerebrospinal fluid (aCSF) or TTX into the SCN of control or experimental rats, respectively, and measuring their drinking activity rhythms (Schwartz et al., 1987). Prior to infusion, both control and experimental rats exhibited free-running drinking rhythms over multiple days, as expected. During the time of infusion, the control, aCSF-infused animals continued to exhibit free-running drinking rhythms. However, the drinking rhythms of the experimental, TTX-infused animals quickly became arrhythmic for the duration of the TTX infusion. When the infusion stopped (and TTX was allowed to wash out of the system), the free-running drinking rhythms of the experimental rats reemerged with a phase predicted from their prior free-running rhythms, suggesting that the circadian pacemaker in the SCN continued to run even though its electrical activity output, and thus its communication to the rest of the brain, was suppressed. However, later experiments by Schwartz demonstrated that depolarizing the SCN by the *in vivo* infusion of high potassium aCSF or of veratridine, a neurotoxin that depolarizes the membrane by blocking the inactivation of voltage-gated sodium channels, is able to phase shift drinking activity rhythms in rats (Schwartz, 1991). Thus, membrane depolarization (but not sodium-dependent action potentials *per se*) appears to directly influence the molecular clockworks and, subsequently, their downstream behavioral output *in vivo*.

In 2006, Andrea Meredith and colleagues investigated the role of particular ion channels involved in circadian rhythms in electrical activity and their behavioral and physiological outputs (Meredith et al., 2006). *Kcnma1*$^{-/-}$ mice, in which the gene encoding the BK calcium-activated is knocked out, exhibit disrupted firing rate rhythms (see **Section 1.3**). Importantly, these mice also exhibit a variety of pacemaker-directed behavioral and physiological deficits, including a severe reduction in the robustness of locomotor activity and body temperature rhythms. Meredith and colleagues later found that transgenically expressing a modified BK channel under the control of the *Per1* promoter so that BK conductance is active throughout the entire circadian cycle (when it is normally only active

during the subjective night) causes similar deficits in locomotor activity rhythms (Montgomery et al., 2013). Finally, in 2011, Takashi Kudo and colleagues identified yet another ion channel necessary for the persistence of coherent locomotor activity rhythms, the fast-delayed rectifier (FDR) potassium channel (Kudo et al., 2011). *Kcnc1*$^{-/-}$; *Kcnc2*$^{-/-}$ double knockout mice, which do not express the FDR potassium channels Kv3.1 or Kv3.2, exhibited extremely disrupted rhythms in locomotor activity, both during a light cycle and under constant darkness. Intriguingly, even though both locomotor and electrical activity rhythms are disrupted in the absence of Kv3.1 and Kv3.2, PER2 protein expression remains rhythmic, suggesting that the molecular clockworks continues to run even in these electrically- and behaviorally-compromised animals.

Undoubtedly, the relationship between electrical activity rhythms and the molecular clockworks and between electrical activity rhythms and behavior remains ambiguous. Is artificially inducing or suppressing firing rate in SCN neurons sufficient to start or stop, respectively, circadian rhythms in gene expression, or is firing rate solely an output of the molecular clockworks? Is altering firing rate *per se* sufficient to entrain circadian behavior? A major hurdle that has hindered the examination of these relationships is the lack of methods to accurately and precisely manipulate firing rate in SCN neurons without confounding ionic or pharmacological stimuli. In **Section 2.2**, I address these questions through a combination of SCN-directed *ex vivo* and *in vivo* optogenetic manipulation of firing rate, real-time PER2::LUC bioluminescence imaging, and locomotor activity monitoring, and conclude that firing rate is fundamental to mammalian circadian pacemaking as both an input onto and an output of the molecular clockworks.

2.2: Manipulating circadian clock neuron firing rate resets molecular circadian rhythms and behavior

Jeff R. Jones[1], Michael C. Tackenberg[1], Douglas G. McMahon[1,2]

[1]Neuroscience Graduate Program, [2]Department of Biological Sciences, Vanderbilt University, Nashville, TN

Adapted from Jones, J.R., Tackenberg, M.C. & McMahon, D.G. Manipulating circadian clock neuron firing rate resets molecular circadian rhythms and behavior. *Nat. Neurosci.* 10.1038/nn.3937 (2015).

Abstract

To examine the interaction between molecular, electrical, and behavioral circadian rhythms, we combined optogenetic manipulation of suprachiasmatic nucleus (SCN) firing rate with bioluminescence imaging and locomotor activity monitoring. Manipulating firing rate reset circadian rhythms both *ex vivo* and *in vivo* and this resetting required spikes and network communication. This suggests that SCN firing rate is fundamental to circadian pacemaking as both an input onto and output of the molecular clockworks.

Introduction

The brain's circadian clock – the suprachiasmatic nucleus (SCN) – provides a unique model for studying the interaction between gene networks and behavior. The individual cellular oscillators that comprise the SCN network exhibit endogenous molecular and electrical rhythms. Additionally, a collection of intrinsic currents allows these neurons to fire action potentials in the absence of synaptic drive and, importantly, fire at elevated frequency (up to 8–12 Hz) during the day while being nearly silent at night (typically <1 Hz; Kuhlman and McMahon, 2006; Colwell, 2011). Network communication by the neuropeptides vasoactive intestinal peptide (VIP), arginine vasopressin (AVP), and the neurotransmitter GABA allow these oscillators to form a tissue-level clock, orchestrating daily changes in physiology and behavior (Welsh et al., 2010; Brancaccio et al., 2013; Freeman et al., 2013; Kudo et al., 2013). Thus interlocking molecular and electrical loops in the SCN interact to drive behavior; however, the precise interplay of these molecular, electrical, and behavioral components of the brain's biological clock remains unknown (Schwartz et al., 1987; Welsh et al., 1995; Herzog et al., 1998; Nitabach et al., 2002; Kuhlman et al., 2003; Yamaguchi et al., 2003).

The inability to precisely manipulate firing rate in SCN neurons without confounding ionic or pharmacological stimuli has hindered the examination of these relationships. To address this problem, we used SCN-directed expression of the optogenetic constructs channelrhodopsin (ChR2) and halorhodopsin (NpHR) to drive or inhibit SCN neuron firing rate, respectively, both *ex vivo* and *in vivo*. Here we show that optogenetic induction or suppression of firing rate within SCN neurons is sufficient to reset the phase and alter the period of the molecular clockworks, that this resetting requires action potentials and VIPergic network communication, and that *in vivo* optogenetic stimulation of the SCN synchronizes behavioral rhythms. We therefore conclude that SCN firing rate is a key component in circadian rhythmicity and entrainment, rather than solely an output of the molecular clock.

Materials and Methods

Animals

Drd1a-Cre (B6.FVB(Cg)-Tg(*Drd1a*-Cre)EY266Gsat/Mmucd, GENSAT; Supplementary Fig. 1) mice were crossed with Cre-dependent ChR2 (Ai27D, B6.Cg-Gt(ROSA)26Sortm27.1(CAG-COP4*H134R/tdTomato)Hze/J, Jackson Laboratories) or NpHR (Ai39, B6;129S-Gt(ROSA)26Sortm39(CAG-hop-/EYFP)Hze/J, Jackson Laboratories) mice to yield *Drd1a*-ChR2 or *Drd1a*-NpHR mice. A subset of *Drd1a*-ChR2 and *Drd1a*-NpHR mice were crossed with PER2::LUC mice (Yoo et al., 2004) congenic on a C57BL/6J background to yield *Drd1a*-ChR2 x PER2::LUC mice or *Drd1a*-NpHR x PER2::LUC mice. All animals used (males and females; no obvious differences were observed between sexes) were ~1–3 months of age, housed in a temperature- and humidity-controlled facility (~22ºC, ~40% humidity) in single-sexed cages of no more than five animals from weaning until experimental use on a 12:12 light/dark (LD; light intensity ~300 lux) cycle, and were provided with food and water *ad libitum*. All animal care and experiments were conducted in concordance with Vanderbilt University's Institutional Animal Care and Use Committee guidelines.

Immunohistochemistry

Drd1a-ChR2 mice were administered a single injection of colchicine (2.5 mM; Sigma, St. Louis, MO) in the lateral ventricle. ~24 hours later, colchicine-injected mice were deeply anesthetized and transcardially perfused with 4% (w/v) paraformaldehyde (PFA; Sigma). Brains were removed and post-fixed with 4% PFA overnight, and cryoprotected in 20% sucrose in PBS. A cryostat was used to obtain 40 µm coronal slices containing the SCN. Slices were then labeled for AVP using rabbit polyclonal anti-vasopressin (1:5000, ab1565, Millipore, Billerica, MA) or VIP using rabbit polyclonal anti-VIP (1:2500, ab43841, Abcam, Cambridge, MA). For cFos experiments, membrane-attached organotypic SCN cultures were fixed for 1 hour in 4% PFA post-ChR2 stimulation and labeled for cFos using rabbit polyclonal anti-cFos (1:1000, ab7963, Abcam). For visualization, slices were incubated with Alexa Fluor 488 goat anti-rabbit IgG (1:500, Invitrogen). Slices were examined under a confocal microscope (LSM510; Zeiss; Thornwood, NY) at 488 nm for Alexa Fluor 488 and 543 nm for ChR2-tdTomato. Colocalization of *Drd1a*-ChR2 and AVP or VIP was determined manually using ImageJ and was defined as an AVP or VIP-positive (i.e., green fluorescent) neuron completely surrounded by red tdTomato membrane-bound fluorescence. ImageJ was also used to perform manual quantification of cFos-positive cell numbers.

Slice preparation and electrophysiological recording

Brains were removed and blocked in cold, oxygenated 95% O_2–5% CO_2 dissecting solution (in mM: 114.5 NaCl, 3.5 KCl, 1 NaH_2PO_4, 1.3 $MgSO_4$, 2.5 $CaCl_2$, 10 D-glucose, and 35.7 $NaCHO_3$). SCN slices (200 µm) were cut on a vibroslicer (WPI, Sarasota, FL) at 4–10°C and transferred directly to an open recording chamber continually superfused with warmed (35 ± 0.5°C) extracellular solution (in mM: 124 NaCl, 3.5 KCl, 1 NaH_2PO_4, 1.3 $MgSO_4$, 2.5 $CaCl_2$, 10 D-glucose, and 26 $NaCHO_3$). Slices were allowed to recover for 1 hour before recording. SCN neurons were visualized using a Leica DMLFS microscope (Leica Microsystems, Buffalo Grove, IL) equipped with near-infrared (IR)-differential interference contrast and fluorescence optics. For cell-attached recordings, patch electrodes (4-6 MΩ) pulled from glass capillaries (WPI) on a multistage puller (DMZ; Zeitz, Martinsried, Germany) were filled with extracellular solution. For whole-cell current-clamp recordings, patch electrodes (8–10 MΩ) were filled with intracellular solution containing, in mM, 135 K-Gluconate, 10 KCl, 10 HEPES, 0.5 EGTA, and 2 mM $MgCl_2$. Recordings were obtained with an Axopatch 200B amplifier (Molecular Devices, Sunnyvale, CA) and monitored online with pClamp 10.0 software (Molecular Devices). Slices were subjected to pulsed blue light (470 nm; 8 Hz; 10 ms duration) from a mounted high-power LED (Thorlabs, Newton, NJ) controlled by a Grass SD-9 stimulus generator (Grass Technologies, Warwick, RI) or continuous yellow light (590 nm) from a mounted high-power LED (Thorlabs). In some experiments, superfused extracellular solution was switched to extracellular solution containing 0.5 µM tetrodotoxin (TTX; Sigma) after 1–2 minutes of whole-cell current clamp recording.

Ex vivo culture and PER2::LUC imaging

Brains from mice killed without anesthesia by cervical dislocation were removed and blocked in cold HBSS supplemented with 100 U/ml penicillin/streptomycin, 10 mM HEPES, and 4.5 mM sodium bicarbonate. Hypothalamic coronal slices (200 µm) containing the SCN were cut on a vibroslicer (WPI) at 4–10°C, trimmed to ~1.5 x 1.5 mm squares, and transferred directly to culture membranes (Millipore) in vacuum grease-sealed 35 mm culture dishes with recording media containing 1.0 ml of DMEM (D-2902; Sigma) supplemented with 3.5 g/L D-glucose, 10 mM HEPES, 25 U/ml penicillin/streptomycin, 2% B27, and 0.1 mM beetle luciferin (Promega, Madison, WI). Slice cultures containing the SCN were maintained in an incubator at 36.8°C. Bioluminescence was monitored in real time with a LumiCycle (Actimetrics). After a minimum of two cycles of bioluminescence recording, slice cultures were removed from the LumiCycle and, while still in the incubator, placed under a custom-built high-power LED array consisting of blue Cree XP-E or yellow Luxeon Rebel LEDs (LEDSupply, Randolph, VT) soldered to an 0.25" aluminum sheet heatsink and driven at 1000 mA using a LEDD1B high-powered LED driver (Thorlabs) and subjected to either pulsed blue

light (470 nm; 8 Hz; 10 ms duration) controlled by a Grass SD-9 stimulus generator (Grass Technologies, Warwick, RI) or continuous yellow light (590 nm) for 1 hour. Light intensity inside the 35 mm culture dish was determined to be 20.1 mW ± 0.5 mW (470 nm LEDs) or 16.27 mW ± 0.3 mW (590 nm LEDs) when driven at 1000 mA using a PM100D Optical Power Meter (Thorlabs). Control unstimulated slices were instead removed from the LumiCycle and kept in the incubator for an equivalent time without stimulation. Slice temperature before and after stimulation was measured with an infrared thermometer (Fluke, Norwich, UK) and was determined to not change (± 0.1°C) after stimulation (data not shown). Slice cultures were then returned to the LumiCycle and bioluminescence was recorded for at least two additional cycles; data were excluded if bioluminescence did not persist for at least five total cycles.

Pharmacological manipulation of PER2::LUC cultures

For some experiments, slices were cultured and recorded as above, but when they were removed from the incubator, slice cultures were either transferred to pre-warmed fresh recording media, fresh recording media containing 0.5 µM TTX, or fresh recording media containing 1 µM [D-p-Cl-Phe^{6},Leu^{17}]-VIP (Tocris cat. no. 3045; Bristol, UK). TTX concentration was selected from Brancaccio et al., 2013 and Kudo et al., 2013; [D-p-Cl-Phe^{6},Leu^{17}]-VIP concentration was based on values from Atkins et al., 2010 and Evans et al., 2013. The original recording media was sealed in its culture dish and kept warm inside the incubator. Slice cultures were then kept in the incubator without stimulation for 1 hour, or stimulated as above; after which all slice cultures were rinsed, transferred to their original recording media, resealed with vacuum grease, and returned to the LumiCycle for further bioluminescence recording.

In vivo optogenetic stimulation and locomotor activity monitoring

Anesthetized mice (100 mg/kg ketamine, 10 mg/kg xylazine) were placed into a stereotaxic device and implanted with a fiber optic cannula (5 mm in length, 400 µm diameter core, 0.39 NA; Thorlabs) sheathed to prevent light leak. The cannula was targeted to the SCN using the coordinates of +0.0 mm anterior and +0.0 mm lateral to bregma. After at least three days of recovery, mice were placed individually into litter-filled cages equipped with an IR motion detector (Spy2, Visonic, Tel Aviv, Israel) inside light-tight boxes, and food and water was provided *ad libitum*. Animals were chronically tethered to a fiber optic cable (400 µm diameter core, 0.39 NA; Thorlabs) attached to the implanted cannula and connected to a high-powered blue (470 nm) LED (Thorlabs) under the control of a LED driver (DC4100; Thorlabs). Mice were kept in constant darkness (DD) and allowed to free-run for at least four days before stimulation. Locomotor activity was monitored in 5 minute bins using ClockLab software (Actimetrics, Evanston, IL). Light pulses (470 nm; 8 Hz; 10 ms duration; 1 hour) were generated at various circadian

times (CTs), where CT 12 is defined as the start of locomotor activity, by a Grass SD-9 stimulus generator attached to the LED driver under the control of a light timer, and repeated daily at the same clock time. Light intensity at the cannula tip was determined to be 10.9 mW ± 0.1 mW when driven at 1000 mA using a PM100D Optical Power Meter (Thorlabs). Calculated irradiances (Yizhar et al., 2011), along with the estimated ChR2 activation threshold (Aravanis et al., 2007) are shown in **Fig. II-8**. Animals were excluded from analysis if they did not successfully free-run in DD during the four days after surgery but before stimulation.

PER2::LUC data analysis

Sample sizes were chosen so as to be sufficient for statistical analysis based upon previous publications detailing similar measurements both *in vivo* and *in vitro* (Gamble et al., 2007; Ruan et al., 2008, 2012). Data analysis was performed blind to genotype, while there were no methods to randomize mice to experimental groups or to blind investigators to genotype for the duration of the experiment. Baseline subtracted bioluminescence data were obtained using a 24 hour running average from the raw data using LumiCycle data analysis software (Actimetrics). Subtracted bioluminescence data were then loaded into Matlab (Mathworks, Natick, MA) for further analysis. Data were smoothed using a Loess local regression filter and a damped sine wave was fit from the beginning of the smoothed data until the time of manipulation. The damped sine wave was then extrapolated past the time of manipulation in order to project the timing of the undisturbed rhythm. Phase shifts were determined by calculating the mean difference in the post-manipulation peaks and troughs of the actual rhythms and the extrapolated unstimulated rhythms on the first and second cycles after stimulation. Period changes were calculated in ClockLab analysis software (Actimetrics) by measuring the best fit line through the calculated acrophases before and after stimulation. For data visualization, smoothed baseline-subtracted bioluminescence rhythms were depicted as double-plotted actograms created using Matlab. CT 12 was defined as the peak of PER2::LUC bioluminescence.

In vivo data analysis

Sample sizes were chosen so as to be sufficient for statistical analysis based upon previous publications detailing similar measurements both *in vivo* and *in vitro* (Gamble et al., 2007; Ruan et al., 2008, 2012). Data analysis was performed blind to genotype, while there were no methods to randomize mice to experimental groups or to blind investigators to genotype for the duration of the experiment. A best fit line was drawn between the times of activity onset until the time at which the change in time of activity onset was less than ± 0.1 hours a day (i.e., when the animal "locked on" to the stimulus) or until cessation of the stimulus (such as in the case of control actograms). If the animal "locked on" to the stimulus as defined above, a second best fit line was drawn between these times of activity

onset. The clock time of the best fit line(s) was then subtracted from the clock time of the daily optogenetic stimuli and the absolute value (i.e., activity onset in hours from time of stimulation) was plotted against days of stimulation for both ChR2+ and control animals.

Statistical analysis

All statistical analyses (Student's *t*-test, One-Way ANOVA, Tukey's HSD, Mann-Whitney *U*) were performed in Matlab, with α defined as 0.05. A Bartlett's multiple-sample test and a Kolmogorov-Smirnov test were used to confirm equal variance and normality. Curves were fit using Matlab's Curve Fitting Toolbox (Mathworks). Data are presented as means ± SEM.

A Supplementary Methods Checklist is available online at http://bit.ly/1DYjszq .

Results

To manipulate firing rate in the SCN, we generated mouse lines that expressed either ChR2 or NpHR under an SCN-directed Cre driver (dopamine receptor D1a; '*Drd1a*-ChR2' or '*Drd1a*-NpHR' mice) and confirmed transgene expression in the SCN using immunohistochemistry (Methods). Optogenetic constructs were highly expressed throughout the SCN in ~90% of AVP^+ and VIP^+ neurons, as well as a high proportion of AVP^-/VIP^- SCN neurons (**Figs. II-1** and **II-2**).

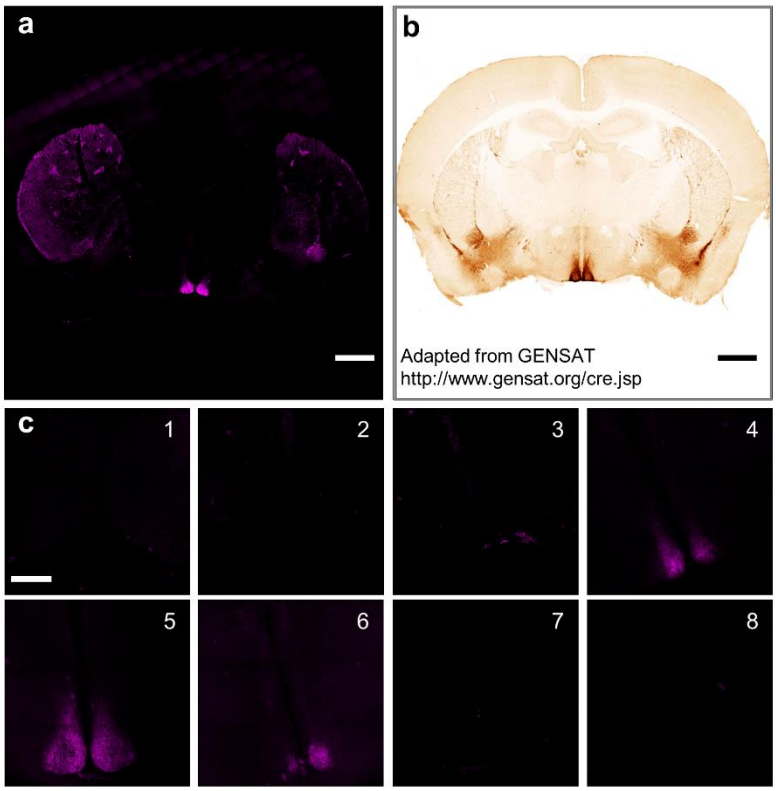

Figure II-1 *Drd1a*-Cre driven ChR2 expression in the SCN.

(**a**) Low-magnification image of a representative *Drd1a*-ChR2 brain slice (n = 2) showing endogenous tdTomato fluorescence (magenta). Note that *Drd1a*-ChR2 is expressed strongly in the SCN; it is also expressed in the striatum, but shows minimal expression in the rest of the section (notably absent along the midline); scale bar, 1 mm.

(**b**) Picture of a Drd1a-Cre brain section adapted from GENSAT's Cre database at http://www.gensat.org/cre.jsp; note that *Drd1a*-Cre (brown) shows a comparable expression pattern to our low-magnification representative *Drd1a*-ChR2 brain section shown in (**a**); scale bar, 1 mm.

(**c**) Representative 200 µm rostral-caudal serial sections of the SCN and hypothalamus (n = 2) from a *Drd1a*-ChR2 mouse showing endogenous tdTomato fluorescence (magenta); scale bar 300 µm.

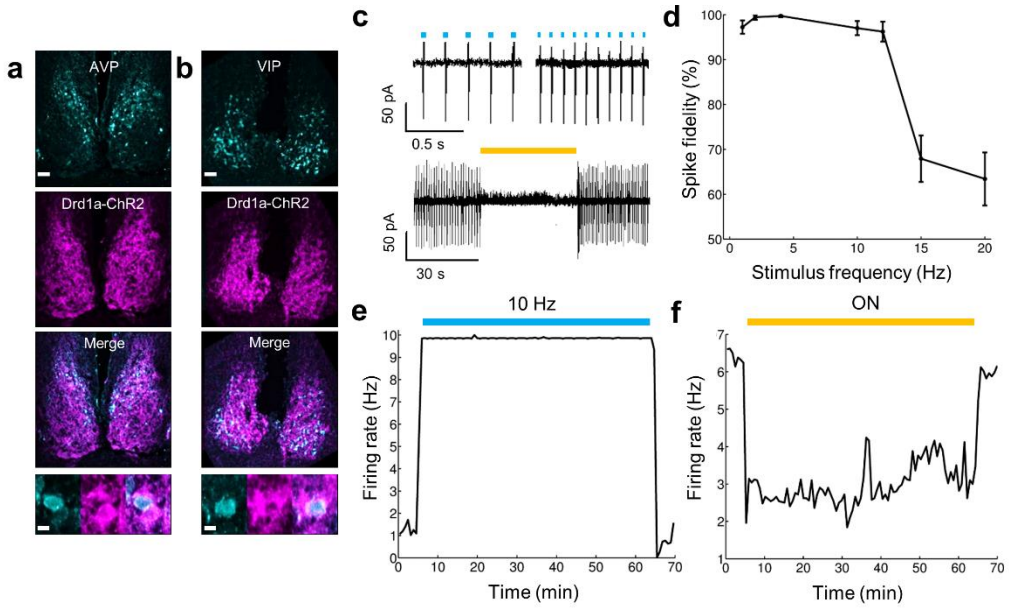

Figure II-2 *Drd1a*-driven optogenetic constructs are expressed in the SCN and can stimulate or inhibit SCN neurons.

(**a**) Immunohistochemical labeling of the SCN for AVP (cyan) and *Drd1a*-ChR2 (magenta); upper scale bar, 50 µm; lower scale bar, 5 µm; n = 5 slices.

(**b**) Immunohistochemical labeling of the SCN for VIP (cyan) and *Drd1a*-ChR2 (magenta); upper scale bar, 50 µm; lower scale bar, 5 µm; n = 5 slices. ChR2 is shown to be expressed across the SCN, with 93.71 ± 1.41% of AVP-positive neurons and 89.65 ± 2.31% of VIP-positive neurons colocalized with ChR2.

(**c**) Action potentials are generated by blue light stimulation in 92.68 ± 2.00% of *Drd1a*-ChR2 SCN neurons; n = 6 slices, 53 cells (top) and inhibited by yellow light in 84.21 ± 3.84% of *Drd1a*-NpHR SCN neurons; n = 5 slices, 37 cells (bottom).

(**d**) The percentage of stimulus pulses that generated action potentials in *Drd1a*-ChR2 SCN neurons in response to a train of blue light pulses is near-100% up to approximately 12 Hz; at higher stimulation frequencies, spike fidelity declines; n = 4 cells per frequency.

(**e**) Representative firing rate histogram showing that *Drd1a*-ChR2 neurons can be driven at 10 Hz for over an hour; after the conclusion of stimulation, firing rate returns to baseline; n = 3 cells.

(**f**) Representative firing rate histogram showing that *Drd1a*-NpHR neurons can be inhibited for over an hour; after the conclusion of inhibition, firing rate returns to baseline; n = 3 cells.

We were able to increase or decrease SCN neuron firing rate *in vitro* for an hour or more with appropriate light input (8 Hz 470 nm for *Drd1a*-ChR2 and continuous 590 nm for *Drd1a*-NpHR SCN neurons, respectively). Optogenetic stimulation of *ex vivo* SCN slices

from *Drd1a*-ChR2 mice at the typical daytime peak of spontaneous firing rate in SCN neurons (470 nm, 8 Hz, 1 hour) resulted in widespread cellular activation in the SCN, with ~90% of ChR2-expressing cells exhibiting gene activation as assayed by cFos immunohistochemistry (**Fig. II-3**).

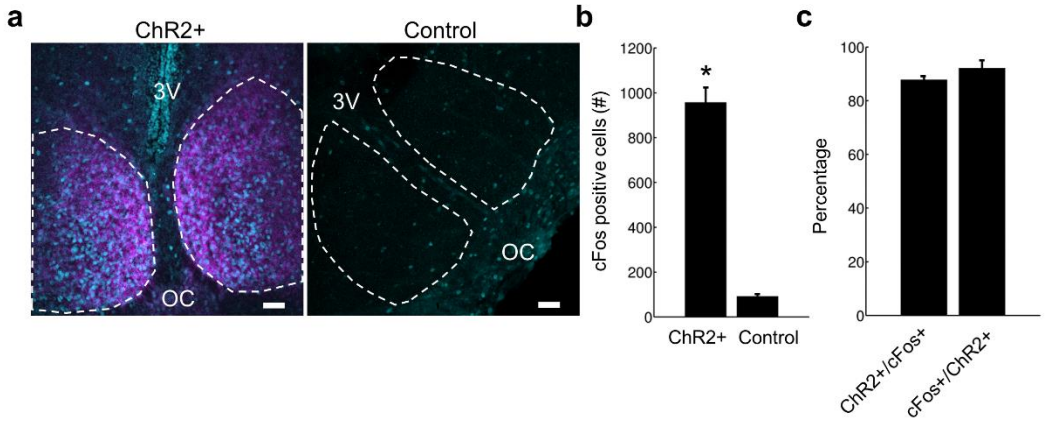

Figure II-3 Optogenetic stimulation of organotypic *Drd1a*-ChR2 SCN slices results in widespread cFos activation.

(**a**) (Left) Representative immunohistochemical labeling of ChR2+ SCN slices for cFos (cyan) and *Drd1a*-ChR2 (magenta); (Right) Representative immunohistochemical labeling of ChR2- (control) SCN slices for cFos (cyan); 3V = third ventricle; OC = optic chiasm; dashed white line = approximate outline of SCN as determined by *Drd1a*-ChR2 fluorescence (ChR2+) or cell density (ChR2-); scale bar, 50 µm; n = 3 slices per genotype.

(**b**) Quantification of the number of cFos-positive cells in the SCN of ChR2+ or ChR2- SCN slices; Student's *t*-test, $p < 0.001$.

(**c**) Quantification of the number of ChR2-positive cells that are also cFos-positive (87.83 ± 0.97%) and the number of cFos-positive cells that are also ChR2-positive (92.17 ± 2.34%) after optogenetic stimulation. Data are presented as means ± SEM.

By crossing *Drd1a*-ChR2 or *Drd1a*-NpHR mice with a PER2::LUC reporter line in which the clock protein PERIOD2 (PER2) is fused to luciferase, we were able to assay the effect of optogenetic manipulation on the molecular clockworks. *Ex vivo Drd1a*-ChR2 x PER2::LUC SCN slices or *Drd1a*-NpHR x PER2::LUC SCN slices were optogenetically stimulated or inhibited, respectively, at varying times relative to the peak of the PER2::LUC rhythm (defined as circadian time 12 [CT 12]). In *Drd1a*-ChR2 x PER2::LUC SCN slices, optogenetic stimulation elicited delaying resets of the molecular clockworks from CT 12–18, advancing resets from CT 18–2, and no or minimal shifts from CT 2–12 (**Figs. II-4a,b**).

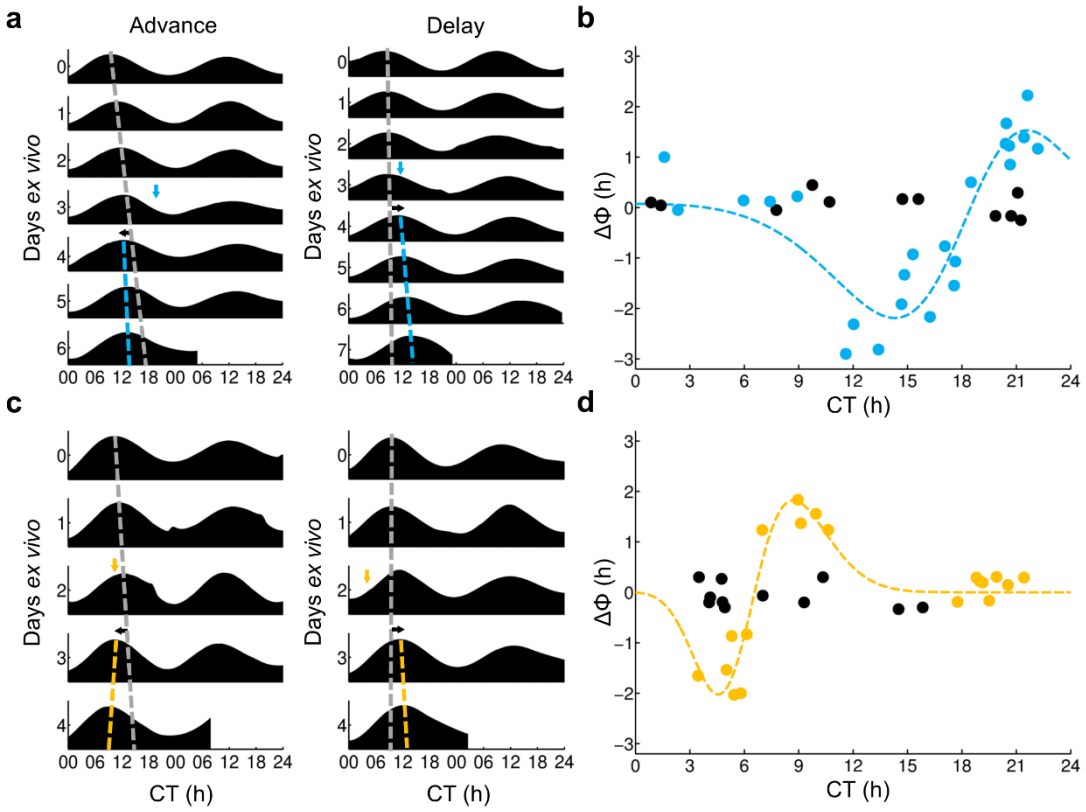

Figure II-4 Optogenetic manipulation of SCN neurons *ex vivo* produces changes in phase.

(**a**) Representative PER2::LUC actograms demonstrating the effects of ChR2-mediated stimulation of *Drd1a*-ChR2 organotypic slices resulting in advances (left) and delays (right). In these traces, the dashed gray line depicts the peak times of the undisturbed pre-stimulation rhythm extrapolated past the time of manipulation; the dashed blue line depicts the peak times of the post-stimulation rhythm; the blue arrow depicts the time of stimulation (470 nm, 1 hour, 8 Hz); and the black arrow depicts the direction of the resulting phase shift.

(**b**) Phase response curve depicting changes of phase of PER2::LUC bioluminescence in *Drd1a*-ChR2 organotypic slices in response to ChR2-mediated stimulation at varying circadian times; dashed line, Gaussian fit, $r^2 = 0.8510$; blue dots, ChR2+, n = 23 slices, 20 animals; black dots, ChR2–, n = 11 slices, 11 animals.

(**c**) Representative PER2::LUC actograms demonstrating the effects of NpHR-mediated inhibition of *Drd1a*-NpHR organotypic slices resulting in advances (left) and delays (right). In these traces, the dashed gray line depicts the peak times of the extrapolated pre-treatment rhythm; the dashed yellow line depicts the peak times of the post-treatment rhythm; the yellow arrow depicts the time of stimulation (590 nm, 1 hour); and the black arrow depicts the direction of the resulting phase shift.

(**d**) Phase response curve depicting changes of phase of PER2::LUC bioluminescence in *Drd1a*-NpHR organotypic slices in response to NpHR-mediated inhibition at varying circadian times; dashed line,

Gaussian fit, $r^2 = 0.8895$; yellow dots, NpHR+, n = 19 slices, 14 animals; black dots, NpHR–, n = 11 slices, 9 animals.

There were also changes in the period of the PER2 rhythm, with period lengthening resulting from delaying stimuli (CT 12–18), period shortening from advancing stimuli (CT 18–24), and no change in period from stimuli that did not result in phase shifts (CT 0–12; **II-5**).

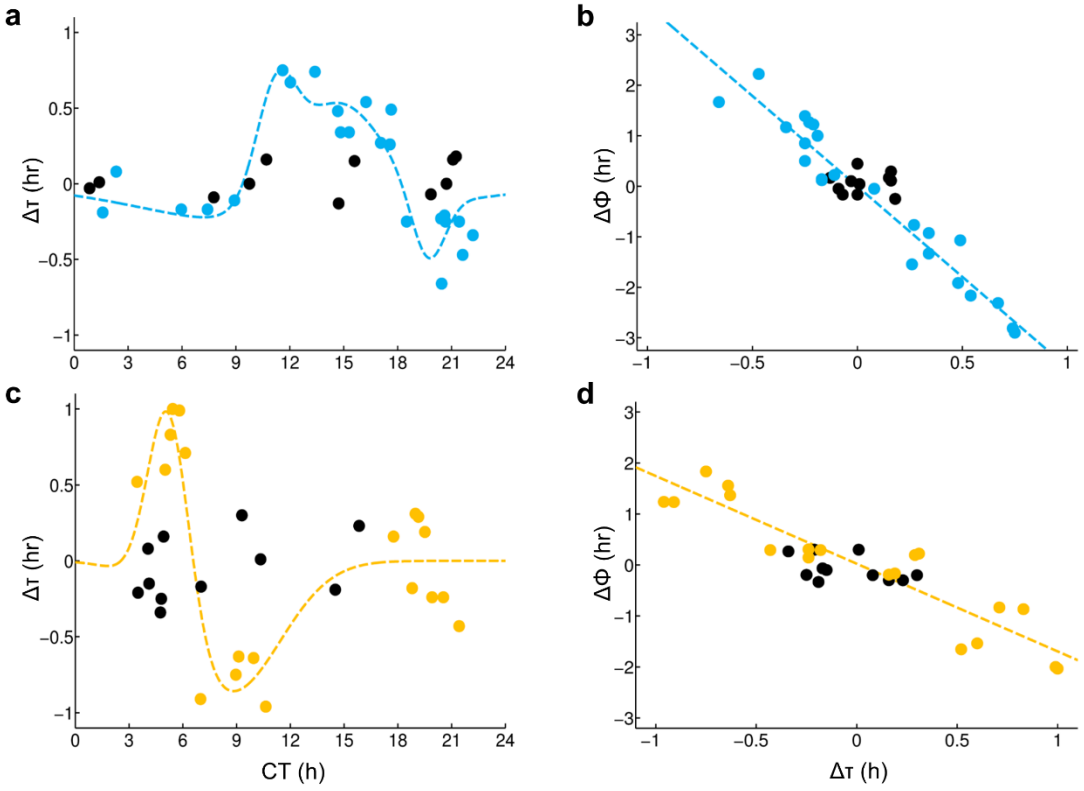

Figure II-5 Optogenetic manipulation of the SCN *ex vivo* produces changes in period that are correlated with changes in phase.

(**a**) Period response curve depicting changes of period in response to ChR2-mediated stimulation in the same slices depicted in Figs. 1a and 1b; dashed line, Gaussian fit, $r^2 = 0.7466$.

(**b**) Changes in phase and changes in period in response to ChR2-mediated stimulation are positively correlated; Pearson's r, $r^2 = 0.9342$, $p<0.001$. For (**a**-**b**), blue dots, ChR2+, n = 23 slices, 20 animals; black dots, ChR2-, n = 11 slices, 11 animals.

(**c**) Period response curve depicting changes of period in response to NpHR-mediated inhibition in the same slices depicted in Figs. 1c and 1d; dashed line, Gaussian fit, $r^2 = 0.6302$.

(**d**) Changes in phase and changes in period in response to NpHR-mediated inhibition are positively correlated; Pearson's r, $r^2 = 0.8565$, $p<0.001$. For (**c**-**d**), yellow dots, NpHR+, n = 19 slices, 14 animals; black dots, NpHR-, n = 11 slices, 9 animals.

Identical optogenetic stimuli delivered to PER2::LUC SCN slices lacking ChR2 did not result in phase shifts or period changes. In *Drd1a*-NpHR x PER2::LUC SCN slices, optogenetic inhibition resulted in a different pattern of resets, with delay resets from CT 0–6, advances from CT 6–12, and no resets from CT 12–24 (**Figs. II-4c,d**). As with ChR2 stimulation, NpHR inhibition resulted in changes in period, with period lengthening from delay-inducing treatments (CT 3–6), period shortening from advancing treatments (CT 9–12), and no change in period if shifts were not induced (CT 12–24; **Fig. II-5**). Identical optogenetic stimuli delivered to PER2::LUC SCN slices lacking NpHR did not result in phase shifts or period changes. In both *Drd1a*-ChR2 x PER2::LUC and *Drd1a*-NpHR x PER2::LUC SCN slices, effects on period and phase were found to persist for 5–6 days (n = 3 slices per genotype, data not shown).

To investigate the roles of action potentials and intercellular communication in ChR2-mediated changes in phase and period of the molecular clockworks, we used *ex vivo* optogenetic stimulation of *Drd1a*-ChR2 x PER2::LUC SCN slices in the presence of the sodium channel blocker tetrodotoxin (TTX) or the VIP receptor blocker [D-p-Cl-Phe^6,Leu^{17}]-VIP (VIPX) . Stimulation during the delay zone (CT 12–18) in control media resulted in phase delays and period lengthening, as before; however, these changes were inhibited when slices were stimulated in media containing TTX or VIPX (**Figs. II-6a,b**; **Fig. II-7**).

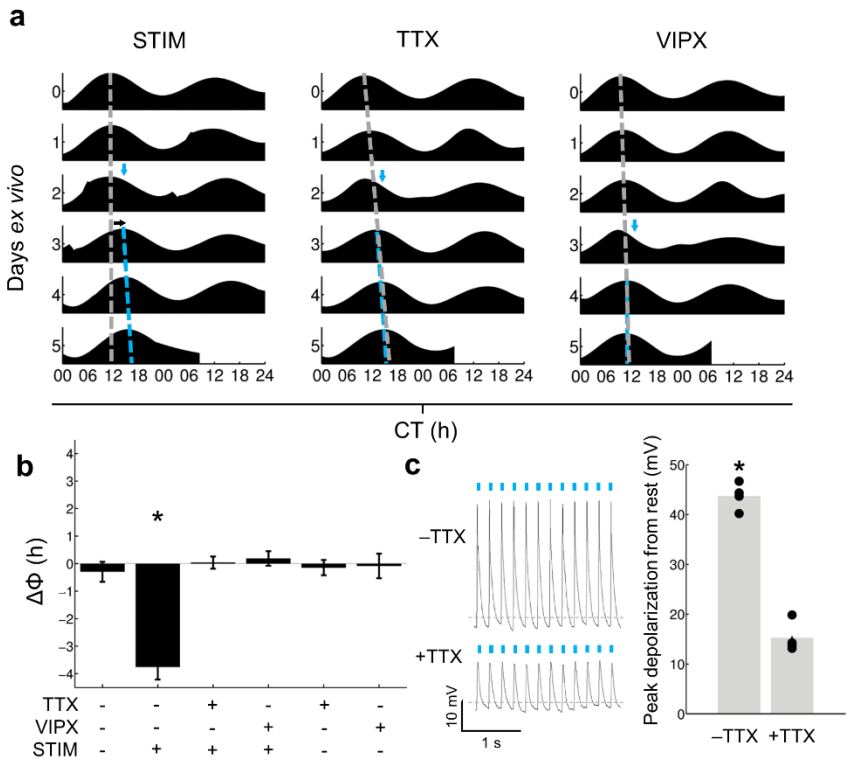

Figure II-6 Pharmacological blockade of action potential generation or VIP signaling ablates phase changes induced by ChR2 stimulation.

(**a**) Representative PER2::LUC actograms of *Drd1a*-ChR2 organotypic slices undergoing a media change followed by ChR2 stimulation (left, 'STIM'; n = 4 slices, 3 animals); a change to media containing 0.5 µM TTX followed by ChR2 stimulation (middle, 'TTX'; n = 6 slices, 5 animals); or a change to media containing 1 µM [D-p-Cl-Phe^{6},Leu^{17}]-VIP followed by ChR2 stimulation (right, 'VIPX'; n = 5 slices, 4 animals); dashed gray line, peak times extrapolated past the time of manipulation in order to project the timing of the undisturbed rhythm; dashed blue line, peak times of post-manipulation rhythms; blue arrow, time of stimulation (470 nm, 1 hour, 8 Hz); black arrow, direction of resulting phase shift, if any.

(**b**) Summary of changes in phase of PER2::LUC rhythms in response to combinations of ChR2 stimulation (470 nm, 1 hour, 8 Hz; 'STIM'), TTX, and/or [D-p-Cl-Phe^{6},Leu^{17}]-VIP ('VIPX'); from left to right, n = 4 slices, 4 animals; 4 slices, 3 animals; 6 slices, 5 animals; 5 slices, 4 animals; 3 slices, 3 animals; and 3 slices, 3 animals; One-Way ANOVA with post-hoc HSD, F: 21.47, $p<0.0001$.

(**c**) (Left) Representative voltage traces in response to ChR2 stimulation in the absence of or presence of TTX (–TTX or +TTX, respectively; dashed gray line in each trace indicates -50 mV); (Right) Peak depolarization amplitudes in response to ChR2 stimulation are significantly reduced in the presence of TTX; Mann-Whitney *U*, p = 0.0286; n = 4 cells. Data are presented as means ± SEM.

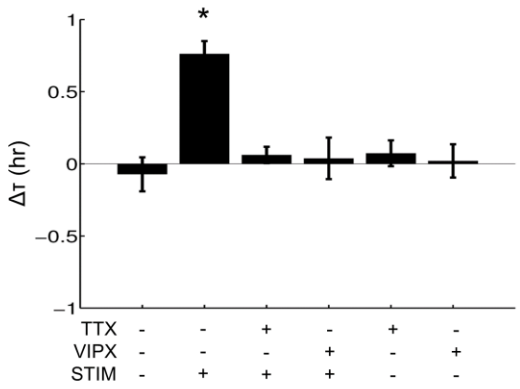

Figure II-7 Pharmacological blockade of action potential generation or VIP signaling ablates period changes induced by ChR2 stimulation.

Summary of changes in period of PER2::LUC rhythms from slices in Fig. 2 in response to combinations of ChR2 stimulation (470 nm, 1 hour, 8 Hz; 'STIM'), TTX, and/or VIPX; One-Way ANOVA with post-hoc HSD, F: 7.92, p=0.0004. Data are presented as means ± SEM.

Importantly, transfer to TTX, VIPX, or control media had no effect on unstimulated *Drd1a*-ChR2 x PER2::LUC SCN slices (**Fig. II-6b**; **Fig. II-7**). To determine the effects of TTX on ChR2-induced depolarization, we performed whole-cell current clamp recording on *Drd1a*-ChR2 neurons from acute SCN slices and measured the response to ChR2 stimulation in the absence or presence of TTX (**Fig. II-6c**). In the absence of TTX, the average peak depolarization amplitude in response to ChR2 stimulation was 43.71 ± 0.47 mV, which included the action potentials riding on top of the ChR2-induced depolarization. In the presence of TTX, however, depolarization by ChR2 stimulation persisted, but was severely reduced in amplitude to 15.25 ± 0.17 mV. In other studies, neural plasticity can be induced by ChR2 stimulation even in the presence of TTX (Goold and Nicoll, 2010); however, our data suggest that in the SCN the subthreshold depolarization induced by ChR2 stimulation is insufficient to reset the circadian clock.

Finally, to investigate the effects of manipulating SCN neuron firing rate on circadian behavior, we optogenetically stimulated the SCN of *Drd1a*-ChR2 mice *in vivo* over multiple days at a frequency similar to that of the daytime firing rate of SCN neurons (Sakai, 2014). While ChR2 stimulation allows exact temporal control of firing rate phase locked to pulsed illumination, NpHR inhibition requires continuous illumination and does not allow for such precise control (**Fig. II-2**). Thus, we chose ChR2 excitation over NpHR inhibition to test the specific role of clock neuron firing rate *in vivo*. Importantly, SCN-targeted expression of ChR2 combined with stereotaxic implantation of SCN-directed fiber optics and a limited range of blue light penetration in the brain allowed for specific activation of the SCN (**Fig. II-8**).

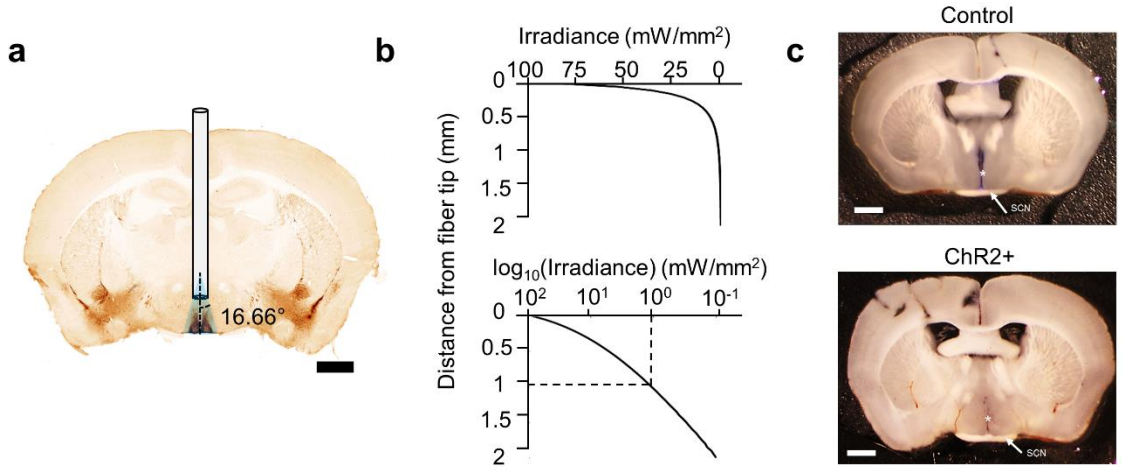

Figure II-8 *In vivo* optogenetic stimulation is localized to the SCN.

(**a**) Schematic representing the brain area illuminated by 470 nm light of sufficient intensity to excite ChR2 as delivered through the stereotaxically implanted fiber optic used in our experiments (400 µM diameter, 0.39 NA). Measured light intensity at the fiber tip of 10.8 mW. The cone of blue shading depicts the distance from the fiber tip at which the irradiance is approximately 1 mW/mm^2, which is the estimated ChR2 activation threshold (see (**b**)); scale bar, 1 mm.

(**b**) Calculated linear (top) and log (bottom) irradiance values attenuate rapidly as distance from fiber tip increases. Calculations were based on a measured light intensity at the fiber tip of 10.8 mW and were performed using the "Brain tissue light transmission calculator" available at www.optogenetics.org. Dashed line in the bottom graph represents an irradiance of 1 mW/mm^2.

(**c**) Representative brain slices (n = 3) from control (top) and ChR2+ (bottom) animals implanted with a fiber optic cannula dipped in blue dye and immediately perfused and sectioned; asterisk depicts approximate location of fiber tip; scale bar, 1 mm.

While control mice that lacked ChR2 expression showed no apparent response to repeated optogenetic stimulation of the SCN, *Drd1a*-ChR2 mice were entrained by the same stimulation, aligning the onset of their locomotor behavioral rhythms to the time of stimulation then free-running after cessation of the stimulus (**Fig. II-9**).

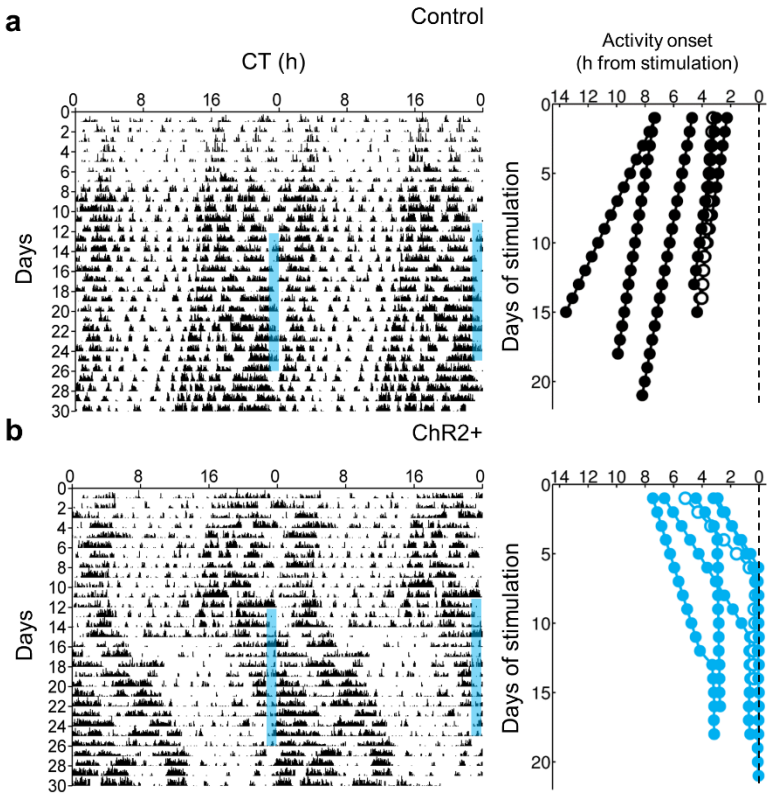

Figure II-9 Repeated stimulation of ChR2 in the SCN *in vivo* results in entrainment.

(**a**) Left, representative double-plotted actogram of locomotor activity for a control ChR2– animal stimulated intracranially with blue light targeted to the SCN with a fiber optic cannula; blue bars represent time of stimulation (1 hour per day, 470 nm, 8 Hz); Right, activity onset time difference from time of stimulation (dashed line; n = 6 trials; black filled circles, n = 5 mice; black open circles, n = 1 mouse re-stimulated after free-running for multiple days).

(**b**) Left, representative double-plotted actogram of locomotor activity for a *Drd1a*-ChR2 animal stimulated intracranially with blue light targeted to the SCN with a fiber optic cannula; blue bars represent time of stimulation (1 hour per day, 470 nm, 8 Hz); Right, activity onset time difference from time of stimulation (dashed line; n = 6 trials; blue filled circles, n = 5 mice; blue open circles, n = 1 mouse re-stimulated after free-running for multiple days).

Control mice continued to free-run independently of the optogenetic stimulus, with their time of activity onset drifting away from the time of stimulation; conversely, *Drd1a*-ChR2 mice entrained to the stimulus, with activity onset progressively moving towards the time of stimulation until activity onset locked on to the time of stimulation or shortly after.

Discussion

The application of optogenetics to the SCN has allowed us to test the fundamental role of firing rate in influencing molecular and behavioral circadian rhythms. Artificial induction or suppression of firing rate across the SCN *ex vivo* has upstream effects on the phase and period of clock gene expression: the pattern of phase shifts elicited by ChR2 stimulation is essentially identical to that of light, which acts on the SCN through depolarizing glutamate release from retinal ganglion afferents (Daan and Pittendrigh, 1976; Ding et al., 1994), while the pattern of phase shifts resulting from NpHR inhibition is similar to clock-resetting by dark pulses or other non-photic stimuli that are thought to act through inhibition of SCN neuron activity (Quintero and McMahon, 1999; Morin and Allen, 2006). Induction of firing rate *in vivo* also has downstream effects on locomotor behavior consistent with its phase-shifting effects observed *ex vivo*, suggesting that increasing SCN firing rate *per se* is potentially behaviorally equivalent to light stimulation in its action on the circadian system. Additionally, our results show that pharmacological blockade of coupling or firing rate prevents phase shifts *ex vivo*, which suggests a stronger role for VIPergic network communication and for action potentials versus sub-threshold depolarizations in the resetting of the molecular clockworks. Together, these data indicate that manipulation of SCN firing rate is sufficient to produce lasting changes within the circadian clock. These results, and the stimulation system used to produce them, will serve as a foundation for future experiments in circadian neurobiology investigating the interaction between the molecular, electrical, and behavioral components of the brain's circadian clock.

Chapter Acknowledgments

We thank H. Iwamoto for assistance with the whole-cell recording experiments and T. Page, C. Johnson, and L. Funkhouser-Jones for helpful discussion and manuscript comments. This work was supported by US National Institutes of Health grants R01 EY015815 (D.G.M.), T32 MH064931 (J.R.J.) and F31 NS082213 (J.R.J.), NSF Graduate Research Fellowship 0909667 (M.C.T.), and a Vanderbilt University Discovery Grant (D.G.M.).

Author Contributions

J.R.J., M.C.T., and D.G.M. prepared the paper. J.R.J. analyzed data. J.R.J. performed all *in vitro* and *ex vivo* experiments. J.R.J. and M.C.T. performed all *in vivo* experiments. J.R.J., M.C.T., and D.G.M. designed experiments.

CHAPTER III

Linking the molecular clockworks to electrical activity rhythms

3.1: Evidence for a relationship between the molecular clockworks and electrical activity rhythms

Whereas **Chapter II** investigated the role circadian rhythms in electrical activity play in regulating the gene expression rhythms and behavior, there is a variety of evidence that suggests the molecular clockworks directly regulates the electrical activity of SCN neurons. The most direct evidence for such a link comes from a number of studies investigating how mutations in core and accessory clock genes affect electrophysiological outputs. As mentioned in **Chapter I**, the *tau* mutation in hamsters discovered by Ralph and Menaker results in animals with a severely reduced period of locomotor activity (Ralph and Menaker, 1988). In 1997, Chen Liu and colleagues used these *tau* mutant hamsters to investigate how this mutation that causes a deficit in circadian behavior affects rhythms expressed by the SCN itself (Liu et al., 1997). Individual SCN neurons from heterozygous and homozygous *tau* mutant and wild-type hamsters were cultured on multielectrode arrays at a low density and their extracellular, spontaneous firing rate rhythms were recorded for up to five days. While the period of electrical activity in wild-type SCN neurons was approximately 23.5 hours, as expected, the period of electrical activity in heterozygous *tau* mutant SCN neurons was approximately 21 hours, and the period of electrical activity in homozygous *tau* mutant SCN neurons was approximately 19 hours. Importantly, the *in vitro*, single-neuron firing rate rhythms for an animal of a given genotype exhibited periods that were correlated with the periods of *in vivo* locomotor activity for animals of the same genotype. However, the range of period lengths in electrical activity for individual SCN neurons of a given genotype was much greater than the range of period lengths in locomotor behavior, which suggests that SCN coupling is important for synchronized rhythmicity (see **Section 1.4**). A few years later, Qing-Jun Meng and colleagues discovered that the *tau* mutation promotes the degradation of PER through its effects on casein kinase 1ε; thus, it appears that the core clock gene *Per* somehow influences electrical activity rhythms in SCN neurons (Meng et al., 2008).

Although the *tau* mutation affects the degradation rate of the molecular clockworks, the molecular clock is still intact in animals with this mutation. In 1998, Erik Herzog and colleagues investigated the effect of a mutation in a core clock gene on electrical activity rhythms in ClockΔ19 mice (See **Section 1.2**), in which exon 19 is deleted from *Clock*, resulting in a reduced ability to activate the transcription of *Per1* (Herzog et al., 1998). As is the case in the *tau* mutant hamster, wild-type, heterozygous, and homozygous ClockΔ19 mutant mice exhibited *in vitro* single-cell firing rate rhythms that mirrored the animal's *in vivo* locomotor activity rhythms. Specifically, wild-type mice and individual SCN neurons

from these mice had normal ~23.5 hour periods of locomotor and electrical activity, respectively; heterozygous ClockΔ19 mice had lengthened ~25 hour periods of locomotor and electrical activity; and homozygous ClockΔ19 mice were electrically and behaviorally arrhythmic. However, a few years later, Wateru Nakamura and colleagues repeated this experiment in both SCN slices and dispersed SCN neurons from wild-type, heterozygous, and homozygous ClockΔ19 mice (Nakamura et al., 2002). They found that wild-type SCN neurons had a period of electrical activity of around 23.5 hours and heterozygous SCN neurons had a period of around 25 hours, as expected. Unlike in the results of Herzog and colleagues, however, nearly 77% of neurons from SCN slices and ~15% of individual dissociated neurons from homozygous ClockΔ19 mice remained rhythmic, exhibiting a period of electrical activity of around 27 hours and clearly demonstrating that the intact SCN network enhances synchrony between SCN neurons. Regardless of the actual effect a homozygous ClockΔ19 mutant has on SCN firing rate, that is, arrhythmicity or a lengthened period, together these results indicate that *Clock* is important for normal circadian electrical activity. Finally, in 2002, Henk Albus and colleagues performed multielectrode array recording in SCN slices from *Cry1*$^{-/-}$; *Cry2*$^{-/-}$ double knockout mice over multiple days (Albus et al., 2002). *Cry* is a necessary component of the negative loop of the TTFL, and unlike *Clock*, *Cry* has two paralogs (see **Section 1.2**); as such, a double knockout is necessary to eliminate *Cry* from the system. Whereas the SCN slice seemed to rescue some of the arrhythmicity observed in individual SCN neurons from homozygous ClockΔ19 mice, SCN slices from homozygous *Cry1*$^{-/-}$; *Cry2*$^{-/-}$ mice were found to be electrically arrhythmic even with an intact SCN network. Thus, *Cry* plays a role in generating electrical activity rhythms that is not redundant with coupling factors within the SCN.

These results with mutant animals clearly indicate a necessary interaction between the molecular clockworks and electrical activity rhythms but raise the question of these two components of the multi-component circadian system interact in a wild-type animal. To address this, Sandra Kuhlman and colleagues in the laboratory of my thesis advisor, Douglas McMahon, generated a line of "*Per1*::d2EGFP" transgenic mice which express a fragment of the *mPer1* promoter that contains both E-box enhancer elements for CLOCK/BMAL1-driven transcription as well as CRE elements for CREB-driven induction (Kuhlman et al., 2000). When activated, this fragment of *mPer1* drives a short half-life version of enhanced GFP which essentially acts as a real-time reporter of E-box and/or CRE-element induction. GFP fluorescence in SCN neurons from these mice can be used as a readout of the state of the molecular clockworks, and electrical activity in individual SCN neurons can be simultaneously recorded using traditional whole-cell or cell-attached electrophysiology. Importantly, it is much more difficult to obtain this single-cell relationship with other methods of visualizing the molecular clockworks, such as *Per1-luc* or PER2::LUC bioluminescence imaging, or of recording electrical activity, such as with a multielectrode array.

In 2003, Kuhlman and colleagues used acute *in vitro* SCN slices from these mice to determine that GFP fluorescence and firing rate in individual SCN neurons was positively correlated after the animal from which the slice was obtained was subjected to a phase-resetting nighttime light pulse (Kuhlman et al., 2003). Similarly, Jorge Quintero and colleagues found that GFP fluorescence and firing rate was also positively correlated in individual neurons from acute SCN slices when recorded during the middle of the day phase of the circadian cycle (Quintero et al., 2003). Thus, these results suggest that a fixed phase relationship may exist between the molecular clockworks and circadian electrical activity, and, indeed, this is supported by a computational model of the SCN that suggests that there is a positive correlation between *Per* mRNA and firing rate in SCN neurons *in silico* (Vasalou and Henson, 2010). Intriguingly, applying either GRP or VIP to the SCN during the night phase of the circadian cycle causes a sustained increase in firing rate that is prevented by the application of antisense oligodeoxynucleotides (αODNs) specific to *Per1*, which may indicate a functional role for *Per1* in linking the molecular clockworks to circadian electrical activity (Gamble et al., 2007; Kudo et al., 2013).

While a correlation exists between *Per1* induction and firing rate, and there is evidence to suggest that *Per1* itself is able to influence electrical activity in the SCN, the functional relationship between these clock components still needs to be determined. Previous multielectrode array experiments explored this question in SCN slices and neurons from clock mutant animals, in which the cycling of the molecular clockworks is completely abolished. Thus, in **Section 3.2**, I have taken a complimentary approach to investigate this key relationship by using a combination of real-time GFP fluorescence monitoring of the state of the molecular clockworks and visually-targeted patch clamp electrophysiology in wild-type, *Per1*$^{-/-}$, and *Per2*$^{-/-}$ mice, which have an intact, but altered molecular clockworks (see **Section 1.2**). I conclude that *Per1* plays a functional and non-redundant role in linking gene expression and firing rate rhythms in individual SCN neurons.

3.2: The core clock gene *Per1* links molecular and electrical circadian rhythms

Jeff R. Jones[1] and Douglas G. McMahon[1,2]

[1]Neuroscience Graduate Program, [2]Department of Biological Sciences, Vanderbilt University, Nashville, TN

Adapted from Jones, J.R. & McMahon, D.G. The core clock gene *Per1* links molecular and electrical circadian rhythms. In preparation.

Abstract

The brain's biological clock, the suprachiasmatic nucleus (SCN), exhibits endogenous 24-hour rhythms in gene expression and spontaneous firing rate; however, the functional relationship between these neuronal rhythms is unknown. Here, we used a *Per1*::GFP transgenic mouse line that allows for the simultaneous quantification of the molecular clock state and firing rate in the SCN to examine the link between these key components of the circadian clock. We find that there are stable population-level and single-cell relationships between E-box-driven clock gene expression and spontaneous firing rate in individual SCN neurons, and that these relationships are independent of light input onto the system or of $GABA_A$ receptor-mediated synaptic activity. Importantly, these relationships persist in the absence of the core clock gene *Per2*, but are abolished in the absence of the homologous clock gene *Per1*. These results suggest that *Per1* plays a unique, non-redundant role in linking gene expression and firing rate rhythms in SCN neurons.

Introduction

Understanding how gene signaling networks influence the activity of neurons and circuits that control behavior is an essential problem in neuroscience. Daily changes in physiology and behavior in mammals are driven by the suprachiasmatic nucleus (SCN), a network of neurons exhibiting endogenous rhythms in gene expression and firing rate in isolation (Welsh et al., 2010; Colwell, 2011). A key unsolved question in circadian neurobiology is how these neuronal rhythms interact to form a coherent pacemaker. Gene expression rhythms in SCN neurons consist of a daily transcriptional / translational feedback loop (TTFL) comprised of the core clock genes *Bmal1*, *Clock*, *Per1/2*, and *Cry1/2* (Mohawk and Takahashi, 2011). Furthermore, firing rate rhythms are produced by a collection of intrinsic ionic currents that allow SCN neurons to spontaneously fire action potentials and, importantly, modulate their firing rates so that they fire quickly during the day and slowly at night (Kuhlman and McMahon, 2006). The central role of the TTFL in driving circadian electrical activity has been supported by studies in which critical clock genes have been eliminated (Liu et al., 1997). Indeed, mice homozygous for a mutation in *Clock* and mice with a double knockout of *Cry1* and *Cry2* were each found to be electrically arrhythmic. However, in each of these mice, the molecular clock is completely disrupted (Herzog et al., 1998; Albus et al., 2002; Nakamura et al., 2002).

A fundamental gap in our knowledge is therefore understanding how an intact circadian molecular clockworks is linked to firing rate rhythms in the SCN. Which clock genes are key? What is the precise relationship between gene expression rhythms and circadian electrical activity? To investigate these questions, we have used our *Per1*::GFP transgenic mouse line in which sequences from the *Per1* gene promoter that contain both E-box

enhancer elements for CLOCK/BMAL1-driven transcription as well as CRE elements for CREB-driven induction drive a short half-life version of enhanced green fluorescent protein (EGFP; Kuhlman et al., 2000; LeSauter et al., 2003). Using this artificial molecular clock-controlled gene – essentially an E-box and CRE element induction reporter – we have previously shown that the degree of activation of this construct correlates with firing rate in individual SCN neurons during the day phase of circadian cycling and following a phase-resetting light pulse at night (Kuhlman et al., 2003; Quintero et al., 2003). Thus, a fixed phase relationship may exist between the molecular clockworks and circadian electrical activity (Colwell, 2011). Intriguingly, resetting SCN neuron firing rate by applying the neuropeptides gastrin releasing peptide (GRP) or vasoactive intestinal peptide (VIP), mediators of light signaling in the SCN that act through CRE element induction, requires the translation of the native *Per1* gene, which suggests a functional role for *Per1* in this relationship (Gamble et al., 2007; Kudo et al., 2013).

Here we report that the phase relationship between the molecular clockworks and circadian electrical activity persists throughout a 24 hour circadian day, and that the knockout of *Per1* abolishes this relationship in individual SCN neurons. Importantly, this role is specific to *Per1*, as the link between circadian gene expression and firing rate rhythms is preserved when the clock gene *Per2* is knocked out. Taken together, these results indicate that the relationship between SCN neuron gene expression rhythms and firing rate is more than correlational, and identify *Per1* as a clock gene that links the molecular clockworks to circadian electrical activity.

Materials and Methods

Animals and housing

Experiments were performed using male and female *Per1*::d2EGFP (*Per1*::GFP or $Per1^{+/+}$; $Per2^{+/+}$), *Per1*::GFP x $Per1^{-/-}$ ($Per1^{-/-}$; $Per2^{+/+}$), *Per1*::GFP x $Per2^{-/-}$ ($Per1^{+/+}$; $Per2^{-/-}$), or *Per1*::GFP x $Per1^{-/-}$ x $Per2^{-/-}$ ($Per1^{-/-}$; $Per2^{-/-}$) mice on a C57BL/6J background, 1–3 months of age (Kuhlman et al., 2003; Ruan et al., 2012). Animals were provided with food and water *ad libitum* and were housed in single-sexed cages of no more than five animals from weaning until experimental use on a 12:12 light/dark (LD) cycle, or, for some experiments, were housed in constant darkness (DD) for at least two weeks before use. All animal care and experimental procedures were conducted in concordance with Vanderbilt University's Institutional Animal Care and Use Committee guidelines.

Behavioral analysis

Wheel-running activity from mice housed in DD was monitored and recorded in 5 minute bins using ClockLab software (Actimetrics, Evanston, IL). Time of activity onset (defined as circadian time 12 [CT 12]) was determined using ClockLab Analysis Software. As *Per1*$^{-/-}$; *Per2*$^{-/-}$ mice are behaviorally arrhythmic, CT could not be defined for this group of mice.

Slice preparation

Mice housed in LD were killed by cervical dislocation without anesthesia in ambient light for dissections occurring between ZT (Zeitgeber time) 0 to 12, where ZT 0 is defined as the time of lights on and ZT 12 is defined as the time of lights off. For dissections occurring between ZT 12–24 for mice housed in LD, or for all dissections from mice housed in DD, mice were killed by cervical dislocation without anesthesia under dim red light (<1 lux). Importantly, dissections occurring in the dark phase have been shown not to affect the phase of electrical activity rhythms in the SCN (vanderLeest et al., 2009). After dissection, brains were quickly removed and blocked in cold, oxygenated 95% O_2–5% CO_2 dissecting solution (in mM: 114.5 NaCl, 3.5 KCl, 1 NaH_2PO_4, 1.3 $MgSO_4$, 2.5 $CaCl_2$, 10 D-glucose, and 35.7 $NaCHO_3$). SCN slices (200 μm) were cut coronally on a vibroslicer (World Precision Instruments, Sarasota, FL) at 4–10ºC and transferred directly to an open recording chamber continually superfused with warmed (35 ± 0.5ºC) extracellular solution (in mM: 124 NaCl, 3.5 KCl, 1 NaH_2PO_4, 1.3 $MgSO_4$, 2.5 $CaCl_2$, 10 D-glucose, and 26 $NaCHO_3$). Slices were allowed to recover for 1 hour before recording.

Electrophysiological recording and imaging

SCN neurons were visualized using a Leica DMLFS microscope (Leica Microsystems, Buffalo Grove, IL) equipped with near-infrared (IR)-differential interference contrast and fluorescence optics. For loose-patch recordings, patch electrodes (4-6 MΩ) pulled from glass capillaries (WPI) on a multistage puller (DMZ; Zeitz, Martinsried, Germany) were filled with extracellular solution. Spontaneous action potential recordings (~5 minutes in duration) from neurons sampled throughout the SCN were obtained with an Axopatch 200B amplifier (Molecular Devices, Sunnyvale, CA) and monitored online with pClamp 10.0 software (Molecular Devices). Recordings were obtained in gap-free mode throughout the day, were sampled at 10 kHz, and were filtered online at 1 kHz. Loose-patch seal resistances ranged from 10–30 MΩ. Slices were used for no more than 6 hours after dissection. Immediately after cessation of electrophysiological recording, an image of the recorded neuron was captured with an exposure time of one second using HCImage acquisition software (Hamamatsu; Bridgewater, NJ) with a cooled CCD camera (Hamamatsu) and an EGFP filter set. All recordings were confirmed to be from GFP^+

neurons by aligning digital images of the same neuron taken under near-IR and GFP fluorescence illumination.

Pharmacology

In some experiments, 20 μM gabazine (SR 95531 hydrobromide; Sigma, St. Louis, MO) was dissolved directly in the extracellular solution and perfused over the slice. Concentrations were chosen based on values from Scott et al., 2010 and Belle et al., 2009.

Data analysis

Image analysis was performed based on methods described in Kuhlman et al, 2003, using ImageJ software with 16-bit digitization. Fluorescence was reported as the intensity of a region of interest containing the cell body divided by the background fluorescence to normalize for differences in baseline fluorescence across preparations and fields. Background fluorescence was defined as the average pixel intensity of two local measurements next to the recorded neuron and the total frame (1024 x 1024 pixels). Average firing rate for the recording period was calculated using Clampex software (Molecular Devices).

Statistical analysis

Sample sizes were chosen so as to be sufficient for statistical analysis based upon previous publications detailing similar measurements. All statistical analyses (Student's *t*-test, One-Way ANOVA, Tukey's HSD, Mann-Whitney *U*) were performed in Matlab, with α defined as 0.05. A Bartlett's multiple-sample test and a Kolmogorov-Smirnov test were used to confirm equal variance and normality. Curves were fit using Matlab's Curve Fitting Toolbox (Mathworks). Data are presented as means ± SEM.

Results

To determine the phase relationship between E-box-driven clock gene expression and spontaneous firing rate in the SCN, we performed visually-targeted loose-patch recording of individual GFP^+ SCN neurons in coronal SCN slices from from wild-type (*Per1*$^{+/+}$; *Per2*$^{+/+}$; Kuhlman et al., 2000) mice sampled around the clock. In these mice the fluorescence intensity of GFP provides a continuous readout of the state of the molecular clockworks at the single-cell level (Quintero et al., 2003). The fluorescence intensity and firing rate of each sampled neuronw as determined over a 5 minute interval to provide a snapshot of both the molecular clockworks and SCN neural activity. We found that both E-box-driven clock gene expression as measured by GFP fluorescence intensity and spontaneous firing rate showed temporal variations consistent with ongoing rhythms at a

population level (**Fig. III-1a;** n = 249 cells, 34 mice; Cosinor fit, $r^2 = 0.2985$, $p < 0.001$ and $r^2 = 0.3267$, $p < 0.001$, respectively).

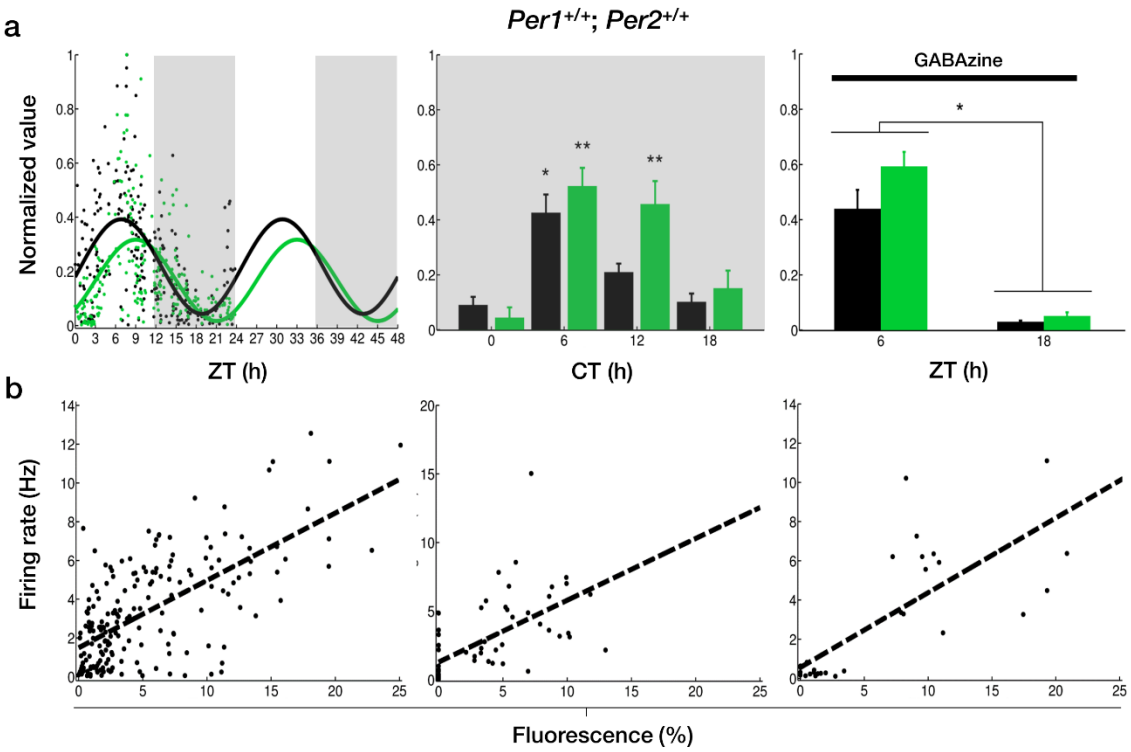

Figure III-1 E-box driven gene expression and spontaneous firing rate are rhythmic and correlated in individual *Per1*$^{+/+}$; *Per2*$^{+/+}$ neurons.

(**a**) *Left*, Average LD (light, white shading; dark, gray shading) fluorescence intensities (green dots) and firing rates (black dots) from individual *Per1*$^{+/+}$;*Per2*$^{+/+}$ SCN neurons recorded throughout the day (n = 249 cells, 34 mice). Fluorescence intensity and firing rate each normalized to the maximum recorded value and population rhythmicity determined using a Cosinor fit; fluorescence intensity (green line), $r^2 = 0.2985$, $p < 0.001$; firing rate (black line), $r^2 = 0.3267$, $p < 0.001$. *Middle*, Average DD (gray shading) fluorescence intensities (green bars) and firing rates (black bars) from individual *Per1*$^{+/+}$;*Per2*$^{+/+}$ SCN neurons recorded throughout the day (n = 58 cells, 10 mice). Fluorescence intensity and firing rate each normalized to the maximum recorded value and population rhythmicity determined using a Kruskal-Wallis ANOVA on Ranks test (fluorescence, $p < 0.001$; firing rate, $p < 0.001$). *Right*, Average LD fluorescence intensity (green bars) and firing rates (black bars) from individual *Per1*$^{+/+}$;*Per2*$^{+/+}$ SCN neurons recorded throughout the day in the presence of GABAzine (n = 32 cells, 4 mice). Fluorescence intensity and firing rate each normalized to the maximum recorded value and population rhythmicity determined using a Mann-Whitney U test (fluorescence, $p < 0.001$; firing rate, $p < 0.001$).

(**b**) *Left*, Fluorescence intensity versus firing rate in individual *Per1*$^{+/+}$;*Per2*$^{+/+}$ SCN neurons recorded throughout the day in LD show a positive, linear correlation (n = 249 cells, 34 mice; Pearson's r, $r^2 = 0.4504$, $p < 0.001$). *Middle*, Fluorescence intensity versus firing rate in individual *Per1*$^{+/+}$;*Per2*$^{+/+}$ SCN neurons recorded throughout the day in DD show a positive, linear correlation (n = 58 cells, 10 mice; Pearson's r, $r^2 = 0.3621$, $p < 0.001$). *Right*, Fluorescence intensity versus firing rate in individual *Per1*$^{+/+}$;*Per2*$^{+/+}$ SCN

neurons recorded throughout the day in LD in the presence of GABAzine show a positive, linear correlation ($n = 32$ cells, 4 mice; Pearson's r, $r^2 = 0.5744$, $p < 0.001$).

The population of recorded SCN neurons exhibited a peak in GFP fluorescence intensity at around Zeitgeber time (ZT) 9.05 and a peak in spontaneous firing rate at around ZT 6.83, where ZT 0 is defined as the time of lights on. The observed population firing rate rhythm was consistently phase-advanced compared to the population rhythm in GFP fluorescence intensity. Importantly, we also found that there was a positive, linear correlation between *Per1* promoter activation as read out by GFP fluorescence intensity and spontaneous firing rate within individual SCN neurons over the course of the 24 hour sampling (**Fig. III-1b**; Pearson's r, $r^2 = 0.4504$, $p < 0.001$). To test whether these results were due to circadian rhythms or diurnal light-driven responses we performed experiments on SCN from mice housed in constant darkness and used their running wheel rhythms to estimate the circadian time (CT) of sampling. At the population level, we found that both GFP fluorescence intensity and spontaneous firing rate remained rhythmic (**Fig. III-1a**; $n = 58$ cells, 10 mice; Kruskal-Wallis ANOVA on Ranks, $p < 0.001$), and that the positive, linear correlation between GFP fluorescence intensity and spontaneous firing rate in individual neurons persisted (**Fig. III-1b**; Pearson's r, $r^2 = 0.3621$, $p < 0.001$). Finally, most SCN neurons are GABAergic (Wagner et al., 1997) and therfore GABAergic transmission represents much of the ongoing rapid synaptic communication in the SCN. We found that when the $GABA_A$-receptor blocker GABAzine was applied to SCN neurons from mice housed under a normal light cycle GFP fluorescence intensity and spontaneous firing rate remained rhythmic at the population level (**Fig. III-1a**; $n = 32$ cells, 4 mice; Mann-Whitney U, $p < 0.001$). Likewise, the positive, linear correlation between GFP fluorescence intensity and spontaneous firing rate in individual neurons again persisted in the presence of this blocker (**Fig. III-1b**; Pearson's r, $r^2 = 0.5744$, $p < 0.001$).

To determine if this observed population- and single-cell stable phase relationship between E-box-driven gene expression and spontaneous firing rate persisted in the absence of the core clock gene *Per1*, we again performed visually-targeted loose-patch recording in individual *Per1*::GFP^+ SCN neurons recorded throughout the day; however, here, we recorded from neurons from *Per1*$^{-/-}$*; Per2*$^{+/+}$ mice in which the core clock gene *Per1* is knocked out. Importantly, in these mice, the E-box-driven production of GFP still acts as a reporter of the molecular clockworks since it is driven by a BMAL1/CLOCK heterodimer even in the absence of the native *Per1* gene. We found that at the population level both E-box-driven clock gene expression as measured by GFP fluorescence intensity and spontaneous firing rate exhibited statistically significant time series variations; however, their phase relationship was radically changed (**Fig. III-2a**; Cosinor fit, $n = 227$ cells, 21 mice; $r^2 = 0.2822$, $p < 0.001$ and $r^2 = 0.3988$, $p < 0.001$, respectively).

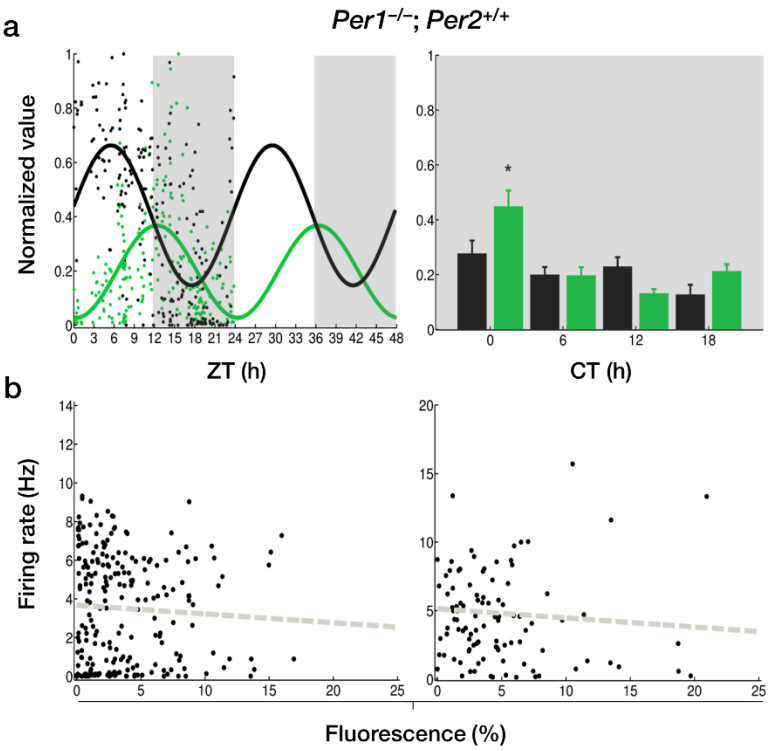

Figure III-2 E-box driven gene expression and spontaneous firing rate are no longer correlated in individual *Per1*$^{-/-}$; *Per2*$^{+/+}$ SCN neurons.

(**a**) *Left*, Average LD (light, white shading; dark, gray shading) fluorescence intensities (green dots) and firing rates (black dots) from individual *Per1*$^{-/-}$;*Per2*$^{+/+}$ SCN neurons recorded throughout the day (n = 227 cells, 21 mice). Fluorescence intensity and firing rate each normalized to the maximum recorded value and population rhythmicity determined using a Cosinor fit; fluorescence intensity (green line), $r^2 = 0.2822$, $p < 0.001$; firing rate (black line), $r^2 = 0.3988$, $p < 0.001$. *Right*, Average DD (gray shading) fluorescence intensities (green bars) and firing rates (black bars) from individual *Per1*$^{-/-}$;*Per2*$^{+/+}$ SCN neurons recorded throughout the day (n = 61 cells, 7 mice). Fluorescence intensity and firing rate each normalized to the maximum recorded value and population rhythmicity determined using a Kruskal-Wallis ANOVA on Ranks test (fluorescence, $p < 0.001$; firing rate, $p = 0.067$).

(**b**) *Left*, Fluorescence intensity versus firing rate in individual *Per1*$^{-/-}$;*Per2*$^{+/+}$ SCN neurons recorded throughout the day in LD are not correlated (n = 227 cells, 21 mice; Pearson's r, $r^2 = 0.0032$, $p = 0.3968$). *Right*, Fluorescence intensity versus firing rate in individual *Per1*$^{-/-}$;*Per2*$^{+/+}$ SCN neurons recorded throughout the day in DD are not correlated (n = 61 cells, 7 mice; Pearson's r, $r^2 = 0.0049$, $p = 0.4831$).

Whereas the phase difference in the peaks of GFP fluorescence intensity and spontaneous firing rate in *Per1*$^{+/+}$*; Per2*$^{+/+}$ SCN neurons was approximately 2.2 hours, SCN neurons from *Per1*$^{-/-}$*; Per2*$^{+/+}$ mice exhibited a delayed peak in GFP fluorescence intensity at around ZT 12.40 and an advanced peak in spontaneous firing rate at around ZT 5.50 – a difference of 6.9 hours. Even more strikingly, the robust correlation between GFP fluorescence intensity and spontaneous firing rate we observed in individual SCN neurons from *Per1*$^{+/+}$*;*

Per2$^{+/+}$ mice was completely lost in individual *Per1*$^{-/-}$*; Per2*$^{+/+}$ SCN neurons (**Fig. III-2a**; Pearson's r, $r^2 = 0.0032$, $p = 0.3968$). In SCN neurons from *Per1*$^{-/-}$*; Per2*$^{+/+}$ mice housed in constant darkness, the correlation between GFP fluorescence intensity and spontaneous firing rate in individual cells remained absent (**Fig. III-2b**; n = 61 cells, 7 mice; Pearson's r, $r^2 = 0.0049$, $p = 0.4831$); at the population level, GFP fluorescence intensity remained rhythmic, while spontaneous firing rate showed a statistical trend towards rhythmicity (**Fig. III-2a**; Kruskal-Wallis ANOVA on Ranks, $p < 0.001$ and $p = 0.067$, respectively).

To determine if the altered population-level and abolished single-cell phase relationship between E-box-driven gene expression and spontaneous firing rate we observed in *Per1*$^{-/-}$*; Per2*$^{+/+}$ SCN neurons was specific to the loss of *Per1*, we performed visually-targeted loose-patch recording in individual *Per1*::GFP^{+} SCN neurons recorded throughout the day from *Per1*$^{+/+}$*; Per2*$^{-/-}$ mice in which the core clock gene *Per2*, a homolog of *Per1*, was knocked out. Surprisingly, both E-box-driven clock gene expression as measured by GFP fluorescence intensity and spontaneous firing rate were rhythmic at a population level (**Fig. III-3a**; Cosinor fit, n = 230 cells, 10 mice; $r^2 = 0.2561$, $p < 0.001$ and $r^2 = 0.4951$, $p < 0.001$, respectively).

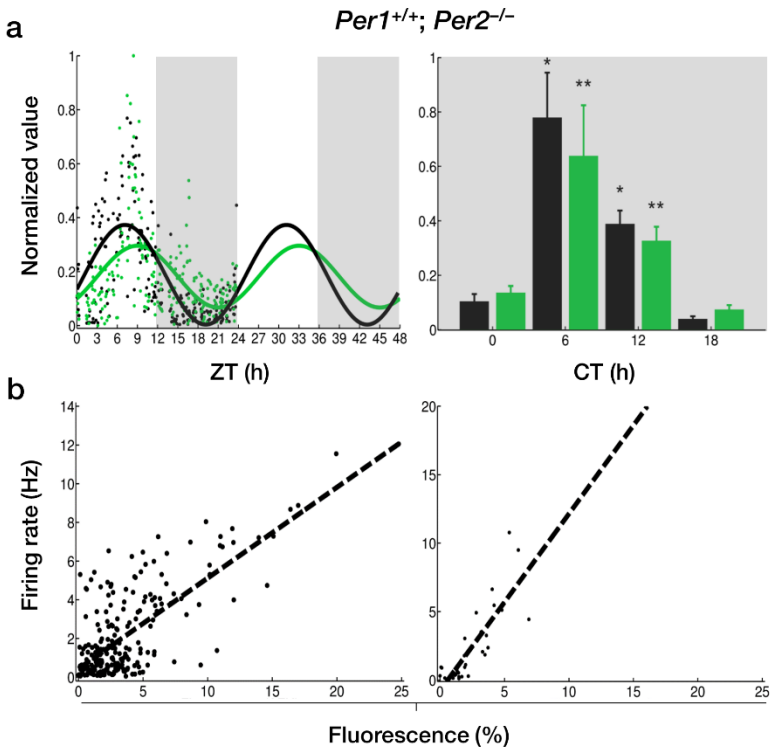

Figure III-3 The correlation between E-box driven gene expression and spontaneous firing rate is preserved in individual *Per1*$^{+/+}$; *Per2*$^{-/-}$ SCN neurons.

(**a**) *Left*, Average LD (light, white shading; dark, gray shading) fluorescence intensities (green dots) and firing rates (black dots) from individual *Per1*$^{+/+}$;*Per2*$^{-/-}$ SCN neurons recorded throughout the day (n = 230 cells, 10 mice). Fluorescence intensity and firing rate each normalized to the maximum recorded value and population rhythmicity determined using a Cosinor fit; fluorescence intensity (green line), $r^2 = 0.2561$, $p < 0.001$; firing rate (black line), $r^2 = 0.4951$, $p < 0.001$. *Right*, Average DD (gray shading) fluorescence intensities (green bars) and firing rates (black bars) from individual *Per1*$^{+/+}$;*Per2*$^{-/-}$ SCN neurons recorded throughout the day (n = 64 cells, 7 mice). Fluorescence intensity and firing rate each normalized to the maximum recorded value and population rhythmicity determined using a Kruskal-Wallis ANOVA on Ranks test (fluorescence, $p < 0.001$; firing rate, $p < 0.001$).

(**b**) *Left*, Fluorescence intensity versus firing rate in individual *Per1*$^{+/+}$;*Per2*$^{-/-}$ SCN neurons recorded throughout the day in LD show a positive, linear correlation (n = 230 cells, 10 mice; Pearson's r, $r^2 = 0.6328$, $p < 0.001$). *Right*, Fluorescence intensity versus firing rate in individual *Per1*$^{+/+}$;*Per2*$^{-/-}$ SCN neurons recorded throughout the day in DD show a positive, linear correlation (n = 64 cells, 7 mice; Pearson's r, $r^2 = 0.7572$, $p < 0.001$).

The population of recorded SCN neurons exhibited a peak in GFP fluorescence intensity at around ZT 9.02 and a peak in spontaneous firing rate at around ZT 7.10, with the observed population firing rate rhythm consistently phase-advanced compared to the population rhythm in GFP fluorescence intensity. These neurons exhibited a peak phase difference of 1.92 hours, similar to that observed in wild-type *Per1*$^{+/+}$*; Per2*$^{+/+}$ SCN neurons. Critically, the single-cell correlation between GFP fluorescence intensity and spontaneous firing rate that was abolished in *Per1*$^{-/-}$*; Per2*$^{+/+}$ SCN neuron was still present in the absence of *Per2* (**Fig. III-3b**; Pearson's r, $r^2 = 0.6328$, $p < 0.001$). In SCN neurons from *Per1*$^{+/+}$*; Per2*$^{-/-}$ mice housed in constant darkness, we continued to observe stable population-level and single-cell phase relationships between GFP fluorescence intensity and spontaneous firing rate (**Fig. III-3a,b**; n = 64 cells, 7 mice; Kruskal-Wallis ANOVA on Ranks, $p < 0.001$; $r^2 = 0.7572$, $p < 0.001$). This single-cell correlation was abolished when *Per1* was concurrently knocked out in SCN neurons from *Per1*$^{-/-}$*; Per2*$^{-/-}$ mice (n = 65 cells, 6 mice; Pearson's r, $r^2 = 0.0036$, $p = 0.5146$; **Fig. III-4**).

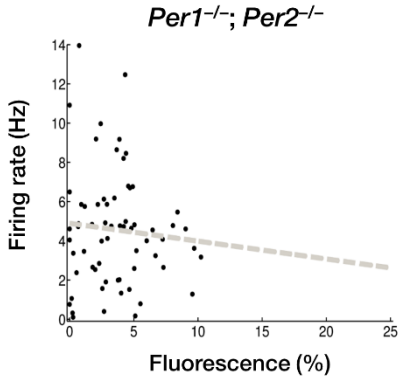

Figure III-4 E-box driven gene expression and spontaneous firing rate are not correlated in individual *Per1*$^{-/-}$; *Per2*$^{-/-}$ SCN neurons.

Fluorescence intensity versus firing rate in individual *Per1*$^{-/-}$;*Per2*$^{-/-}$ SCN neurons recorded throughout the day in DD are not correlated (n = 65 cells, 6 mice; Pearson's r, $r^2 = 0.0036$, $p = 0.5146$).

Discussion

To investigate the precise relationship between gene expression rhythms and circadian electrical activity in the SCN, and to determine which clock genes are involved in this link, we recorded from and subsequently performed real-time fluorescence imaging of the state of the molecular clockworks in *Per1*::GFP^{+} SCN neurons throughout the circadian day. We found that there exists a stable phase relationship between E-box-driven gene expression and spontaneous firing rate in individual *Per1*$^{+/+}$; *Per2*$^{+/+}$ SCN neurons, with firing rate rhythms consistently phase leading gene expression rhythms by about 2.2 hours. In SCN neurons from *Per1*$^{-/-}$; *Per2*$^{+/+}$ mice in which the core clock gene *Per1* is knocked out – which, importantly, maintain circadian rhythmicity in the molecular clockworks and locomotor behavior (Bae et al., 2001; Liu et al., 2007 – but see Pendergast et al., 2009; Ruan et al., 2012) – this relationship is abolished. However, in SCN neurons from *Per1*$^{+/+}$; *Per2*$^{-/-}$ mice, in which *Per2*, a close homolog of *Per1*, is knocked out, the phase relationship between circadian rhythms in gene expression and firing rate is restored. These results therefore demonstrate that *Per1* is necessary for linking the molecular clockworks to membrane electrical activity.

The finding that there exists a stable phase relationship between E-box driven gene expression and spontaneous firing rate across an entire circadian day expands upon previous studies from our lab showing that there is a correlation between these two components of the circadian clock at midday and after a phase-resetting light pulse at night (Kuhlman et al., 2003; Quintero et al., 2003). Here we not only show that this correlation persists in neurons sampled across 24 hours, but that gene expression rhythms consistently lag behind spontaneous firing rate rhythms. Importantly, *Per1*::GFP expression in a wild-type animal peaks at approximately the same time as the peak of native PER1 protein expression (which peaks approximately two to four hours after the peak of native *Per1* mRNA expression; LeSauter et al., 2003), and our observed time of peak spontaneous firing rate is also consistent with that found in other studies (Green and Gillette, 1982; Meijer et al., 1997 – but see Belle et al., 2009). Thus, by simultaneously measuring the state of the molecular clock and electrical activity in individual neurons, we were able to for the first time determine the instantaneous circadian relationship between these two key components of the circadian clock in individual SCN neurons. This newly established single-cell relationship therefore predicts that an increase in firing rate precedes an increase in translation of PER1 (although it may occur concurrently with the transcription of *Per1* itself). The traditional multi-component model of the mammalian circadian clock proposes that firing rate is solely an output or readout of the state of the molecular clock; however, these results suggest that firing rate, peaking ~2.2 hours before

the peak of GFP fluorescence and thus the peak of PER1 translation, must in some way be an input onto the molecular clock.

How, though, could an ostensible output of the molecular clock instead affect the state of the molecular clock itself? The most likely candidate for this connection is yet another component of neuronal circadian rhythms – daily oscillations in intracellular second messengers, including Ca^{2+} and cAMP (Brancaccio et al., 2013). Some SCN neurons can exhibit spike frequency rhythms on genetic backgrounds in which gene cycling is absent, suggesting that the ionic mechanisms at the membrane can oscillate in a circadian manner without an intact TTFL (Nakamura et al., 2002). Similarly, genetic or physiological blockade of the spike frequency rhythm in *Drosophila* (dORK channel) or mouse (TTX) leads to run-down of clock gene cycling in clock neurons (Nitabach et al., 2002; Yamaguchi et al., 2003). This is likely due to blunting of cellular calcium rhythms as chelation of extracellular Ca^{2+} or buffering intracellular Ca^{2}, also blunts gene expression rhythms (Lundkvist et al., 2005; Harrisingh et al., 2007). Finally, another intracellular messenger, cAMP, which in SCN neurons is primarily controlled by VIP intercellular communication through VPAC2 receptors, is also critical for sustained gene and spike rhythms (Harmar et al., 2002; Aton et al., 2005; Maywood et al., 2006).

Our results also demonstrate that the core clock gene *Per1* is necessary for the persistence of the single-cell correlation between the molecular clock and circadian rhythms in firing rate. While in wild-type SCN neurons from *Per1*::GFP mice this correlation is clearly evident, in SCN neurons in which *Per1* is knocked out, this correlation is abolished. However, in neurons where *Per2* is knocked out, and, importantly, *Per1* is present, this correlation is reestablished. Whereas GFP fluorescence intensity reliably predicts firing rate (and vice versa) in $Per1^{+/+}; Per2^{+/+}$ and $Per1^{+/+}; Per2^{-/-}$ SCN neurons, there is no predictive relationship between fluorescence intensity and firing rate in $Per1^{-/-}; Per2^{+/+}$ neurons. A brightly-fluorescent $Per1^{-/-}; Per2^{+/+}$ neuron is just as likely to have a high or low firing rate, and, conversely, a high firing rate neuron is just as likely to be brightly- or dimly-fluorescent. Thus, not only do these results demonstrate that *Per1* is necessary for a single-cell molecular clockworks/membrane relationship, but also that *Per2* does not compensate, suggesting disparate roles for the homologous clock genes *Per1* and *Per2*. Previous studies have shown differing roles for these two clock genes in their effect on the molecular clockworks (Bae et al., 2001; Schwartz et al., 2011), firing rate rhythms (Sugiyama et al., 2004), and locomotor behavior (Spoelstra et al., 2004), and, intriguingly, the constitutive overexpression of *Per1* impairs both molecular and behavioral rhythms (Numano et al., 2006) . Thus, these results expand upon the role of *Per1* in the generation of circadian rhythms and demonstrate that *Per1* in and of itself is key for the link between the molecular clockworks and the membrane in individual neurons of the SCN.

Chapter Acknowledgments

This work was supported by US National Institutes of Health grants R01 EY015815 (D.G.M.), T32 MH064931 (J.R.J.) and F31 NS082213 (J.R.J.).

Author Contributions

J.R.J. and D.G.M. prepared the paper. J.R.J. analyzed data. J.R.J. performed all experiments. J.R.J. and D.G.M. designed experiments.

CHAPTER IV

Conclusions

Through the work presented in this dissertation, I addressed the important question of the relationship between gene networks, neurons, circuits, and behavior using the brain's biological clock – the suprachiasmatic nucleus – as a model system (**Fig. IV-1**).

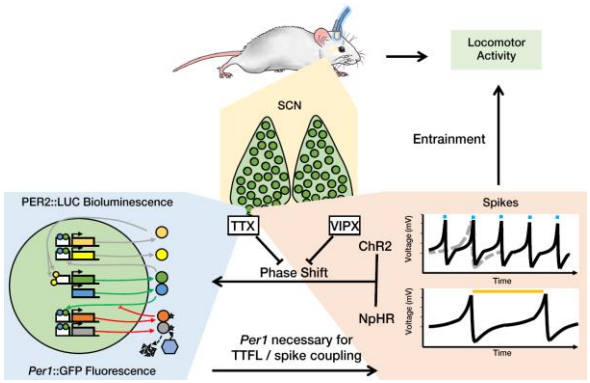

Figure IV-1 Linking molecular, electrical, and behavioral rhythms in the brain's biological clock.

In **Chapter II**, I combined *in vivo* and *in vitro* optogenetics with real-time bioluminescence imaging of the molecular clockworks and locomotor activity monitoring to demonstrate that manipulating firing rate can reset the molecular clockworks and entrain behavior. Unexpectedly, optogenetic resetting required both action potentials (as opposed to subthreshold depolarization) and VIPergic network communication. From this, I concluded that firing rate in and of itself is fundamental to circadian pacemaking. To investigate this relationship from the other direction, in **Chapter III**, I used visually-targeted patch-clamp electrophysiological recording combined with real-time GFP fluorescence imaging of clock gene expression to demonstrate that the core clock gene *Per1* is necessary for the persistence of the relationship between the molecular clockworks and electrical activity. Thus, together, these results suggest that there is a bidirectional relationship between clock gene expression and circadian electrical activity such that firing rate is both an output of and an input onto the molecular clockworks.

How, though, can membrane electrical activity in SCN neurons feed onto the molecular clockworks? Intracellular calcium levels are likely a principal mediator of this relationship, as levels of calcium within SCN neurons also exhibit circadian rhythms which peak at approximately CT 7.2 as measured by the genetically encoded calcium indicators Yellow Cameleon 3.60 or GCaMP3 (Enoki et al., 2012; Brancaccio et al., 2013). Importantly, the phase of intracellular calcium rhythms precedes *Per* and *Cry* gene expression rhythms as

read out by *Per1-luc*, *Cry1-luc*, or PER2::LUC. According to my results in *Per1*::GFP SCN neurons, the peak of intracellular calcium therefore falls between the peak of firing rate rhythms (ZT 6.8) and the peak of gene expression rhythms (ZT 9). Indeed, Ryosuke Enoki presented new data at the 2014 Society for Neuroscience meeting in which he used simultaneous multielectrode array recording, calcium imaging, and bioluminescence imaging to determine that firing rate peaks before intracellular calcium rhythms, which in turn peaks before PER2::LUC bioluminescence (Brancaccio et al., 2014). The daily rhythm of calcium in SCN neurons as measured by the calcium-sensitive dye fura-2 is blunted by the application of TTX or L-type calcium blockers (Colwell, 2000), and, importantly, the *in vitro* stimulation of the retinohypothalamic tract induces a rise in intracellular calcium levels (Irwin and Allen, 2010), which again supports the hypothesis that there is a connection between intracellular calcium and electrical activity. However, other studies have shown that ryanodine-sensitive intracellular calcium rhythms peak before firing rate rhythms and persist in the presence of TTX (Ikeda et al., 2003).

Whatever the actual temporal order of calcium and firing rate rhythms in the SCN, it is clear that intracellular calcium itself is able to drive the molecular clockworks, as blocking calcium influx reversibly blocks gene expression rhythms in both the mammalian SCN and in *Drosophila* (Lundkvist et al., 2005; Harrisingh et al., 2007). An increase in intracellular calcium, such as that due to influx through L-type calcium channels during neural activity, is an ubiquitous second messenger. Intracellular calcium is able to activate a calcium/calmodulin-dependent protein kinase to in turn activate CREB (calcium/cAMP response element binding protein), which then binds to the CRE elements of the *Per* promoter to activate clock gene transcription (Brancaccio et al., 2014). Calcium levels within SCN neurons are also modulated by VIP-mediated signaling, as the VPAC2 receptor is a G protein-coupled receptor that increases intracellular calcium levels through a Gq pathway. Importantly, VIP also increases levels of intracellular cAMP (cyclic adenosine monophosphate) through a Gs pathway that increases the activity of adenylyl cyclase (Brancaccio et al., 2013). cAMP can, in turn, activate protein kinase A or EPAC (exchange protein activated by cAMP) to activate CREB, which again binds to the CRE elements of the *Per* promoter. Both cAMP levels and CRE element transcriptional activity are rhythmic in the SCN, and indeed, inhibiting adenylyl cyclase (and thus lowering intracellular levels of cAMP) lengthens the period of PER2::LUC bioluminescence (O'Neill et al., 2008). The ability of VIP to mediate an increase in calcium or cAMP is especially important in light of my data in **Chapter II** that suggests that the presence of VIP is necessary to optogenetically reset the molecular clockworks (Jones et al., 2015).

Whereas intracellular signaling through calcium and/or cAMP is likely the mechanism by which membrane events are translated to the molecular clockworks within SCN neurons, surprisingly, much less is known about how gene expression rhythms can, in turn, influence circadian electrical activity. As previously mentioned, a number of knockout and

correlational studies (and, indeed, my own work presented in **Chapter III**) strongly suggest that there is a direct link between these components of the mammalian circadian system; however, there has been much less research on a potential mechanism that would allow for this relationship. One possibility is that the molecular clockworks works as a transcriptional regulator of various ion channels whose conductances contribute to rhythmic firing rate SCN neurons (Meijer and Michel, 2015). Indeed, a variety of ion channels found in the SCN exhibit transcriptional rhythms, including calcium-activated BK potassium channels, TASK1 and TASK2 twin-pore potassium channels, and L-type calcium channels (Colwell, 2011). The transcriptional rhythmicity of these channels may be regulated by the CLOCK/BMAL1 heterodimer acting on E-box elements of their promoters. Although the precise half-life of ion channel proteins within the SCN is difficult to determine, it is likely that the synthesis and degradation of ion channels (via endocytosis and subsequent ubiquitination) with a half-life of between two and 12 hours could generate the rhythmic currents that are the hallmark of SCN neurons (Meijer and Michel, 2015).

Another way the molecular clockworks could influence SCN electrical activity is through the trafficking of ion channels, as opposed to their synthesis and degradation *per se*. The insertion or removal of ion channels from the plasma membrane, such as AMPA receptors that are trafficked to and away from the membrane during long-term potentiation or long-term depression, respectively, is a common feature of many types of neural activity (Derkach et al., 2007). As such, it is possible that electrical activity and firing rate in SCN neurons could also be modulated by the trafficking of various ion channels, such as Kv3.1 channels, which are rhythmically expressed in the SCN and are bound to the kinesin 1 heavy chain and thus can be directly targeted to the membrane (Itri et al., 2005; Xu et al., 2010). Finally, the most likely mechanism by which the molecular clockworks influences the membrane (or, perhaps, the mechanism that accounts for the majority of this influence) is the post-translational modification of ion channels themselves. This post-translational modification may occur through the action of various clock-controlled signaling and second messenger pathways, such as those involving calcium and cAMP. Indeed, the ryanodine receptor (particularly RYR2), which mediates the release of intracellular calcium from the endoplasmic reticulum, is rhythmically expressed in the SCN and the promoter region of *RYR2* contains E-box elements for CLOCK/BMAL1 heterodimer-mediated activation (Pfeffer et al., 2009). In other brain regions, calcium and cAMP mediate kinase- and phosphatase-dependent changes in the phosphorylation state, and thus the conductance, of ion channels (Park et al., 2008). As such, it is likely that rhythmic kinase and phosphatase activity regulated by daily rhythms in intracellular calcium and cAMP can open and close ion channels involved in setting the firing rate of SCN neurons.

The work presented in this dissertation aimed to understand the links between the different components of the mammalian multi-component circadian system and, as such, can be considered "basic" science. However, expanding our fundamental knowledge of how circadian rhythms work in a healthy brain is essential for understanding the translational nature of how the dysregulation of circadian clock components may negatively impact human health. A variety of sleep disorders and other diseases have a large circadian component, including those that are heritable and thus have a genetic basis. One of such disorders is familial advanced sleep phase syndrome (FASPS), in which patients have persistent three or four hour advances sleep onsets due to a missense mutation in the human *Per2* gene; another is delayed sleep phase syndrome (DSPS), in which patients have a chronic inability to fall asleep due to one of a variety of core clock gene polymorphisms, including mutations in *Clock*, *casein kinase 1ϵ*, or *Per3* (Toh et al., 2001; von Schantz, 2008). Importantly, clock gene mutations have also been implicated in neuropsychiatric and affective disorders in both mice and humans, including alcohol consumption (*Per2*), bipolar disorder (*Clock*; Takahashi et al., 2008). My results from **Chapter III** suggesting that *Per1* is necessary for the link between the molecular clockworks and the membrane are particularly interesting in light of *Per1*'s association with bipolar disorder, schizophrenia, and autism as determined by a number of genome-wide association studies (GWAS; Nicholas et al., 2007; McCarthy et al., 2012).

A number of other widespread circadian-related maladies such as jet lag or shift work disorder (or, possibly, seasonal affective disorder) are fundamentally due to the SCN's inability to instantly phase shift or reset in response to light (Lewy et al., 2007; Gamble et al., 2011; Yamaguchi et al., 2013). In **Chapter II**, I found that artificially resetting SCN electrical activity using optogenetics can entrain locomotor activity rhythms *in vivo*; thus, this newfound knowledge of how to reset the SCN could potentially lead to treatment for these disorders. Optogenetics has presently not been implemented in humans, although this possibility is currently being explored by other researchers (Williams and Denison, 2013). A major obstacle that must be overcome for optogenetics to be used in the clinic is that patients would have to undergo invasive surgery to implant an optical fiber and gene therapy to virally-transfect SCN neurons with light-sensitive opsins. However, my finding that circadian behavior can be reset optogenetically could potentially translate to the clinic through "chronopharmacology" – knowing what time of day would be best to take a drug that affects SCN neural activity to reset behavioral rhythms (Dallmann et al., 2014). Thus, the findings and, possibly, technologies presented in this dissertation may ultimately serve to bridge the gap from basic circadian neurophysiology to helping human patients in the clinic.

APPENDIX A

Future directions

Long-term optogenetic stimulation of *ex vivo* SCN slices

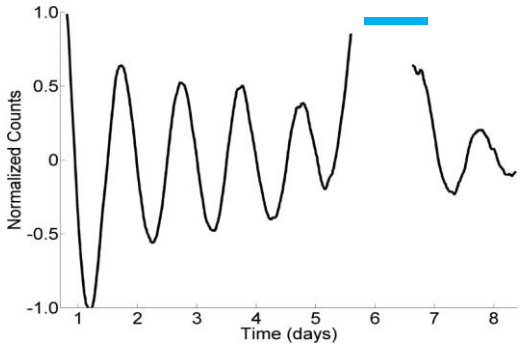

Figure A-1 *Ex vivo* bioluminescence rhythms persist after over 24 hours of ChR2 stimulation.

While my dissertation research shows that one hour of optogenetic stimulation at various times of day is able to reset the molecular clock, it does not address whether firing rate rhythms in and of themselves are necessary for rhythms in the molecular clock. One way to address this would be continuous optogenetic stimulation over a long time scale to eliminate the daily variation in firing rate; **Fig. A-1** shows that such stimulation is possible for up to 24 hours without affecting the bioluminescence output of the molecular clock.

Increasing firing rate *in vivo* restores disrupted behavioral rhythms

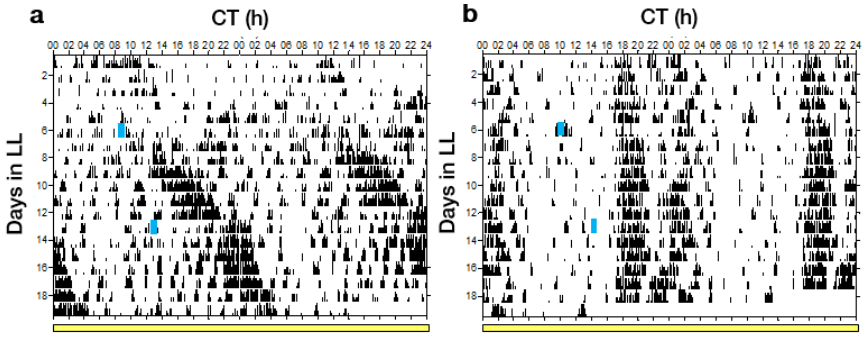

Figure A-2 Locomotor rhythms are restored by optogenetic stimulation in mice raised in constant light.

Some mice born and raised in constant light become behaviorally arrhythmic (Ohta et al., 2005). Curiously, a single one hour pulse of optogenetic stimulation is able to restore locomotor activity rhythms in these arrhythmic animals (**Fig. A-2a**); the same pulses do not affect a control littermate (**Fig. A-2b**).

CLARITY and SeeDB allow the optical clearing of brain tissue

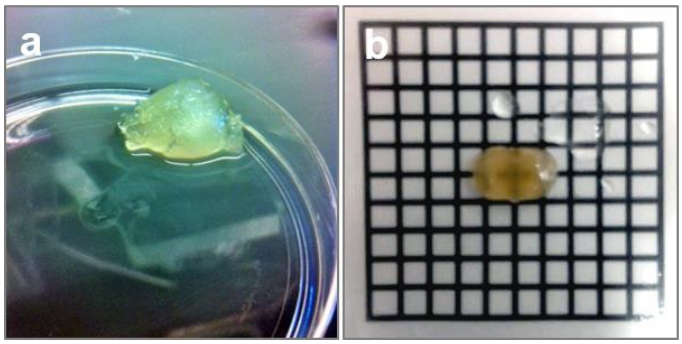

Figure A-3 Optically transparent mouse brains.

The *Per1*::GFP mouse line developed by the McMahon lab provides the unprecedented ability to view the molecular clock state of individual SCN neurons in real time as GFP fluorescence. Importantly, these mice could be used to investigate the four-dimensional (that is, three-dimensional over time) clock gene expression pattern in the SCN. To image the entire SCN, it would need to be optically transparent, and indeed, there are a number of methods available to optically clear brain tissue, such as CLARITY (**Fig. A-3a**; Chung et al., 2013) and SeeDB (**Fig. A-3b**; Ke et al., 2013).

Calcium imaging of SCN neurons

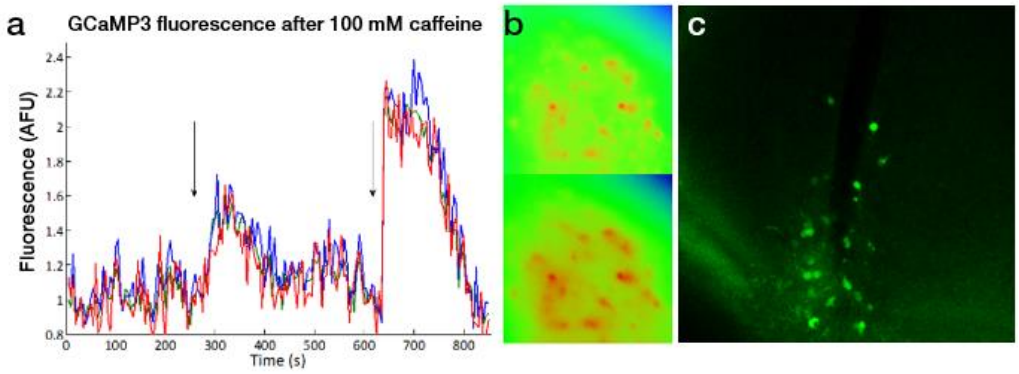

Figure A-4 GCaMP3 fluorescence after caffeine or optogenetic stimulation.

In the SCN, calcium imaging, when integrated over a longer time scale, is essential for measuring intracellular calcium levels in individual neurons (Brancaccio et al., 2013). When imaged over a shorter time scale, calcium imaging can be used as an optical readout of action potentials in the entire network. I have used adeno-associated viruses (AAVs)

encoding the genetically-encoded calcium indicator GCaMP3 to transfect organotypic SCN slices (**Fig. A-4c**) and have shown that GCaMP fluorescence increases in response to both caffeine (**Fig. A-4a**), which is an activator of the ryanodine receptor, and ChR2 stimulation (**Fig. A-4b**). A number of other AAVs for optogenetics, calcium imaging, and voltage imaging (Cao et al., 2013) are stored in the -80°C freezer in the McMahon lab and are listed in **Table D-6**.

Combined single-cell fluorescence imaging and optogenetic manipulation

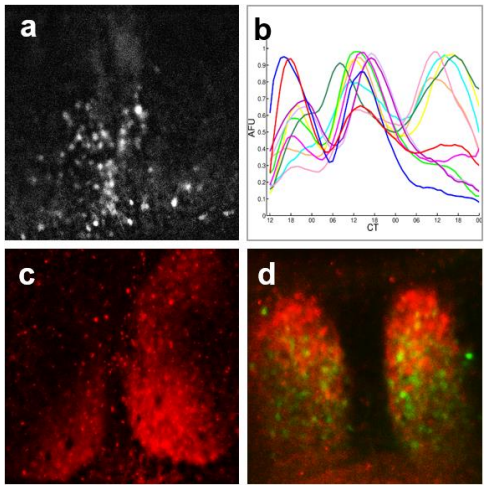

Figure A-5 AAV transfection of the red-shifted opsin C1V1 in *Per1*::GFP SCN slices.

Finally, in **Chapter II**, I demonstrated the effects of optogenetic manipulation on bioluminescence intensity as a readout of the molecular clockworks. However, in these experiments, I measured population bioluminescence from the entire SCN slice. It is important to know how optogenetic resetting affects the single-cell rhythms within the SCN. This can be accomplished through the imaging of PER2::LUC in individual SCN neurons (Evans et al., 2013), or, through the method that I had attempted, the single-cell imaging of *Per1*::GFP neurons (Ciarleglio et al., 2009). **Fig. A-5a** is a confocal image of GFP expression in a cultured SCN slice, and **Fig. A-5b** shows the individual GFP fluorescence rhythms over time. These animals can be virally transfected with an optogenetic construct such as in **Fig. A-5c**, where I used AAV to transfect the red-shifted channelrhodopsin variant C1V1 to minimize spectral overlap (**Fig. A-5d**).

APPENDIX B

Matlab code

Background

First and foremost, I would like to thank Robert Barretto, my post-doctoral mentor during my rotation in Charles Zuker's lab at Columbia. He did not appreciate my use of Excel for graphing and for performing calculations. If I was to succeed as a neuroscientist, I would need to learn how to program, and if I wanted to program, I might as well learn Matlab. And with that, I began a long, grueling process in which I taught myself how to code through brute force. I spent many hours figuratively bashing my head against the keyboard until, slowly yet surely, my programs actually did something. I learned about matrices and arrays, structures and loops; I learned about data acquisition and transistor-transistor logic.

Ultimately, I was able to write code to control a classical conditioning system for a mouse. The mouse would be presented with a tone or a flash of light along with a sweet or bitter tastant, in the hopes that we could condition an aversive licking behavior in response to the tone or light in the absence of the bitter tastant. I used Matlab to control the fluid lines, to generate tones and light flashes, to record video, and to analyze and plot all the collected data; basically, this was a crash course in "how to do everything possible in Matlab." I was able to take my newfound knowledge of Matlab with me to Vanderbilt, where I used Matlab for essentially everything, from automated data analysis to optogenetic stimuli presentation to statistics and figure creation.

Presented in this section are useful Matlab programs (".m files") that I created during my time in graduate school or links to useful programs that I found online, along with a brief description of their purpose and use.

actogramcode.m

This program plots Lumicycle data as a double-plotted actogram.

```
twofour = x.*24;
start = 24;
startpoint = 8;
z = start+startpoint;
endpoint = z+48;
days = [1:10];

for i = 1:length(days);
```

```
array{i} = find(twofour > (z + (days(i)-1).*24) & twofour < ((z +
((days(i)-1).*24))+48));

end

for i = 1:length(days);

% dropzer{i} = ysmooth(array{i})./max(ysmooth(array{i}));
notdropzer{i} = ysmooth(array{i})./max(ysmooth(array{i}));
% notdropzer{i} = y(array{i})./max(y(array{i}));
% dropzer{i}(dropzer{i}<0)=0;

end

figure;
for i = 1:length(days);
h(i) = subplot(length(days),1,i);
ex = twofour(array{i});
y1 = notdropzer{i}+(abs(min(notdropzer{i})+1));
y2 = ones(length(notdropzer{i}),1).*-1.5;
y1 = y1.';
y2 = y2.';
shadedplot(ex,y1,y2,'k','k');
% plot(twofour(array{i}),(notdropzer{i}+abs(min(notdropzer{i}))),'.k')
% plot(twofour(array{i}),(notdropzer{i}),'k','LineWidth',1)
% area(twofour(array{i}),notdropzer{i})
set(gca,'Box','off','XTickLabel',[],'YTickLabel',[],'XTick',((max(twofo
ur(array{i})) - min(twofour(array{i})))/2) +
min(twofour(array{i})),'YTick',[],'YLim',[-1.5
1.5],'XLim',[min(twofour(array{i})) (min(twofour(array{i})+47))]);
% set(gca,'YLim',[-1.5 1.5],'XLim',[min(twofour(array{i}))
max(twofour(array{i}))]);
end

set(gcf,'Color','white');
```

batchprocessfr.m

This program automatically analyzes firing rate data from pCLAMP saved in an Excel format. It requires both xlsread1.m and xlswrite1.m, available at the Mathworks File Exchange.

```
%%  Batch Process Firing Rate
%   This program takes raw spike time data from spiketimes.xlsx and
%   converts them into firing rate histograms for each recorded cell.
It
%   also plots the calculated mean firing rate and standard deviations
in
%   froutput.xls.
```

```
%%
%   This program requires both xlsread1 and xlswrite1, both downloaded
from
%   Mathworks File Exchange.  Place both of those files in the same
file
%   directory as this M file.  Be sure to edit the 'Excel =
%   evalin('base','Excel');' line in each program to read 'Excel =
%   evalin('caller','Excel');' or this program will not work.


%%   Reads from an Excel file organized as follows:
%   Column A, Row 1: DATE (eg. 121010)      Column B, Row 1: etc.
%   Column A, Row 2: CELL NUMBER (eg. 7)    Column B, Row 2: etc.
%   Column A, Row 3: TIME (eg. 1810)        Column B, Row 3: etc.
%   Column A, Rows 4-end: SPIKE TIMES       Column B, Row 4-end: etc.

%% Initializes xlsread1 (faster version of xlsread)
Excel = actxserver ('Excel.Application');
File='C:\Users\Jeff\Dropbox\Matlab\spiketimes.xlsx';   %   Replace with
input file location and extension
if ~exist(File,'file')
    ExcelWorkbook = Excel.Workbooks.Add;
    ExcelWorkbook.SaveAs(File,1);
    ExcelWorkbook.Close(false);
end
Excel.Workbooks.Open(File);
%%  Imports data from Excel and plots histograms
[status,sheets] = xlsfinfo(File);   %   Gets sheet names from Excel
file.


collets = 'A':'Z';  %   Sets up letters corresponding to columns in
Excel file
%   Maximum of 26 cells per sheet, so I recommend separating cells into
%   sheets by date of recording.


subx = 2;   %   How many figures wide you want the combined figure (eg.
2)
suby = 3;   %   How many figures tall you want the combined figure (eg.
3)
pos = 1;    %   Start position for figure placement in combined figure

for i = 1:length(sheets);   %   Looks at each sheet in the Excel file

    for x = 1:length(collets)   %   Looks at all columns (A-Z)
        thiscol = collets(x);
        xlsrange = sprintf('%c4:%c%d', thiscol, thiscol, 10000);    %
Looks at spike times from start to end of given column
%   Need to find a way to replace 10000 with actual end of column
%   range
```

```
        xlsdate = sprintf('%c1:%c1', thiscol, thiscol); %   Looks at
the date in the given column
        xlstime = sprintf('%c3:%c3', thiscol, thiscol); %   Looks at
the time in the given column, eg. A3:A3
        xlscell = sprintf('%c2:%c2', thiscol, thiscol); %   Looks at
the cell number in the given column, eg. A2:A2

%   Sets up a structure containing the firing times, date, time,
%   and cell number for each neuron
        neuron.firing{i} = xlsread1(File,sheets{i},xlsrange);
        neuron.date{i} = xlsread1(File,sheets{i},xlsdate);
        neuron.time{i} = xlsread1(File,sheets{i},xlstime);
        neuron.cell{i} = xlsread1(File,sheets{i},xlscell);

%   Checks to see if column is empty (eg. column Z in a sheet that
%   only has cells in columns A through E)
        if isempty(neuron.firing{i}) == 1;
            neuron.firing{i} = NaN;
        end

        bins(1:length(neuron.firing)) = NaN;    %   Preallocates bins

%   Calculates 1 second bins
        for j = 1:length(neuron.firing);
            bins(j) = ((max(neuron.firing{j})-
min(neuron.firing{j}))/1000);
        end

        for k = 1:length(neuron.firing)

%   Skips cells that don't exist
            if isnan(neuron.firing{k}) == 1;
                continue
            else

%   Calculates firing rate mean and standard deviation
            histomean = mean(hist(neuron.firing{k},bins(k)));
            histostd =  std(hist(neuron.firing{k},bins(k)));

%   Plots histograms for each cell
            m = rem(pos-1,(subx*suby))+1;
            if m == 1;
                figure;
            end
                subplot(suby,subx,m);hist(neuron.firing{k},bins(k))
                axis tight
                xlabel('Time (ms)')
                ylabel('Firing Rate (Hz)')
                legend(['Mean ' num2str(histomean) ' Std '
num2str(histostd)],'Location','SouthOutside')    %   Adds a legend with
the mean and std firing rate
```

```
%   Titles each figure appropriately
                title([num2str(neuron.date{i}) ' '
num2str(neuron.time{i}) ' cell #' num2str(neuron.cell{i})])  %
Outputs "MMDDYY HHMM cell ##"
                final.date{pos} = neuron.date{i};
                final.time{pos} = neuron.time{i};
                final.cell{pos} = neuron.cell{i};
                final.mean{pos} = histomean;
                final.std{pos} = histostd;
                pos = pos + 1;
            end
        end
    end
end
%%  Closes xlsread1
Excel.ActiveWorkbook.Save;
Excel.Quit
Excel.delete
clear Excel

%%  Initializes xlswrite1
Excel = actxserver('Excel.Application');
File = 'C:\Users\Jeff\Dropbox\Matlab\froutput.xls';   %   Replace with
output file location and extension
%   xlswrite1 can only save as .xls, if you try to save as .xlsx, you
will get an error.
if ~exist(File,'file');
    ExcelWorkbook = Excel.workbooks.Add;
    ExcelWorkbook.SaveAs(File,1);
    ExcelWorkbook.Close(false);
end
Excel.Workbooks.Open(File);

%%  Saves data in output Excel file
  for l = 1:(pos-1);
      output.data{l} = [final.date{l} final.time{l} final.cell{l}
final.mean{l} final.std{l}]; % Excel Column A: Date, B: Time, C: Cell#,
D. Mean Firing Rate, E. Std Firing Rate
      finalrange = sprintf('A%d:E%d',l,l);
      xlswrite1(File,output.data{l},'Sheet1',finalrange);
  end

%%  Closes xlswrite1
Excel.ActiveWorkbook.Save;
Excel.Quit
Excel.delete
clear Excel

%%  Initializes xlsread1
Excel = actxserver ('Excel.Application');
File='C:\Users\Jeff\Dropbox\Matlab\froutput.xls';   %   Replace with
output file location and extension
if ~exist(File,'file')
```

```
    ExcelWorkbook = Excel.Workbooks.Add;
    ExcelWorkbook.SaveAs(File,1);
    ExcelWorkbook.Close(false);
end
Excel.Workbooks.Open(File);

%%  Plots firing rate vs. time graph
for n = 1:(pos-1)
xlstime = sprintf('B%d:B%d', n, n);
timing = num2str(xlsread1(File,'Sheet1', xlstime));
timing = sprintf('%04d',str2num(timing));
%%%
graph.dectime{n} = (60*str2double(timing([1 2])) + str2double(timing([3
4])))/1440; %   Reads and converts HHMM military time to decimal time
(fraction of 24 hours)
    if isnan(graph.dectime{n})
        continue
    else
%%%

xlsfr = sprintf('D%d:D%d', n, n);
graph.fr{n} = xlsread1(File,'Sheet1',xlsfr);    %   Reads firing rate
from Excel file
    if isnan(graph.fr{n})
        continue
    else
xlserr = sprintf('E%d:E%d', n, n);
graph.err{n} = xlsread1(File,'Sheet1',xlserr);  %   Reads standard
deviation from Excel file
    if isnan(graph.err{n})
        continue
    else
    end
    end
end
end

figure;
%   Plots a graph of firing rate (Hz, Y axis) versus time (hrs, X
axis),
%   with standard deviation error bars
for o = 1:(pos-1)
    errorbar(graph.dectime{o},graph.fr{o},graph.err{o},'ok')
    hold on
end

set(gca,'XTick',0:0.05:1)
set(gca,'XTickLabel',[0000 0112 0224 0336 0448 0600 0712 0824 0936 1048
1200 1312 1424 1536 1648 1800 1912 2024 2136 2248 2400])
axis([-.01 1.01 0 20])
xlabel('Time (hr)')
ylabel('Firing Rate (Hz)')
title('Firing Rate vs. Time')
```

```
ylims=get(gca,'ylim');
xlims=get(gca,'xlim');
xrange=xlims(2)-xlims(1);
yrange=ylims(2)-ylims(1);
xpos=xlims(1)+0.9*xrange;
ypos=ylims(1)+0.95*yrange;
text(xpos,ypos,['n = ' num2str(pos-1)],'BackgroundColor',[1 1 1])    %
Displays total cell count on graph

%%  Closes xlsread1
Excel.ActiveWorkbook.Save;
Excel.Quit
Excel.delete
clear Excel

%   If the program causes an error, you may have instances of Excel
open
%   because Matlab did not have a chance to close them.  This could
mess up
%   further instances of this program, so CTRL ALT DEL and close Excel
%   manually.
```

convtime.m

This program converts 24 hour time into a single number.

```
% This program takes time in 24-hour time format HHMM and converts it
to a single number.
% Ex. 1:15 PM = 1315 = 795

for i = 1:length(times);
    b = num2str(times(i));
    if length(b) == 1;
        hrs = 0;
        mins = str2double(b([1]));
        newtime.hrs{i} = hrs.*60;
        newtime.mins{i} = mins;
        newtime.newtime{i} = newtime.hrs{i} + newtime.mins{i};
    elseif length(b) == 2;
        hrs = 0;
        mins = str2double(b([1 2]));
        newtime.hrs{i} = hrs.*60;
        newtime.mins{i} = mins;
        newtime.newtime{i} = newtime.hrs{i} + newtime.mins{i};
    elseif length(b) == 3;
        hrs = str2double(b(1));
        mins = str2double(b([2 3]));
        newtime.hrs{i} = hrs.*60;
        newtime.mins{i} = mins;
        newtime.newtime{i} = newtime.hrs{i} + newtime.mins{i};
    else
        hrs = str2double(b([1 2]));
```

```
        mins = str2double(b([3 4]));
        newtime.hrs{i} = hrs.*60;
        newtime.mins{i} = mins;
        newtime.newtime{i} = newtime.hrs{i} + newtime.mins{i};
    end
end
```

ledcontroller.m

This program controls the LED for brain slice optogenetic stimulation.

```
%%% LED CONTROLLER v 1.0, 2/8/11
%%% By Jeff Jones, Vanderbilt University
% This program sends a TTL pulse to an LED control to control the speed
and
% duration of LED flashes.

function varargout = ledcontroller(varargin)
%   Begin initialization code - DO NOT EDIT
gui_Singleton = 1;
gui_State = struct('gui_Name',       mfilename, ...
                   'gui_Singleton',  gui_Singleton, ...
                   'gui_OpeningFcn', @ledcontroller_OpeningFcn, ...
                   'gui_OutputFcn',  @ledcontroller_OutputFcn, ...
                   'gui_LayoutFcn',  [] , ...
                   'gui_Callback',   []);
if nargin && ischar(varargin{1})
    gui_State.gui_Callback = str2func(varargin{1});
end

if nargout
    [varargout{1:nargout}] = gui_mainfcn(gui_State, varargin{:});
else
    gui_mainfcn(gui_State, varargin{:});
end
%   End initialization code - DO NOT EDIT

%   Executes just before ledcontroller is made visible.
function ledcontroller_OpeningFcn(hObject, eventdata, handles,
varargin)

%   This function has no output args, see OutputFcn.
%   hObject    handle to figure
%   eventdata  reserved - to be defined in a future version of MATLAB
%   handles    structure with handles and user data (see GUIDATA)
%   varargin   command line arguments to ledcontroller (see VARARGIN)

%   Choose default command line output for ledcontroller
handles.output = hObject;

%   Update handles structure
```

```
%   Adds a toolbar to the figure
%   set(hObject,'toolbar','figure');

%   Initializes radio button toolbar
set(handles.buttons,'SelectionChangeFcn',@buttons_SelectionChangeFcn);

%   Stores data in the figure
guidata(hObject, handles);

%   Initializes digital I/O line
%   Select device:  Rig Comp Dev1, Lab Comp Dev2
dio = digitalio('nidaq','Dev1');
addline(dio,0,'out');

%   Outputs from this function are returned to the command line.
function varargout = ledcontroller_OutputFcn(hObject, eventdata,
handles)
%   varargout  cell array for returning output args (see VARARGOUT);
%   hObject    handle to figure
%   eventdata  reserved - to be defined in a future version of MATLAB
%   handles    structure with handles and user data (see GUIDATA)

%   Get default command line output from handles structure
varargout{1} = handles.output;

function input1_on_Callback(hObject, eventdata, handles)
%%% This function controls the ON editbox

%   hObject    handle to input1_on (see GCBO)
%   eventdata  reserved - to be defined in a future version of MATLAB
%   handles    structure with handles and user data (see GUIDATA)

%   Converts the ON editbox string into a number
input = str2double(get(hObject,'String'));

%   Checks to see if ON editbox is empty; if so, defaults to zero
if (isempty(input))
     set(hObject,'String','0')
end

%   Stores data in the figure
guidata(hObject, handles);

function input1_on_CreateFcn(hObject, eventdata, handles)
%%% This function controls the ON editbox

%   hObject    handle to input1_on (see GCBO)
%   eventdata  reserved - to be defined in a future version of MATLAB
%   handles    empty - handles not created until after all CreateFcns
called
```

```
%   Sets background to Windows default (white)
if ispc && isequal(get(hObject,'BackgroundColor'),
get(0,'defaultUicontrolBackgroundColor'))
    set(hObject,'BackgroundColor','white');
end

function input2_off_Callback(hObject, eventdata, handles)
%%% This function controls the OFF editbox

%   hObject    handle to input2_off (see GCBO)
%   eventdata  reserved - to be defined in a future version of MATLAB
%   handles    structure with handles and user data (see GUIDATA)

%   Converts the OFF editbox string into a number
input = str2double(get(hObject,'String'));

%   Checks to see if OFF editbox is empty; if so, defaults to zero
if (isempty(input))
     set(hObject,'String','0')
end

%   Stores data in the figure
guidata(hObject, handles);

function input2_off_CreateFcn(hObject, eventdata, handles)
%%% This function controls the OFF editbox

%   hObject    handle to input2_off (see GCBO)
%   eventdata  reserved - to be defined in a future version of MATLAB
%   handles    empty - handles not created until after all CreateFcns
called

%   Sets background to Windows default (white)
if ispc && isequal(get(hObject,'BackgroundColor'),
get(0,'defaultUicontrolBackgroundColor'))
    set(hObject,'BackgroundColor','white');
end

function durationedit_Callback(hObject, eventdata, handles)
%%% This function controls the DURATION editbox

%   hObject    handle to durationedit (see GCBO)
%   eventdata  reserved - to be defined in a future version of MATLAB
%   handles    structure with handles and user data (see GUIDATA)

%   Converts the DURATION editbox string into a number
input = str2double(get(hObject,'String'));

%   Checks to see if DURATION editbox is empty; if so, defaults to zero
if (isempty(input))
```

```
     set(hObject,'String','0')
end

%   Stores data in the figure
guidata(hObject, handles);

%   Executes during object creation, after setting all properties.
function durationedit_CreateFcn(hObject, eventdata, handles)
%%% This function controls the DURATION editbox

%   hObject    handle to durationedit (see GCBO)
%   eventdata  reserved - to be defined in a future version of MATLAB
%   handles    empty - handles not created until after all CreateFcns
called

%   Sets background to Windows default (white)
if ispc && isequal(get(hObject,'BackgroundColor'),
get(0,'defaultUicontrolBackgroundColor'))
    set(hObject,'BackgroundColor','white');
end

function start_Callback(hObject, eventdata, handles)
%%% This function controls the START pushbutton

%   hObject    handle to start (see GCBO)
%   eventdata  reserved - to be defined in a future version of MATLAB
%   handles    structure with handles and user data (see GUIDATA)

%   Reads the pulse DURATION, ON time, and OFF time
duration = get(handles.durationedit,'String');
a = get(handles.input1_on,'String');
b = get(handles.input2_off,'String');

%   Calculates the frequency from the ON and OFF time
ontime = str2double(a);
offtime = str2double(b);
total = ontime + offtime;
freq = num2str(1/total);

%   Calculates the number of ON OFF periods for a given DURATION
numofperiods = round(str2double(freq)*str2double(duration));
durationperiod = str2double(duration);
if durationperiod == 0;
    return
end

%   Initializes digital I/O line
dio = digitalio('nidaq','Dev1');
addline(dio,0,'out');

%   Initializes functions
```

```
%   LIGHT ON
    if offtime == 0;
        set(dio, 'TimerPeriod', durationperiod);
        set(dio, 'TimerFcn', {@const, numofperiods, ontime});
        set(dio, 'UserData', 0);
        putvalue(dio.Line(1), 1);
        start(dio);
%   LIGHT PULSES
    else
        set(dio, 'TimerPeriod', offtime);
        set(dio, 'TimerFcn', {@puton, numofperiods, ontime, offtime});
        set(dio, 'UserData', 0);
        putvalue(dio.Line(1), 0);
        start(dio);
    end

%  Executes ON PULSES
    function puton(obj, str, numofperiods, ontime, offtime)
        obj.TimerFcn = {@putoff, numofperiods, ontime, offtime,};
        obj.TimerPeriod = offtime;
        putvalue(obj.Line(1), 1);
%   Ends function when DURATION met
        if (obj.UserData == numofperiods)
            obj.TimerFcn = ' ';
            putvalue(obj.Line(1), 0);
            stop(obj);
        end
        obj.UserData = obj.UserData +1;

%   Executes OFF PULSES
     function putoff(obj, str, numofperiods, ontime, offtime)
        obj.TimerFcn = {@puton, numofperiods, ontime, offtime};
        obj.TimerPeriod = ontime;
        putvalue(obj.Line(1), 0);

%   Executes LIGHT ON
    function const(obj, str, numofperiods, ontime)
        putvalue(obj.Line(1), 0);
        stop(obj);

function manualtoggle_Callback(hObject, eventdata, handles)
%%% This function controls the MANUAL togglebutton

%   hObject    handle to manualtoggle (see GCBO)
%   eventdata  reserved - to be defined in a future version of MATLAB
%   handles    structure with handles and user data (see GUIDATA)

%   Initializes digital I/O line
dio = digitalio('nidaq','Dev1');
addline(dio,0,'out');

%   Checks to see if the togglebutton is pressed
```

```
isPushed = get(hObject,'Value');

%   Turns light ON when pressed
if isPushed
    set(handles.ticbox,'String','...');
    tic
    set(hObject, 'String', 'ON');
    putvalue(dio,1);
%   Turns light OFF when pressed again, reports time pressed
else
    set(handles.ticbox,'String',toc);
    set(hObject, 'String', 'OFF');
    putvalue(dio,0);
end

function update_Callback(hObject, eventdata, handles)
%%% This function controls the UPDATE pushbutton

%   hObject    handle to update (see GCBO)
%   eventdata  reserved - to be defined in a future version of MATLAB
%   handles    structure with handles and user data (see GUIDATA)

%   Reads the pulse ON time and OFF time
a = get(handles.input2_off,'String');
b = get(handles.input1_on,'String');

%   Calculates the frequency from the ON and OFF times
total = str2double(a) + str2double(b);
freq = num2str(1/total);

%   Displays the frequency in Hz
set(handles.output_freq,'String',freq);

%   Selects current axes
axes(handles.output_axes)
cla(handles.output_axes)

%   Plots the waveform of the ON and OFF pulses
hold on
for i = 0:((1/(str2double(a)+str2double(b)))-1)
    line([(i*str2double(b)+i*str2double(a))
((i+1)*str2double(b)+i*str2double(a))],[0 0])
    line([((i+1)*str2double(b)+i*str2double(a))
((i+1)*str2double(b)+i*str2double(a))],[1 0])
    line([((i+1)*str2double(b)+i*str2double(a))
((i+1)*str2double(b)+(i+1)*str2double(a))],[1 1])
    line([((i+1)*str2double(b)+(i+1)*str2double(a))
((i+1)*str2double(b)+(i+1)*str2double(a))],[1 0])
end
hold off

%   Sets the axes dimensions, turns off the axes background
```

```
axis([-.05 1.05 -.05 1.05])
axis off

%   Stores data in the figure
guidata(hObject, handles);

%   Executes during object creation, after setting all properties.
function ticbox_CreateFcn(hObject, eventdata, handles)
%%% This function controls the TICBOX editbox

%   hObject    handle to ticbox (see GCBO)
%   eventdata  reserved - to be defined in a future version of MATLAB
%   handles    empty - handles not created until after all CreateFcns
called

%   Sets background to Windows default (white)
if ispc && isequal(get(hObject,'BackgroundColor'),
get(0,'defaultUicontrolBackgroundColor'))
    set(hObject,'BackgroundColor','white');
end

function buttons_SelectionChangeFcn(hObject, eventdata)
%%% This function controls the RADIO BUTTON PANEL

%   Retrieves figure data
handles = guidata(hObject);

%   Switch function so that only one button can be pressed at a time
%   Gets tag of current object
switch get(eventdata.NewValue,'Tag')
%   Sets ON and OFF pulses to 1 and 0 when ON radio button is selected
    case 'onbutton'
        set(handles.input1_on,'String','1');
        set(handles.input2_off,'String','0');

%   Sets ON and OFF pulses to 0.5 and 0.5 when 1 Hz radio button is
%   selected
    case 'onehz'
      set(handles.input1_on,'String','0.5');
      set(handles.input2_off,'String','0.5');

%   Sets ON and OFF pulses to 0.1 and 0.1 when 5 Hz radio button is
%   selected
    case 'fivehz'
      set(handles.input1_on,'String','0.1');
      set(handles.input2_off,'String','0.1');

%   Sets ON and OFF pulses to 0.05 and 0.05 when 10 Hz radio button is
%   selected
    case 'tenhz'
      set(handles.input1_on,'String','0.05');
      set(handles.input2_off,'String','0.05');
```

```
%   Execute if none of the above apply
    otherwise

end

%   Stores data in the figure
guidata(hObject, handles);
```

phaseshifter.m

This program analyzes Lumicycle data for phase shifts occurring after optogenetic stimulation by extrapolating the data past the time of stimulation.

```
%% Defines x (time) and y (count) values from array a
x = a(:,1);
y = a(:,2);

%% Smooths counts using a loess filter
ysmooth = smooth(y,(length(x)./max(x)),'sgolay');

%% Finds peaks and troughs of smoothed curve
[maxsmoothloc] = peakfinder(ysmooth,1,[],1);
[minsmoothloc] = peakfinder(ysmooth,1,[],-1);

%% Plots smoothed curve
% % % Blue
plot(x,ysmooth,'Color',[(0/255) (176/255) (240/255)],'LineWidth',10)
% Yellow
% plot(x,ysmooth,'Color',[(255/255) (192/255) (0/255)],'LineWidth',10)
hold on

%% Plots max and min lines of smoothed curve
for i = 1:length(maxsmoothloc)
% %     % Blue
    line([x(maxsmoothloc(i)) x(maxsmoothloc(i))],[-150
150],'Color',[(0/255) (176/255) (240/255)],'LineStyle','--
','LineWidth',2)
%     Yellow
%     line([x(maxsmoothloc(i)) x(maxsmoothloc(i))],[-150
150],'Color',[(255/255) (192/255) (0/255)],'LineStyle','--
','LineWidth',2)
end
for j = 1:length(minsmoothloc)
% %     % Blue
    line([x(minsmoothloc(j)) x(minsmoothloc(j))],[-150
150],'Color',[(0/255) (176/255) (240/255)],'LineStyle','--
','LineWidth',2)
%     Yellow
```

```
%     line([x(minsmoothloc(j)) x(minsmoothloc(j))],[-150
150],'Color',[(255/255) (192/255) (0/255)],'LineStyle','--
','LineWidth',2)
end
hold on

%% Finds where stimulation time occurred
tenderv = abs(diff(y))>(0.5*(max(diff(y))-min(diff(y))));
val = find(tenderv==1);

valbig = find(val>100);
pretime = x(1:val(valbig(1)));
precount = y(1:val(valbig(1)));

%% Fits a damped sine wave to the data from t = 0 to t = stimulation
model = fittype(@(A,f,phi,z,x) (A.*cos(f*x + phi).*exp(-z*x)));
fitobject = fit(pretime,precount,model);

% Plots predicted curve
pred = fitobject.A.*cos(fitobject.f*x+fitobject.phi).*exp(-
fitobject.z*x);
hold on
plot(x,pred,'Color',[(0/255) (0/255) (0/255)],'LineWidth',10);
hold on

% Finds max and min lines of predicted curve
[maxpred] = peakfinder(pred,1,[],1);
[minpred] = peakfinder(pred,1,[],-1);
hold on
for i = 1:length(maxpred)
    line([x(maxpred(i)) x(maxpred(i))],[-150 150],'Color',[(0/255)
(0/255) (0/255)],'LineStyle','--','LineWidth',2)
end
for j = 1:length(minpred)
    line([x(minpred(j)) x(minpred(j))],[-150 150],'Color',[(0/255)
(0/255) (0/255)],'LineStyle','--','LineWidth',2)
end

% Plots raw data
hold on
plot(x,y,'.k');

% Sets axes
boundsup = ceil(max(precount)./10).*10;
boundsdown = floor(min(precount)./10).*10;

axis([0 ceil(max(x)) boundsdown boundsup]);

% Determines phase shift
% % phi = (x(maxpred) -

% Determines predicted POST peaks and troughs
```

```
posttime = x;

posttime(1:length(pretime)) = [];

predpost = fitobject.A.*cos(fitobject.f*posttime+fitobject.phi).*exp(-
fitobject.z*posttime);
% % hold on
% % plot(posttime,predpost,'Color','r','LineWidth',10);
% % hold on

[maxpostpred] = peakfinder(predpost,1,[],1);
[minpostpred] = peakfinder(predpost,1,[],-1);

% % hold on
% % for i = 1:length(maxpostpred)
% %     line([posttime(maxpostpred(i)) posttime(maxpostpred(i))],[-100
100],'Color','r','LineStyle',':')
% % end
% % for j = 1:length(minpostpred)
% %     line([posttime(minpostpred(j)) posttime(minpostpred(j))],[-100
100],'Color','r','LineStyle',':')
% % end

% Determines actual POST peaks and troughs

ysmoothpost = ysmooth;

ysmoothpost(1:(length(pretime))) = [];

[maxpostsmooth] = peakfinder(ysmoothpost,1,[],1);
[minpostsmooth] = peakfinder(ysmoothpost,1,[],-1);

% % hold on
% % for i = 1:length(maxpostsmooth)
% %     line([posttime(maxpostsmooth(i)) posttime(maxpostsmooth(i))],[-
100 100],'Color','b','LineStyle',':')
% % end
% % for j = 1:length(minpostsmooth)
% %     line([posttime(minpostsmooth(j)) posttime(minpostsmooth(j))],[-
100 100],'Color','b','LineStyle',':')
% % end

% Calculates average POST phase difference

phimax = {};

if length(maxpostsmooth) <= length(maxpostpred)
    len = length(maxpostsmooth);
else
    len = length(maxpostpred);
end
```

```
for l = 2:(len-1)
    phimax.struct(l) =  ((posttime(maxpostsmooth(l)) -
posttime(maxpostpred(l)))).*24;
end

postphimax = phimax.struct.';

phimin = {};

if length(minpostsmooth) > length(minpostpred)
    lan = length(minpostsmooth);
else
    lan = length(minpostpred);
end

for l = 2:(lan-1)
    phimin.struct(l) = ((posttime(minpostsmooth(l)) -
posttime(minpostpred(l)))).*24;
end

postphimin = phimin.struct.';

postphimean = mean([postphimin; postphimax])

postphisem = std([postphimin; postphimax])./sqrt(length([postphimin;
postphimax]))
```

APPENDIX C

Primers

Table C-1 Primer information

Name	Sequence	Direction	Band size (bp)	If band is present, this means:
ChR2 WT	5'-AAG GGA GCT GCA GTG GAG TA-3'	F	299	DOES NOT HAVE ChR2
ChR2 WT	5'-CCG AAA ATC TGT GGG AAG TC-3'	R		
ChR2 MU	5'-GGC ATT AAA GCA GCG TAT CC-3'	F	300	HAS ChR2
ChR2 MU	5'-CTG TTC CTG TAC GGC ATG G-3'	R		
Drd1a F1	5'-GCT ATG GAG ATG CTC CTG ATG GAA-3'	F	340	HAS Drd1aCre
CreGS R2	5'-CGG CAA ACG GAC AGA AGC ATT-3'	R		
NpHR WT	5'-TCC CAA AGT CGC TCT GAG TT-3'	F	242	DOES NOT HAVE NpHR
NpHR WT	5'-CTT TAA GCC TGC CCA GAA GA-3'	R		
NpHR MU	5'-ATA TCC TGC TGG TGG AGT GG-3'	F	190	HAS NpHR
NpHR MU	5'-GCC ACG ATA TCC AGG AAA GA-3'	R		
P1	5'-CTG TGT TTA CTG CGA GAG T-3'	1		
P2	5'-GGG TCC ATG TGA TTA GAA AC-3'	2	230	DOES NOT HAVE LUC on this allele
P3	5'-TAA AAC CGG GAG GTA GAT GAG A-3'	3	650	HAS LUC on this allele

Per1::GFPF	5'-CCT GGT CGA GCT GGA CGG CGA CGT AAA-3'	F	700	HAS GFP on this allele
Per1::GFPR	5'-CCG GCG GGA AGC CAT GGC TAA GCT T-3'	R		
Per1F	5'-CAG TAC TTC TCT TTC TAC ATC-3'	F	774	HAS WILD TYPE PER1 on this allele
Per1R	5'-CAT TGC TAT CAC TGG AGG AG-3'	R		
Per1NeoF	5'-TGC CCC AAA GGC CTA CCC GC-3'	NeoF	540	HAS MUTANT PER1 (i.e., KO) on this allele
Per2F	5'-AGA ACT TGT TGC TCC TGC TT-3'	F	810	HAS WILD TYPE PER2 on this allele
Per2R	5'-GGA AGC TTG TAA GGG GTG GT-3′	R		
Per2Neo	5'-TGC CCC AAA GGC CTA CCC GC-3'	NeoF	400	HAS MUTANT PER2 (i.e., KO) on this allele

APPENDIX D

Reagents

Electrophysiology solutions

Table D-1 Electrophysiology dissecting solution
1L in filtered H_2O

Reagent	Concentration	Molecular Weight	Actual Amount
NaCl	114.5 mM	58.44 g/mol	6.69138 g
KCl	3.5 mM	74.55 g/mol	0.260925 g
NaH2PO4-2H2O	1 mM	156.01 g/mol	0.15601 g
MgSO4-7H2O	1.3 mM	246.47 g/mol	0.320411 g
CaCl2-2H2O	2.5 mM	147.01 g/mol	0.367525 g
D(+)-glucose	10 mM	180.16 g/mol	1.8016 g
NaHCO3	35.7 mM	84.01 g/mol	2.999157 g

Table D-2 Electrophysiology recording solution
1L in filtered H_2O

Reagent	Concentration	Molecular Weight	Actual Amount
NaCl	124 mM	58.44 g/mol	7.24656 g
KCl	3.5 mM	74.55 g/mol	0.260925 g
NaH2PO4-2H2O	1 mM	156.01 g/mol	0.15601 g
MgSO4-7H2O	1.3 mM	246.47 g/mol	0.320411 g
CaCl2-2H2O	2.5 mM	147.01 g/mol	0.367525 g
D(+)-glucose	10 mM	180.16 g/mol	1.8016 g
NaHCO3	26 mM	84.01 g/mol	2.18426 g

Table D-3 Electrophysiology intracellular solution
500 ml in filtered H_2O

Reagent	Concentration	Molecular Weight	Actual Amount
K-gluconate	135 mM	234.25 g/mol	15.8119 g
KCl	10 mM	74.55 g/mol	0.37275 g

HEPES	10 mM	238.3 g/mol	1.1915 g
EGTA	0.5 mM	380.35 g/mol	0.0951 g
MgCl2	2 mM	203.3 g/mol	0.2033 g

Lumicycle solutions

Table D-4 Lumicycle slicing solution

Reagent	**Amount**
Sterile H2O	600 ml
HBSS 10x	100ml
PenStrep 10000U/ml	10 ml
7.5% NaHCO3	5 ml
HEPES 1M	10 ml

pH 7.2
Bring up to 1 L with sterile H_2O
Vacuum filter and keep at 4°C

Table D-5 Lumicycle culture medium

Reagent	Amount
Sterile H2O	800 ml
DMEM	1 container
B27 50x	20 ml
7.5% NaHCO3	4.7 ml
HEPES 1M	10 ml
PenStrep 10000U/ml	2.5 ml
D-glucose	7.78 ml

pH 7.2
Bring up to 1 L with sterile H_2O
Vacuum filter and keep at 4°C

Virus stocks

Table D-6 Stock viruses in -80°C freezer

Box	Tube Color	Virus	Cre-dependent?	Common name	Purpose	Titer (GC/ml)
1	-	AAV2/1.Syn.ChR2(H134R).eYFP.WP.hGH	No	ChR2	Optical depolarization	1.81e13
1	-	AAV2/1.hSynapsin.TurboRFP.RBG	No	RFP	Control fluorophore	2.82e13
1	-	AAV2/1.EF1a.DIO.eNpHR-eYFP.WP.hGH	Yes	NpHR	Optical hyperpolarization	4.28e12
1	-	AAV2/1.EF1a.DIO.hChR2(H134R).EYFP.WPRE.hGH	Yes	ChR2	Optical depolarization	1.58e13
1	-	AAV2/1.hSynap.GCaMP3.WPRE.SV40	No	GCaMP	Calcium indicator	?
1	-	AAV2/1.hSynap.Flex.GCaMP3.WPRE.SV40	Yes	GCaMP	Calcium indicator	6.00e12
1	-	rAAV5/Ef1a-DIO-C1V1(E122T/E162T)-TS-mCherry	Yes	C1V1	Red-shifted optical depolarization	4.00e12
1	-	rAAV5/Ef1a-DIO-hChR2(C128S-D156A)-mCherry	Yes	SSFO	Step-function depolarization	4.00e12
1	-	rAAV2/Ef1a-DIO-C1V1(E122T/E162T)-TS-mCherry	Yes	C1V1	Red-shifted optical depolarization	3.00e12
2	Blue	AAV1.Syn.RCaMP1h.WPRE.SV40	No	RCaMP	Red-shifted calcium indicator	1.65e13
2	Yellow	AAV1.hSyn.ArcLightD.WPRE.SV40	No	ArcLight	Voltage indicator	2.38e13

REFERENCES

Albus H, Bonnefont X, Chaves I, Yasui A, Doczy J, van der Horst GT, Meijer JH (2002) Cryptochrome-deficient mice lack circadian electrical activity in the suprachiasmatic nuclei. Curr Biol 12:1130–1133.

Aravanis AM, Wang L-PP, Zhang F, Meltzer LA, Mogri MZ, Schneider MB, Deisseroth K (2007) An optical neural interface: in vivo control of rodent motor cortex with integrated fiberoptic and optogenetic technology. J Neural Eng 4:S143–56.

Atkins N, Mitchell JW, Romanova EV, Morgan DJ, Cominski TP, Ecker JL, Pintar JE, Sweedler JV, Gillette MU (2010) Circadian integration of glutamatergic signals by little SAAS in novel suprachiasmatic circuits. PLoS ONE 5:e12612.

Aton SJ, Colwell CS, Harmar AJ, Waschek J, Herzog ED (2005) Vasoactive intestinal polypeptide mediates circadian rhythmicity and synchrony in mammalian clock neurons. Nat Neurosci 8:476–483.

Bae K, Jin X, Maywood ES, Hastings MH, Reppert SM, Weaver DR (2001) Differential functions of mPer1, mPer2, and mPer3 in the SCN circadian clock. Neuron 30:525–536.

Belle MD, Diekman CO, Forger DB, Piggins HD (2009) Daily electrical silencing in the mammalian circadian clock. Science 326:281–284.

Brancaccio M, Maywood ES, Chesham JE, Loudon AS, Hastings MH (2013) A Gq-Ca2+ axis controls circuit-level encoding of circadian time in the suprachiasmatic nucleus. Neuron 78:714–728.

Bunger MK, Wilsbacher LD, Moran SM, Clendenin C, Radcliffe LA, Hogenesch JB, Simon MC, Takahashi JS, Bradfield CA (2000) Mop3 is an essential component of the master circadian pacemaker in mammals. Cell 103:1009–1017.

Cermakian N, Monaco L, Pando MP, Dierich A, Sassone-Corsi P (2001) Altered behavioral rhythms and clock gene expression in mice with a targeted mutation in the Period1 gene. EMBO J 20:3967–3974.

Colwell CS (2011) Linking neural activity and molecular oscillations in the SCN. Nat Rev Neurosci 12:553–569.

Daan S, Pittendrigh CS (1976) A functional analysis of circadian pacemakers in nocturnal rodents. Journal of comparative physiology 106:267–290.

Debruyne JP (2008) Oscillating perceptions: the ups and downs of the CLOCK protein in the mouse circadian system. J Genet 87:437–446.

Debruyne JP, Noton E, Lambert CM, Maywood ES, Weaver DR, Reppert SM (2006) A clock shock: mouse CLOCK is not required for circadian oscillator function. Neuron 50:465–477.

Depetris-Chauvin A, Bemi J, Aranovich EJ, Muraro NI, Beckwith EJ, Ceriani MF (2011) Adult-specific electrical silencing of pacemaker neurons uncouples molecular clock from circadian outputs. Curr Biol 21: 1783–1793.

Ding JM, Chen D, Weber ET, Faiman LE, Rea MA, Gillette MU (1994) Resetting the biological clock: mediation of nocturnal circadian shifts by glutamate and NO. Science 266:1713–1717.

Evans JA, Leise TL, Castanon-Cervantes O, Davidson AJ (2013) Dynamic interactions mediated by nonredundant signaling mechanisms couple circadian clock neurons. Neuron 80:973–983.

Feldman JF, Hoyle MN (1973) Isolation of circadian clock mutants of Neurospora crassa. Genetics 75:605–613.

Freeman GM, Nakajima M, Ueda HR, Herzog ED (2013) Picrotoxin dramatically speeds the mammalian circadian clock independent of Cys-loop receptors. J Neurophysiol 110:103–108.

Gamble KL, Allen GC, Zhou T, McMahon DG (2007) Gastrin-releasing peptide mediates light-like resetting of the suprachiasmatic nucleus circadian pacemaker through cAMP response element-binding protein and Per1 activation. J Neurosci 27:12078–12087.

Goold CP, Nicoll RA (2010) Single-cell optogenetic excitation drives homeostatic synaptic depression. Neuron 68:512–528.

Green D, Gillette R (1982) Circadian rhythm of firing rate recorded from single cells in the rat suprachiasmatic brain slice. Brain Research 245:198200.

Guillaumond F, Dardente H, Giguère V, Cermakian N (2005) Differential control of Bmal1 circadian transcription by REV-ERB and ROR nuclear receptors. J Biol Rhythms 20:391–403.

Harmar AJ, Marston HM, Shen S, Spratt C, West KM, Sheward WJ, Morrison CF, Dorin JR, Piggins HD, Reubi JC, Kelly JS, Maywood ES, Hastings MH (2002) The VPAC(2) receptor is essential for circadian function in the mouse suprachiasmatic nuclei. Cell 109:497–508.

Harrisingh MC, Wu Y, Lnenicka GA, Nitabach MN (2007) Intracellular Ca2+ regulates free-running circadian clock oscillation in vivo. J Neurosci 27:12489–12499.

Herzog ED, Takahashi JS, Block GD (1998) Clock controls circadian period in isolated suprachiasmatic nucleus neurons. Nat Neurosci 1:708–713.

Hogenesch JB, Chan WK, Jackiw VH, Brown RC, Gu YZ, Pray-Grant M, Perdew GH, Bradfield CA (1997) Characterization of a subset of the basic-helix-loop-helix-PAS superfamily that interacts with components of the dioxin signaling pathway. J Biol Chem 272:8581–8593.

Ikeda M, Nomura M (1997) cDNA cloning and tissue-specific expression of a novel basic helix-loop-helix/PAS protein (BMAL1) and identification of alternatively spliced variants with alternative translation initiation site usage. Biochem Biophys Res Commun 233:258–264.

Konopka RJ, Benzer S (1971) Clock mutants of Drosophila melanogaster. Proc Natl Acad Sci USA 68:2112–2116.

Kudo T, Tahara Y, Gamble KL, McMahon DG, Block GD, Colwell CS (2013) Vasoactive intestinal peptide produces long-lasting changes in neural activity in the suprachiasmatic nucleus. J Neurophysiol 110:1097–1106.

Kuhlman SJ, Silver R, Sauter LJ (2003) Phase resetting light pulses induce Per1 and persistent spike activity in a subpopulation of biological clock neurons. J Neurosci 23:1441-1450.

Kuhlman SJ, McMahon DG (2006) Encoding the ins and outs of circadian pacemaking. J Biol Rhythms 21:470–481.

Kuhlman SJ, Quintero JE, McMahon DG (2000) GFP fluorescence reports Period 1 circadian gene regulation in the mammalian biological clock. Neuroreport 11:1479-1482.

Kurabayashi N, Hirota T, Sakai M, Sanada K, Fukada Y (2010) DYRK1A and glycogen synthase kinase 3beta, a dual-kinase mechanism directing proteasomal degradation of CRY2 for circadian timekeeping. Mol Cell Biol 30:1757–1768.

LeSauter J, Yan L, Vishnubhotla B, Quintero JE, Kuhlman SJ, McMahon DG, Silver R (2003) A short half-life GFP mouse model for analysis of suprachiasmatic nucleus organization. Brain Res 964:279–287.

Liu AC, Welsh DK, Ko CH, Tran HG, Zhang EE, Priest AA, Buhr ED, Singer O, Meeker K, Verma IM, Doyle FJ, Takahashi JS, Kay SA (2007) Intercellular coupling confers robustness against mutations in the SCN circadian clock network. Cell 129:605–616.

Liu C, Weaver DR, Strogatz SH, Reppert SM (1997) Cellular construction of a circadian clock: period determination in the suprachiasmatic nuclei. Cell 91:855–860.

Lowrey PL, Shimomura K, Antoch MP, Yamazaki S, Zemenides PD, Ralph MR, Menaker M, Takahashi JS (2000) Positional syntenic cloning and functional characterization of the mammalian circadian mutation tau. Science 288:483–492.

Lowrey PL, Takahashi JS (2011) Genetics of circadian rhythms in Mammalian model organisms. Adv Genet 74:175–230.

Lundkvist GB, Kwak Y, Davis EK, Tei H, Block GD (2005) A calcium flux is required for circadian rhythm generation in mammalian pacemaker neurons. J Neurosci 25:7682–7686.

Mackey SR (2007) Biological Rhythms Workshop IA: molecular basis of rhythms generation. Cold Spring Harb Symp Quant Biol 72:7–19.

Maywood ES, Reddy AB, Wong GK, O'Neill JS, O'Brien JA, McMahon DG, Harmar AJ, Okamura H, Hastings MH (2006) Synchronization and maintenance of timekeeping in suprachiasmatic circadian clock cells by neuropeptidergic signaling. Curr Biol 16:599–605.

Meijer JH, Schaap J, Watanabe K, Albus H (1997) Multiunit activity recordings in the suprachiasmatic nuclei: in vivo versus in vitro models. Brain research 753: 322-327.

Merrow M, Mazzotta G, Chen Z, Roenneberg T (2006) The right place at the right time: regulation of daily timing by phosphorylation. Genes Dev 20:2629–2633.

Minami Y, Ode KL, Ueda HR (2013) Mammalian circadian clock: the roles of transcriptional repression and delay. Handb Exp Pharmacol:359–377.

Mohawk JA, Takahashi JS (2011) Cell autonomy and synchrony of suprachiasmatic nucleus circadian oscillators. Trends Neurosci 34:349–358.

Morin LP, Allen CN (2006) The circadian visual system, 2005. Brain Res Rev 51:1–60.
Nakamura W, Honma S, Shirakawa T, Honma K (2002) Clock mutation lengthens the circadian period without damping rhythms in individual SCN neurons. Nat Neurosci 5:399–400.

Nitabach MN, Blau J, Holmes TC (2002) Electrical silencing of Drosophila pacemaker neurons stops the free-running circadian clock. Cell 109:485–495.

Nitabach MN, Wu Y, Sheeba V, Lemon WC, Strumbos J, Zelensky PK, White BH, Holmes TC (2006) Electrical hyperexcitation of lateral ventral pacemaker neurons desynchronizes downstream circadian oscillators in the fly circadian circuit and induces multiple behavioral periods. J Neurosci 26: 479–489.

Numano R, Yamazaki S, Umeda N, Samura T, Sujino M, Takahashi R, Ueda M, Mori A, Yamada K, Sakaki Y, Inouye ST, Menaker M, Tei H (2006) Constitutive expression of the Period1 gene impairs behavioral and molecular circadian rhythms. Proc Natl Acad Sci USA 103:3716–3721.

Pendergast JS, Friday RC, Yamazaki S (2009) Endogenous rhythms in Period1 mutant suprachiasmatic nuclei in vitro do not represent circadian behavior. J Neurosci 29:14681–14686.

Quintero JE, Kuhlman SJ, McMahon DG (2003) The biological clock nucleus: a multiphasic oscillator network regulated by light. J Neurosci 23:8070-8076.

Quintero JE, McMahon DG (1999) Serotonin modulates glutamate responses in isolated suprachiasmatic nucleus neurons. J Neurophysiol 82:533–539.

Ralph MR, Menaker M (1988) A mutation of the circadian system in golden hamsters. Science 241:1225–1227.

Ruan G-X, Allen GC, Yamazaki S, McMahon DG (2008) An autonomous circadian clock in the inner mouse retina regulated by dopamine and GABA. PLoS Biol 6:e249.

Ruan G-X, Gamble KL, Risner ML, Young LA, McMahon DG (2012) Divergent roles of clock genes in retinal and suprachiasmatic nucleus circadian oscillators. PLoS ONE 7:e38985.

Sakai K (2014) Single unit activity of the suprachiasmatic nucleus and surrounding neurons during the wake-sleep cycle in mice. Neuroscience 260:249–264.

Schwartz WJ, Gross RA, Morton MT (1987) The suprachiasmatic nuclei contain a tetrodotoxin-resistant circadian pacemaker. Proc Natl Acad Sci USA 84:1694-1698.

Schwartz WJ, Tavakoli-Nezhad M, Lambert CM, Weaver DR, de la Iglesia HO (2011) Distinct patterns of Period gene expression in the suprachiasmatic nucleus underlie circadian clock photoentrainment by advances or delays. Proc Natl Acad Sci USA 108:17219–17224.

Spoelstra K, Albrecht U, van der Horst GT, Brauer V, Daan S (2004) Phase responses to light pulses in mice lacking functional per or cry genes. J Biol Rhythms 19:518–529.

Sugiyama T, Yoshioka T, Ikeda M (2004) mPer2 antisense oligonucleotides inhibit mPER2 expression but not circadian rhythms of physiological activity in cultured suprachiasmatic nucleus neurons. Biochem Biophys Res Commun 323:479–483.

Sun ZS, Albrecht U, Zhuchenko O, Bailey J, Eichele G, Lee CC (1997) RIGUI, a putative mammalian ortholog of the Drosophila period gene. Cell 90:1003–1011.

Takahashi JS, Hong H-KK, Ko CH, McDearmon EL (2008) The genetics of mammalian circadian order and disorder: implications for physiology and disease. Nat Rev Genet 9:764–775.

Tei H, Okamura H, Shigeyoshi Y, Fukuhara C, Ozawa R, Hirose M, Sakaki Y (1997) Circadian oscillation of a mammalian homologue of the Drosophila period gene. Nature 389:512–516.

Van der Horst GT, Muijtjens M, Kobayashi K, Takano R, Kanno S, Takao M, de Wit J, Verkerk A, Eker AP, van Leenen D, Buijs R, Bootsma D, Hoeijmakers JH, Yasui A (1999) Mammalian Cry1 and Cry2 are essential for maintenance of circadian rhythms. Nature 398:627–630.

Vitaterna MH, King DP, Chang AM, Kornhauser JM, Lowrey PL, McDonald JD, Dove WF, Pinto LH, Turek FW, Takahashi JS (1994) Mutagenesis and mapping of a mouse gene, Clock, essential for circadian behavior. Science 264:719–725.

Welsh DK, Logothetis DE, Meister M, Reppert SM (1995) Individual neurons dissociated from rat suprachiasmatic nucleus express independently phased circadian firing rhythms. Neuron 14:697–706.

Welsh DK, Takahashi JS, Kay SA (2010) Suprachiasmatic nucleus: cell autonomy and network properties. Annu Rev Physiol 72:551–577.

Yamaguchi S, Isejima H, Matsuo T, Okura R, Yagita K, Kobayashi M, Okamura H (2003) Synchronization of cellular clocks in the suprachiasmatic nucleus. Science 302:1408–1412.

Yizhar O, Fenno LE, Davidson TJ, Mogri M, Deisseroth K (2011) Optogenetics in neural systems. Neuron 71:9–34.

Yoo S-HH, Yamazaki S, Lowrey PL, Shimomura K, Ko CH, Buhr ED, Siepka SM, Hong H-KK, Oh WJ, Yoo OJ, Menaker M, Takahashi JS (2004) PERIOD2::LUCIFERASE real-time reporting of circadian dynamics reveals persistent circadian oscillations in mouse peripheral tissues. Proc Natl Acad Sci USA 101:5339–5346.

Zheng B, Larkin DW, Albrecht U, Sun ZS, Sage M, Eichele G, Lee CC, Bradley A (1999) The mPer2 gene encodes a functional component of the mammalian circadian clock. Nature 400:169–173.